THE MOLECULAR BASIS OF SEROTYPE 1 REOVIRUS GLYCAN INTERACTIONS AND THE FUNCTION OF GLYCAN-BINDING IN PATHOGENESIS

By

Jennifer Stencel-Baerenwald

Dissertation

Submitted to the Faculty of the

Graduate School of Vanderbilt University

In partial fulfillment of the requirements

for the degree of

DOCTOR OF PHILOSOPHY

in

Microbiology and Immunology

December 2014

Nashville, Tennessee

Approved:

Terence S. Dermody, M.D.

D. Borden Lacy, Ph.D.

Kelli Boyd, D.V.M., Ph.D.

Eric Sebzda, Ph.D.

John Williams, Ph.D.

ACKNOWLEDGEMENTS

I am grateful for the financial support of the Structural Analysis of Reovirus Attachment Mechanisms grant (R01 076983) awarded to T.S. Dermody and T. Stehle and a Vanderbilt Graduate School Dissertation Enhancement Grant that afforded me the opportunity to participate in crystallography studies with the Stehle laboratory at the University of Tübingen. Additionally, I am thankful for the generosity of the Lamb family and their continuous support of the Lamb Center for Pediatric Research.

I am forever indebted to my mentor Dr. Terry Dermody, for the training he provided in his laboratory. I could not have asked for a better mentor. Terry displays unwavering devotion to his trainees and creates a collaborative and cohesive laboratory environment for his team. Terry is a gifted scientist and writer who leads by example. Working with Terry has improved my writing, critical thinking skills, and ability to present data.

I thank lab managers Dr. Andrea Pruijssers and Denise Wetzel for running a smooth ship during my time in the Dermody lab. I would like to thank Andrea Pruijssers for her ability to make sure that we were always taken care of and helping to create a collaborative environment for the lab. I would like to thank Denise Wetzel for her wealth of knowledge about reovirus and Dermody-lab history and persistence when ordering particularly difficult reagents.

I am grateful for the opportunity to have worked with such wonderful graduate students during my time in the Dermody laboratory. I would like to thank Alison Ashbrook, Magda Bokiej, Judy Brown, Joshua Doyle, Johnna Frierson, Jonathan Knowlton, Caroline Lai, Danica Sutherland, and Paula Zamora for their feedback and your friendship. I had the opportunity to overlap with some of you for years and others

for mere months, but I learned so much from each of you. I thank Alison Ashbrook for her pointed questions and smiling face. Dr. Maga Bokiej for early morning discussions; Judy Brown for her enthusiasm and general willingness to help; Dr. Joshua Doyle, for his good-natured, daily dose of sarcasm in the Wilson lab and for discussions about life and science; Dr. Johnna Frierson for her cheerful demeanor and knack for organizing lab events; Jonathan Knowlton for his wealth of medical knowledge and translation of medical terms, Caroline Lai for showing me the ropes in lab and at the gym; Danica Sutherland for her thoroughness, enthusiasm, and discussions; and Paula Zamora, my fellow Wilson-lab mate, for her questions and for always telling me where I can find snacks.

My labmates in the Dermody lab made lab enjoyable regardless of the experimental outcome of the day. I would like to thank Dr. Bernardo Mainou for always being willing to lend a hand in experimental design as well as invaluable discussions about careers in science; Dr. Jenn Konopka-Anstadt for her friendship and advice on anything ranging from neuronal cell-culture and manuscript preparation to wedding planning; and Jason Iskarpatyoti for his willingness to always lend a hand, inside or out of lab. I would like to thank Dr. Greg Wilson for his knowledge as the reovirus historian as well as his friendly demeanor and genuine helpfulness. I would like to thank Dr. Sarah Katen, for her gorgeous cakes and help on anything ranging from an aliquot of antibody to a tutorial on STD-NMR. I would like to thank Solomiia Khomandiak for her curiosity and cheerful personality; Dr. Laurie Silva for her advice on experimental design and work-life balance; and Dr. Allen Wu, for helpful discussions.

I cannot begin to thank my longtime Dermody-Wilson labmates Miné Ikizler and Karl Boehme. I would like to thank Miné Ikizler for her assistance in and outside of lab. Miné has taught me so much about molecular virology, careers in science, and hems when she so graciously stepped up to go wedding dress shopping with me. Dr. Karl

Boehme taught me everything I know about viral plaque assays and organ titration. More importantly, Karl was correct with his weekly mantra of “it’s your career…” and I thank him for leading by example and showing us how to take ownership of our future in science.

I grateful for the insight and guidance I received from all members of my thesis committee: Drs. Borden Lacy, Kelli Boyd, Jim Chappell, Eric Sebzda, and John Williams. I appreciate discussions with Dr. Borden Lacy about careers in science as well as her helpful questions; learning so much about histology and mouse pathology during meetings with Dr. Kelli Boyd; Dr. Jim Chappell’s wealth of knowledge about reovirus and reovirus-sialic acid interactions; Eric Sebzda’s unique perspective, insightful questions, and introducing me to useful tools such as Gene Atlas; and John Williams for his enthusiasm and curiosity towards mouse pathogenesis studies, and line of questioning that facilitated future experimental design.

I would like to thank Eve Anderson and Janet Shelton in Pediatric Infectious Disease for their invaluable administrative support. I also would like to thank Jean Tidwell for her support of the students in the Department of Microbiology and Immunology.

I am so grateful for the opportunity to work with the Stehle lab. I thank Dr. Thilo Stehle for his helpful advice particularly during our bi-monthly conference calls, feedback on writing, and the collaborative environment that Thilo Stehle and Terry Dermody create between the labs. I am so thankful to have had the chance to work and co-publish with Dr. Kerstin Reiss, a talented crystallographer and biochemist. Kerstin performed all of the T1 σ1 crystallography shown in this thesis. I greatly appreciate the time we have spent together in person conferences and the occasions in which we could work and visit in our respective cities. I am grateful for the chance to work alongside Dr. Dirk Reiter. Working with Dirk has been a unique experience and he has taught me so much

about crystallography, biochemistry, coffee machines, aging wine, and preparation of German knüdel. I am thankful for the chance to collaborate with Melanie Dietrich. She, like Thilo, Kerstin, and Dirk, is a fantastic structural biologist. I have much enjoyed getting to know her. I am grateful for her help generating the mutant σ1 proteins. Finally, I am thankful for the chance to have met and worked with Bärbel Balum who performed the NMR spectroscopy data presented in this thesis.

I am grateful for the Animal Care Personnel and Veterinary Staff at Vanderbilt University and their assistance in keeping the animals used in this research clean and safe.

I would like to thank Dr. Daniel Colvin and the rest of the Vanderbilt Small Animal Imaging Core for technical assistance with the MRI studies. I thank Dr. Dapeng Zhou (MD Anderson Cancer Center) for providing the $GM2^{-/-}$ mice for use in these studies.I am grateful for Drs. Ty Abel and Kelli Boyd for the assistance with the histology presented in this thesis. I have had the opportunity to learn so much about brain pathology from each of them.

I appreciate the training in immunology and critical thinking that I received from Dr. Bana Jabri. Developing the data presented in Appendix 1 in collaboration with her laboratory has been rewarding.

I thank Dr. Barbara Osborne, my very first PI, for introducing me to research and her vote of confidence. I became interested in research while working in the Osborne lab during my time as an undergraduate at UMass. It was through her guidance and mentorship that I first learned to develop experimental ideas and follow my passion.

I also thank my family, for without them, I would not be who or where I am today. I thank my grandparents for shaping my perspective on the world and really teaching me the value of an education. I am forever grateful for their insight on navigating through work and life. I would like to thank my aunt Rikay for teaching me the importance and

relevance of mathematics from an early age. I am grateful for her continued interest in my education. I am thankful for my brother, Jason, for his continued support, friendship, and shared interest in medical science. I cannot begin to thank my parents for their love, support, and vote of confidence. They taught me to work hard and strive for perfection while leading a balanced life. They helped me to do so by always putting the needs of my brother and I before theirs. When I was young, I always asked my mother why she had to go to work, but now, I wish I could thank her for showing me how to be a successful career woman, mother, and wife. I thank my father for always being there and instilling in me a sense of reason an logic, something that is required in both science and everyday life. I also thank my husband Devin for always believing in and supporting me. I appreciate his patience and willingness to shuffle schedules and life around for experiments as well as his general understanding that 15 lab minutes is about an hour, sometimes two, on an actual clock. I am so lucky to have him with me through these adventures, and I look forward to the future.

TABLE OF CONTENTS

LIST OF TABLES

LIST OF FIGURES

CHAPTER I

INTRODUCTION

Overview

Viruses are obligate intracellular pathogens that must adhere to and enter cells to initiate an infectious cycle. Receptors expressed on the host cell surface attach the virus to target cells and serve as a determinant of host range and tissue tropism. Since receptor engagement governs the susceptibility of cells to infection, insight into receptor utilization can enhance an understanding of more general principles of ligand-receptor interactions, shed light on the contribution of receptor engagement to disease, and potentially aid in the design of antiviral drugs and viral vectors.

It is common for viruses to bind multiple receptors to facilitate efficient viral entry. Human immunodeficiency virus (HIV) binds primary receptor CD4 (1) and co-receptor CCR5 or CXCR4 (2, 3), adenovirus utilizes both coxsackie virus and adenovirus receptor (CAR) (4) and integrins during entry (5, 6), and mammalian orthoreoviruses, herein referred to as reoviruses, use sialylated glycans (7-10), junctional adhesion molecule A (JAM-A) (11, 12), integrins (13, 14), and Nogo receptor 1 (NgR1) (15). The contribution of individual receptors to viral disease is not completely understood.

Reoviruses display serotype-dependent pathology, with serotype 1 (T1) strains causing hydrocephalus (16) and serotype 3 (T3) strains causing

encephalitis (17), but the basis for these serotype-specific differences is not known. T1 and T3 reoviruses engage the same known proteinaceous receptors (11, 15), yet they interact with distinct glycans. This observation suggests that differences in glycan utilization contribute to serotype-specific differences in tropism.

This thesis describes results of experiments I conducted to understand the molecular basis of T1 reovirus-glycan interactions and define the contribution of glycan engagement to T1 reovirus-mediated disease. In Chapter 1, I present data identifying GM2 as a specific carbohydrate bound by T1 reovirus. In Chapter 2, I show data that define residues in the T1 reovirus σ1 attachment protein required for functional GM2 engagement. In Chapter 3, I describe findings from *in vivo* experiments demonstrating that T1 reovirus-GM2 interactions influence hydrocephalus severity in mice. Taken together, these results establish a determinant of reovirus serotype-specific disease, deepen an understanding of the function of glycan binding in viral tropism, and may facilitate design of therapeutic reovirus vectors.

Virus-Receptor Interactions

Many viruses use cell-surface carbohydrates such as glycosaminoglycans (GAGS) (18-21), blood group antigens (22, 23), and sialylated glycans (7, 8, 24-27) to facilitate attachment and entry. Some viruses, such as influenza virus, appear to engage sialic acid as a primary receptor (26), while others, such as reovirus, engage sialic acid as an initial adhesive event prior to binding a

proteinaceous attachment receptor, in a process known as adhesion strengthening (7, 11). Sialic acid is amongst the oldest known virus receptors (28), and many enveloped and nonenveloped viruses bind some form of sialic acid to facilitate entry.

Sialic acid containing glycans are common virus receptors

Sialic acid, also known as neuraminic acid, is a nine-carbon monosaccharide ubiquitously expressed in higher vertebrates (29). In the host, sialic acids function in cell-cell adhesion, cell signaling, especially within the immune system, and development (30, 31). Genetic defects in sialic acid biosynthesis are exceedingly rare (32). The five carbon of neuraminic acid is frequently modified with an N-acetyl group (Neu5Ac), which can be further hydroxylated to form N-glycolylneuraminic acid (Neu5Gc) (29). Additional modifications can involve acetylation, methylation, and sulfation of various hydroxyl groups. Sialic acid is often α-linked from the two carbon via different linkages to carbohydrate chains found on the nearby saccharides of glycoproteins and glycolipids. Glycoproteins are polypeptide moieties with glycans attached via the nitrogen atom of an asparagine side chain (N-linked) or the oxygen atom of a serine or threonine side chain (O-linked). Gangliosides are amphipathic glycosphingolipids containing a hydrophobic ceramide tail and a hydrophilic head with a sialylated carbohydrate moiety (33). Glycoproteins (34-36) and gangliosides (35) can function as viral attachment factors. Virus

interactions with terminal sialic acid moieties of glycoproteins and gangliosides are usually of low affinity and strengthened by the multivalency of the virus.

Viruses and gangliosides

Gangliosides are divided into three main classes, the asialo-series, a-series, and b-series (37). The gangliosides discussed further in this thesis are a-series gangliosides. GM3, the simplest a-series ganglioside, is formed when GM3 synthase catalyzes the addition of an α2,3-linked sialic acid onto a lactose moiety with a ceramide tail. GM3 is the precursor of GM2 (Figure I-1), which is processed when GM2/GD2 synthase adds an N-acetylgalactosamine (GalNAc) to GM3. GM2 is the precursor for gangliosides GM1 and GD1a. Gangliosides are required for normal development as mice lacking GM3 and GM2 synthases die as embryos (38). Gangliosides also serve as receptors for several non-enveloped viruses. For example, murine norovirus recognizes sialic acid on GD1a and GT1b, and GM1 is a receptor for human rotavirus strains KU, MO, DS-1, and Wa (39). Additionally, GD1a and GT1B are receptors for murine polyomavirus (mPyV) and simian virus 40 (SV40) recognizes GM1 (25).

Studying sialic-acid virus interactions

While viruses have been known for some time to use cell-surface sialic acid to initiate infection, recent advances in glycan microarray (glycan array) screening technology (40) have rapidly accelerated studies of carbohydrate-binding ligands. Coupled with new structural information about how viruses bind

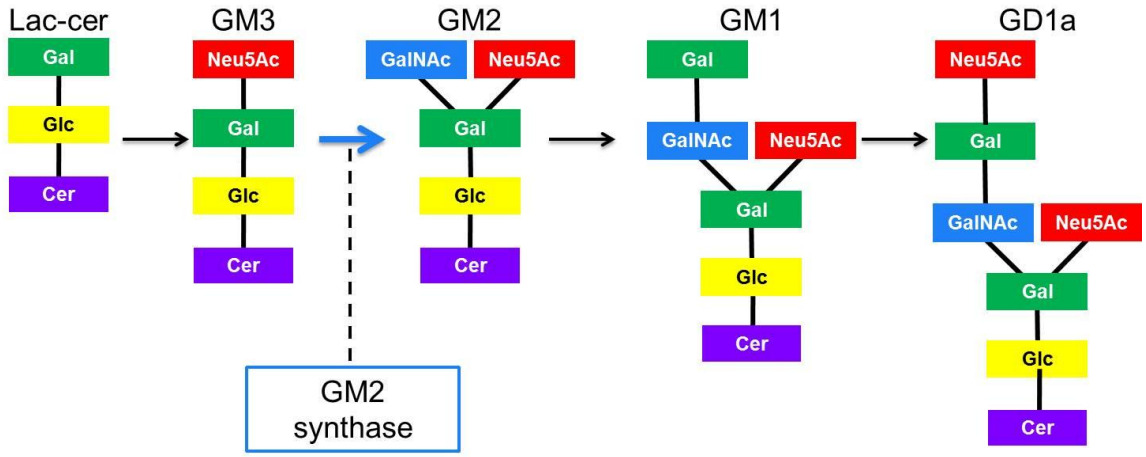

Figure I-1. A-series ganglioside biosynthesis pathway. Lactose-ceramide (Lac-cer) is comprised of a ceramide bound glucose (glc) linked to a galactose (gal) and servers as the precursor for ganglioside synthesis. GM3 synthase catalyzes the addition of an α2,3-linked sialic acid or neuraminic acid (Neu5Ac) to the galactose moiety. GM2 is generated when GM2 synthase catalyzes the addition of a N-acetylgalactosamine (GalNAc) to the GM3 precursor. This step is indicated with a blue arrow and box. GM2 can be further processed to form gangliosides GM1 and GD1a. Gangliosides GM3, GM2, and GM1 will be discussed further in this thesis with emphasis on GM2 and GM2 synthase. (Figure adapted from Furukawa et al. 2002 (37)).

to sialylated glycans as well as the advent of reverse genetics (41, 42), virus-glycan interactions can now be analyzed in unprecedented detail. Historically, a requirement for virus-sialic acid binding was investigated using cell-based assays in which viral infectivity was monitored following treatment with sialic acid-binding lectins or enzymatic removal of sialic acid using various types of neuraminidases. Certain biantennary glycans including ganglioside GM1, are resistant to neuraminidase treatment (43). Moreover, sensitivity is limited to the linkage-basis of the sialic acid moiety. Glycan array screening allows finer differences in virus-glycan binding preferences to be discerned and augments the classical approach by enabling rapid, high-throughput screening of numerous glycans as potential virus receptors (40, 44-46). This technology has been used to identify carbohydrate ligands of adenovirus (36), influenza virus (47, 48), polyomavirus (49), rotavirus (22, 23), and reovirus (10), among others. Glycan array screening also has been highly valuable in identifying glycan specificity differences among related virus strains (47, 50, 51).

Viruses that engage sialylated receptors

Influenza virus-sialic acid interactions are well-studied. The hemagglutinin protein (HA) of influenza virus binds sialic acid to adhere the virus to the cell-surface. Receptor-binding specificities strongly influence host range, with avian strains preferring α2,3-linked sialic acid and human strains preferring α2,6-linked sialic acid (26, 52). Glycan array studies have highlighted more distinct glycan-binding preferences for specific strains (53). Influenza virus

interacts with sialic acid at multiple points during its infectious cycle. Binding of HA to cell-surface sialic acid initiates infection, but the virus must remove sialic acid from the cell surface and its glycoproteins to allow viral release. This function is mediated by a virus-encoded neuraminidase (NA), which is an important target of antiviral therapy (54, 55). NA cleavage specificities are finely tuned to HA binding preferences to facilitate viral exit. Thus, the HA and NA proteins must function in concert for efficient replication and infection (56, 57).

Certain **adenovirus** types bind to sialic acid. For example, the species D adenovirus 37 (Ad37) agglutinates human red blood cells (58) in a neuraminidase-sensitive manner (59, 60). These findings indicate a requirement for sialic acid binding by this adenovirus type. Glycan array screening demonstrated that Ad37 binds specifically to the GD1a glycan on O-linked glycoproteins (36). Soluble GD1a diminishes the capacity of Ad37 to bind and infect human corneal epithelial cells, suggesting that GD1a serves as a functional receptor for at least some adenoviruses.

Polyomaviruses also engage cell-surface sialic acid for efficient infection. Glycan array screening identified LSTc, a linear pentasaccharide that contains an α2,6-linked sialic acid, as a glycan receptor for human JC polyomavirus (JCV) (49). GD1a and GT1b are receptors for mouse polyomavirus (mPyV) (25). Polyomavirus binding to glycans mediates attachment, but in the case of mPyV, GD1a also facilitates transport of the virus to the endoplasmic reticulum (ER) prior to nuclear delivery (35, 61). The GD1a glycan present on both gangliosides and glycoproteins can bind mPyV. However, the GD1a ganglioside and not a

glycoprotein is responsible for viral trafficking to the ER (35), highlighting an additional role for sialylated glycans in viral infection.

Rotaviruses are nonenveloped double-stranded RNA viruses from the *Reoviridae* family. Rotavirus attachment is dependent on glycans and mediated by the trimeric outer-capsid protein, VP4 (62). Rotavirus infectivity is enhanced following proteolytic cleavage of the VP4 trimer into N-terminal VP8* and C-terminal VP5* subunits. The VP8* subunit serves as the viral hemagglutinin and binds to glycans (63), while the VP5* subunit facilitates membrane penetration (64). Animal rotaviruses tend to engage terminal sialic acid-containing receptors (65-70) and display neuraminidase-sensitive infectivity. Some human rotaviruses, such as the Wa strain, bind ganglioside GM1 (71). Neuraminidase cannot remove sialic acid from glycans such as GM1 and, thus, these strains were incorrectly presumed not to engage sialylated glycans. Yet, not all rotavirus strains bind sialylated glycans. A combination of glycan array screening and crystallographic analysis of VP8* from the human sialidase-insensitive strain HAL1166, P[14] VP4 genotype, demonstrated that this virus specifically engages A-type histo blood group antigen (HBGA) (22). HBGAs are oligosaccharides expressed on erythrocytes and epithelial cells and also present in mucosal secretions.

Perturbing virus-sialic acid interactions

Virus-sialic acid interactions can be altered with surprisingly few mutations. For example, two amino acid changes in the 1918 HA receptor-

binding site shift the binding preference of the virus from α2,6- to α2,3-linked sialic acid (47). The virus that binds α2,3-linked sialic acid retains virulence in ferrets but is incapable of droplet transmission, unlike the α2,6-linked sialic acid-binding strain (72). A switch in avian H5N1 from α2,3-linked to α2,6-linked sialic acid allows spread in ferrets by direct contact but is not sufficient to allow droplet transmission (73). Therefore, further adaptations are required to potentiate pandemic spread.

GM1 serves as a functional receptor for polyomavirus SV40 (25). An SV40-GM1 escape mutant containing only three amino acid changes from wildtype virus binds to cells less efficiently and is not neutralized by soluble GM1. This mutant displays enhanced capacity to infect cells with low GM1 expression, likely the result of binding to another ganglioside (74). B series gangliosides GD3, GD2, GD1b, and GT1b share a common α2,8-linked motif and function as receptors for human BK polyomavirus (BKPyV) (51). Structure-guided mutagenesis studies using the crystal structures of BKPyV in complex with GD3 and SV40 in complex with GM1 demonstrated that a single amino acid substitution in BKPyV switches receptor specificity in cell culture to that of GM1 (51). These findings provide a framework for targeting viruses to new receptors.

Virus-glycan engagement influences host range and pathogenesis

Zoonotic transmission of viruses often results from alterations in receptor specificity. The binding preference of human influenza virus strains for α2,6-linked sialic acid and avian strains for α2,3- linked sialic acid (48, 52) mirrors the

pattern of sialic acid expression of the target host as defined by lectin-based immunohistochemistry. In humans, α2,6-linked sialic acid is expressed on ciliated tracheal epithelial cells (75) and epithelial cells in the sinuses, pharynx, and bronchioles (76). Nonciliated cells of the lower respiratory tract express α2,3-linked sialic acid (75, 76). In birds, α2,3-linked sialic acid is the dominant form in the respiratory and intestinal tracts. The switch in receptor specificity from avian α2,3-linked to human α2,6-linked sialic acid is a major factor in the emergence of pandemic influenza viruses. The 1918 H1N1, 1957 H2N2, 1968 H3N2, and 2009 H1N1 strains were not of human origin but acquired human α2,6-linked sialic acid receptor-binding specificity (47, 77-79). In contrast, highly pathogenic avian H5N1 influenza virus strains have a strict requirement for α2,3-linked sialic acid and consequentially spread inefficiently from birds to humans. However, the virus can replicate in the lower respiratory tract of humans where α2,3-linked sialic acid is expressed. Therefore, H5N1 strains are virulent in humans. These observations also indicate that sialic acid-binding influences influenza virus tropism within the host (80).

Mutations that shift influenza virus binding specificity from avian to human receptors are not always conserved among HA types. Mutations that shift H1 HA from α2,3- to α2,6-linked sialic acid do not result in α2,6-linked sialic acid binding by the H5 HA. These mutations only alter the affinity of H5 HA for α2,3-linked sialic acid. In contrast, mutations that convert H3 viruses from avian to human receptor specificity allow H5N1 binding to α2,6-linked sialic acid (81).

In addition to linkage variations, sialic acid modifications also can influence infectivity. The HA protein of human H3 viruses binds Neu5Ac and does not replicate in the duck intestine. However, the addition of two mutations confers binding to Neu5Gc and permits replication in ducks. Neu5Gc is expressed in areas targeted by the mutant virus, suggesting that recognition of Neu5Gc is important for infection (82). While it is certainly well studied, the intimate relationship between sialic acid and viral disease is not unique to influenza virus.

Polyomavirus tropism also is affected by virus-sialic acid interactions. Polyomaviruses transform cells in culture, but only some mPyV strains induce tumors in mice (83). Small-plaque-forming virus, RA, induces few tumors in mice, whereas the large-plaque-forming strain, PTA, is highly tumorigenic (84, 85). Residue 91 of the major capsid protein VP1, which is contained within the sialic acid-binding pocket, dictates this phenotype (86-89). Glycine at position 91, as seen in RA, accommodates straight-chain and branched sialyloligosaccharides, while glutamic acid at this position, as seen in PTA, does not accommodate branched sialyloligosaccharides (87-89). A G91E mutation in RA increases tumorogenicity in mice, while the reciprocal E91G mutation in PTA attenuates disease (90), thus providing an unambiguous link between a single amino acid substitution and disease severity. Attenuation of RA strains is thought to be a consequence of binding to branched sialyloligosaccharides that serve as pseudoreceptors and route the virus to non-productive entry pathways.

Human BKPyV binds GD3, whereas SV40 binds GM1. A mutation in BKPyV switches sialic acid-binding preference from GD3 to GM1. Moreover, the mutant displays species-specific tropism. BKPyV K68S is specific for GM1-Neu5Ac, the common form of GM1 found in humans. Conversely, SV40 prefers GM1-Neu5Gc, the common form in apes (51). Preference for Neu5Gc in SV40 is achieved by a larger, more polar pocket that can accommodate the hydroxyl group of the glycolyl chain. These observations raise the possibility that polyomavirus species jumps are mediated by changes in sialic acid-binding specificity.

Alterations in glycan-binding capacity influence rotavirus disease outcome. Silencing the expression of ganglioside synthesis genes using RNA interference decreases ganglioside production and diminishes the capacity of human, bovine, porcine, and simian rotaviruses to infect cells *in vitro* (91). Sialic acid binding also influences pathogenesis in mice. Administration of bovine submaxillary mucin, which contains sialic acid, prevents gastroenteritis and diminishes rotavirus shedding in these animals (92). Ovine erythrocytes, which are naturally covered with sialic acid, also block rotavirus replication (92). Concordantly, neuraminidase treatment of these red blood cells negates the therapeutic effect (92). Reoviruses also engage sialylated glycans, and these virus-carbohydrate interactions influence tropism in the host.

Reoviruses

Reovirus background

Reoviruses are nonenveloped viruses with icosahedral symmetry. Virions contain 10 segments of dsRNA that are divided into three classes based on size. The three large gene segments, L1, L2, and L3, encode proteins λ3, λ2, and λ1, respectively, which are approximately 140 kDa in size. The three medium segments, M1, M2, and M3, encode μ2, μ1, and μNS, respectively, which are about 80 kDa in size. The small segments are designated S1, S2, S3, and S4. S1 encodes both σ1, the viral attachment protein (93) and subject of this thesis, and σ1s, a nonstructural protein required for reovirus cell-cycle arrest (94, 95). It is noteworthy that all of the mutations engineered in the S1 gene in my studies are not within the σ1s reading frame and can be definitively associated with σ1. The S2, S3, and S4 gene segments encode σ2, σNS, and σ3, respectively. While σ1s is 14,000 kDa in size, all other proteins encoded by reovirus S genes are approximately 40-50 kDa. (Table I-1). These ten segments of dsRNA are encapsidated within two concentric protein shells, the outer capsid and inner core. The outer capsid is comprised of σ1, σ3, and μ1 (Figure I-2). Most children are seropositive for reovirus by five years of age (96). Reovirus causes mild respiratory illness or gastroenteritis. In rare cases, reovirus disseminates in newborn infants and causes central nervous system disease (97).

Reoviruses have a broad host range in nature, infecting nearly all mammals. Reovirus is a tractable experimental system for studies of virus-receptor interactions, viral cell entry, and viral pathogenesis because they

Gene segment	Protein products
L1	λ3
L2	λ2
L3	λ1
M1	μ2
M2	μ1
M3	μNS
S1	σ1 and σ1s
S2	σ2
S3	σNS
S4	σ3

Table I-1. Reovirus gene segments and protein products. The reovirus gene segments and corresponding proteins are shown.

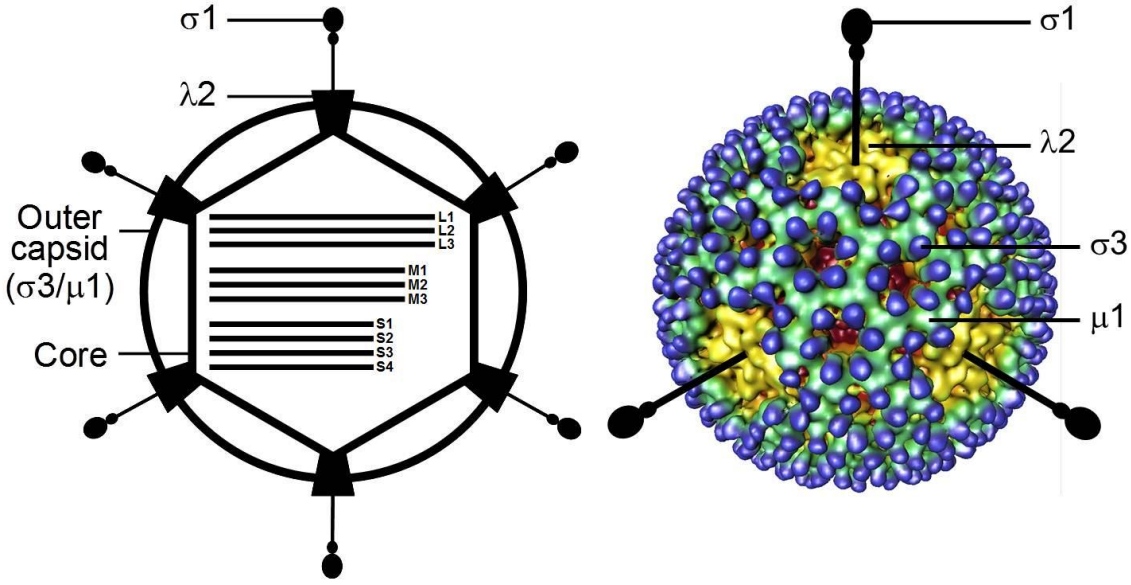

Figure I-2. The reovirus virion. Schematic of a reovirus virion (left). Reovirus particles are composed of two concentric protein shells, the outer capsid and inner core. The inner core contains the viral genome consisting of ten segments of double-stranded RNA. Cryo-electron micrograph image reconstruction of a reovirus virion (right). Outer capsid protein σ3 (blue) is removed during virion disassembly in infected cells. Pentameric λ2 protein (yellow) forms the base for insertion of the σ1 attachment protein (added in black). (Figure adapted from Nason et al. 2001 (98)).

produce high titer, facilitating biochemical and biophysical studies, and the virus and host can be manipulated genetically to define determinants of pathogenesis in each.

A history of common laboratory strains

There are three serotypes of reoviruses, designated as serotype 1, 2, and 3 that are represented by prototype strains type 1 Lang (T1L), type 2 Jones (T2J), and type 3 Dearing (T3D). Prototype strain T1L was isolated in 1951 from a healthy child (99), while prototype strains T2J and T3D were isolated from the stools of children with diarrhea also in the early 1950s (99-101).

Reovirus reverse genetics

Classically, isolation of viral mutants incapable of binding receptors required propagating viruses in the presence of excess soluble receptor to select for escape mutants in a process termed forward genetics. For most viruses, including reovirus, it is now possible to rationalize mutations, sometimes using structural data, and generate single and multiple point mutants using a process termed reverse genetics. In the reovirus reverse genetics system (41, 42), cDNAs corresponding to each of the reovirus gene segments are encoded on plasmids, either alone or in combination. The cDNAs are flanked by the promoter sequence for T7 polymerase and the hepatitis delta virus (HDV) ribozyme. The plasmids are transfected into baby hamster kidney (BHK) cells that constitutively express T7 polymerase, thus driving transcription of the plasmid-encoded

reovirus genes. The HDV ribozyme cleaves the cDNA, ensuring that the 3' ends of the transcripts are in their native form.

Once inside cells, host ribosomes translate the mRNAs, yielding reovirus proteins. Replication complexes form and drive negative-strand RNA synthesis. Infectious virions form and, following a few replication cycles, the BHK-T7 cells are frozen and thawed to release all reovirus virions. Supernatants are then used to infect L cells and generate reovirus stocks (41, 42). Site-directed mutagenesis can be used to generate plasmids encoding mutant viral cDNAs, thereby enabling directed engineering of mutant viruses.

Reovirus tropism

After peroral inoculation, reovirus infects M cells on the surface of Peyer's patches in the intestine (102, 103) and disseminates to sites of secondary replication including the heart, liver, and brain (104). Reovirus displays serotype-dependent pathology in the central nervous system (CNS) of newborn mice, which are highly susceptible to infection and disease.

T1 reovirus, the subject of this thesis, spreads via hematogenous routes, infects ependymal cells that line the brain ventricles, and causes hydrocephalus (16, 105-107). Disease begins with acute ependymitis, followed by hydrocephalus (16, 108). Affected mice display dilation of the lateral and third ventciles, with some animals developing intraventricular hemorrhage. Compression of the midbrain leads to aqueductal stenosis. The majority of the reovirus-infected foci are ependymal cells, but occasional neuronal necrosis

occurs at limited sites (106). Ependymal cells succumb to necrosis, and the ependymal layer is denuded over the course of infection (16, 108). Inflammatory infiltrate and debris subsequently block the aqueduct (106). Both the ependymal cells and choroid plexus are irregular and vary in cellular density. In some cases, tissue grows into the ventricular cavities, resulting in obstruction (108). Reovirus titers are often below the level of detection by the time of disease onset (107). Thus, reovirus-induced obstructive hydrocephalus is a consequence of damage to the ependyma and chorid plexus.

Conversely, T3 reovirus disseminates via neural and hematogenous routes (12, 104, 109), infects CNS neurons, and causes lethal encephalitis (17, 110-112). Encephalitis is associated with neuronal apoptosis and an influx of inflammatory cells (111, 113). While damage is observed in the neurons directly, T3 antigen is not detected in the ependymal cells (17, 114).

Age restriction and immunity

Reovirus displays age-dependent pathology. Mice 8 days of age and younger die following infection with T3 reovirus, while mice 10 days of age and older survive (115) (Wu and Dermody, unpublished observations). Mice inoculated between 10 and 21 days of life display less severe patchy encephalitis in comparison to those inoculated on or before the eighth day of life (115). Intracranial inoculation with T1L results in lower titers in the brains of older animals relative to their younger counterparts (115). Mechanisms by which reovirus disease is restricted to the very young are not well understood.

However, it is possible that differences in receptor expression, immune system function, or both contribute to this phenomenon.

Immune system function contributes to protection against viral disease. Transfer of reovirus-immune adult splenocytes protects neonatal mice from T1-induced hydrocephalus. This protection is diminished if either $CD4^+$ or $CD8^+$ T cells are depleted. While reovirus-immune cells protect neonatal mice from T3D-induced encephalitis following intramuscular inoculation, these cells do not protect neonatal mice from T3D-induced encephalitis resulting from direct intracranial inoculation (116). T3-specific antibody 9BG5 decreases viral spread within the CNS but does not influence reovirus titers at sites of primary infection (117, 118). The addition of functional T cells and immunoglobulin benefits the host, and alternatively, the absence of these functional cells in otherwise healthy animals worsens disease. Adult severe combined immunodeficiency (SCID) mice, which lack functional Peyer's patches, B cells, and T cells, succumb to a lethal hepatitis. Transfer of reovirus-immune Peyer's patch cells can protect these animals (119). Taken together, these findings suggest that the developed immune system in adult mice contributes to resistance against reovirus-mediated disease.

Contribution of the S1 gene to serotype-specific disease

The viral S1 gene, which encodes σ1 and σ1s, determines serotype-dependent differences in CNS disease (17, 104, 110, 120), likely through differential engagement of cell-surface receptors. This phenomenon was

demonstrated using reassortant reoviruses 3HA1, comprised of 9 segments of strain T3D and a T1L S1 gene, and the reciprocal 1HA3 reassortant, containing a T3D S1 gene in an otherwise T1L genetic background. T1L and 3HA1 cause hydrocephalus but not encephalitis in mice, whereas T3D and 1HA3 result in a lethal encephalitis but not hydrocephalus (17, 114). T1L and 3HA1 bind to ependymal cells, while T3D reovirus and 1HA3 do not. T1L binds similarly to adult and neonatal ependymal cells (105), suggesting that age-mediated disease is not a consequence of altered receptor expression, at least by ependymal cells.

Reovirus attachment protein σ1

The σ1 protein, encoded by the S1 gene, serves as the reovirus attachment protein for all serotypes. It is a long, filamentous trimer that extends from the λ2 protein at the five-fold vertices of the virion icosahedron (121-123). The σ1 protein is partitioned into three structurally-distinct domains, an N-terminal α-helical coiled-coil tail, a central body formed from a triple β-spiral, and a C-terminal eight-stranded β-barrel head (9, 123, 124) (Figure I-3). The N-terminal tail inserts into the virion and the head projects away from the virion surface (121).

Reovirus receptors

T1 and T3 reovirus use immunoglobulin superfamily member JAM-A as a receptor (11, 125). JAM-A is expressed at tight junctions in polarized cells and on some leukocytes (126-129). The head domain of both T1 and T3 σ1 proteins

binds to JAM-A with high affinity using virtually identical binding surfaces (130) (Kirchner-Stettner and Stehle, unpublished) (Figure I-3). Studies using JAM-A-null mice indicate that JAM-A promotes hematogenous spread of reovirus (12). Expression of JAM-A in endothelial cells is required for hematogenous spread, while hematopoietic JAM-A is dispensable (Lai and Dermody, unpublished). JAM-A is not required for reovirus infection of the murine intestine and brain (12) and likely does not contribute to serotype-specific disease.

A second proteinaceous receptor for reovirus, NgR1, was identified using a genome-wide siRNA screen (15). This leucine rich-repeat protein (131-134) regulates axonal pasticity during development and prevents axonal regeneration in adults (135, 136). The NgR1 binding site on the reovirus virion has not been defined. However, reovirus virions, but not infectious subvirion particles (ISVPs), an assembly intermediate displaying an altered conformer of σ1 and loss of σ3, bind NgR1. This observation suggests that NgR1 binds a conformation-specific form of σ1, outer-capsid protein σ3, or perhaps both (15). The effect of NgR1 engagement on disease is not known. NgR1 mediates T3 reovirus infection of neurons *in vitro* (15); however, overexpression of NGR1 in CHO cells also permits T1L to infect these otherwise non-susceptible cells. Thus, the function of NgR1 in serotype-specificity is not clear but is an area of active exploration (Konopka-Anstadt and Dermody, unpublished).

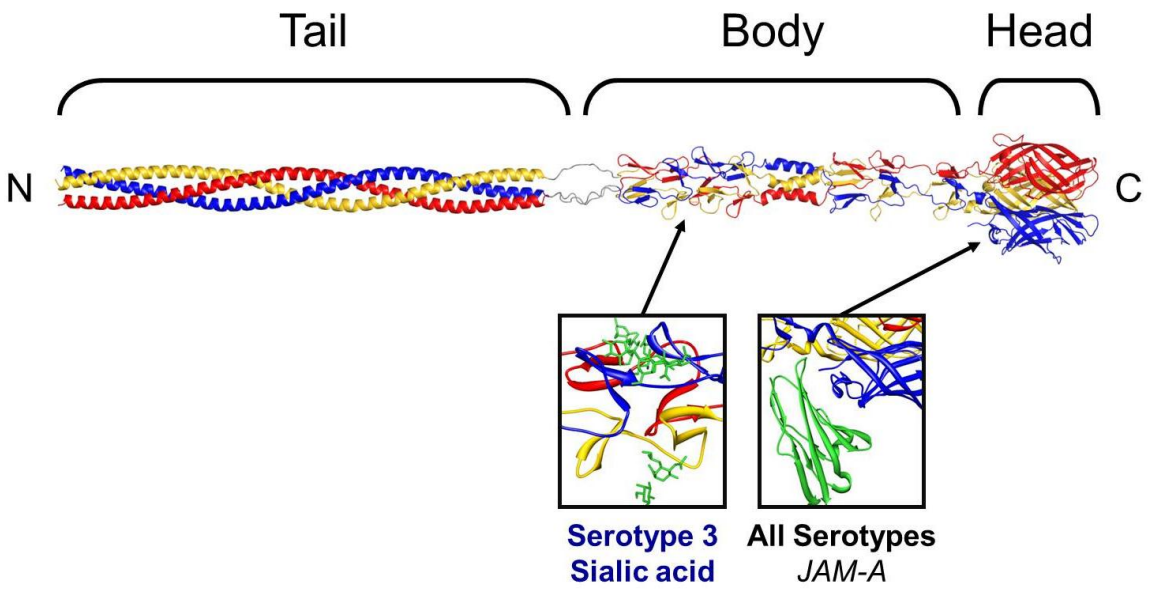

Figure I-3. Model of reovirus σ1 attachment protein. The σ1 attachment protein is depicted with experimentally determined structures shown in blue, red, and yellow, indicating the individual monomers comprising the trimeric protein; modeled regions are shown in gray. The tail, body, and head domains are indicated. The T1 and T3 JAM-A- binding site and T3 sialic-acid-binding site are indicated. Structures of these virus-receptor interactions are shown as insets. (Figure adapted from Chappell et al. 2002 (123), Reiter et al. 2011 (9), Reiss et al. 2012 (10), and Dietrich and Stehle, unpublished).

Serotype-dependent glycan binding by reovirus

Reoviruses were first appreciated to bind glycans through hemagglutination experiments conducted more than 50 years ago (137). Hemagglutination is a carbohydrate-dependent process, as treatment with sodium periodate diminishes hemagglutination capacity (137). T1 reovirus agglutinates erythrocytes of human and non-human primates, whereas T3 reovirus agglutinates erythrocytes from a variety of mammalian species. Interestingly, T1 reovirus agglutinates human erythrocytes more efficiently than does T3 reovirus. T3 binds to glycophorin on erythrocytes, whereas T1 reovirus does not (138). TheT3 σ1 sialic acid binding site is in the body domain (8, 9), while the T1 σ1 carbohydrate-binding site was thought to be beneath the head domain, as assessed by hemagglutination studies using chimeric σ1 molecules (8). Such differences in hemagglutination behavior suggest that T1 and T3 reovirus bind distinct glycans.

While the precise carbohydrate ligands of T3 reovirus σ1 are not known, the T3 σ1-sialic acid interaction is well characterized. T3 σ1 binds α2,3-, α2,6-, and α2,8-linked Neu5Ac using the loop connecting β-spirals two and three in the body domain(9). A bidentate salt bridge between the sialic acid carboxylate and Arg202 of T3 σ1 forms a key interaction between virus and glycan. This salt bridge is required for the interaction, as an arginine to tryptophan substitution at residue 202 abolishes sialic acid-binding capacity (9). Additionally, hydrogen bonds between the hydroxyl, acetyl, and glycerol groups of sialic acid and the backbone carbonyl groups of T3 σ1 strengthen the interaction.

Glycan binding capacity alters T3 reovirus disease. Binding of T3 reovirus to sialic acid enhances dissemination from the intestine to sites of secondary replication including the brain, heart, and liver. T3 reoviruses differing only in the capacity to engage sialic acid display marked differences in tissue tropism in mice (139). Strain $T3SA^+$ binds sialic acid, whereas $T3SA^-$ differs by a single residue in σ1 and cannot engage this carbohydrate (139). $T3SA^+$ infects and injures the bile duct epithelium, resulting in an oily hair syndrome, whereas isogenic strain $T3SA^-$ does not induce this damage (139). T3D binds sialylated glycans and replicates to higher titers in the murine spinal cord and brain compared with a mutant containing an arginine-to-tryptophan substitution at residue 202 in the σ1 body domain (140). While neuraminidase treatment had been shown to reduce T1L binding to rabbit Peyer's patch explants (141), the importance of glycan engagement in T1 reovirus pathogenesis had not been investigated prior to my thesis work.

Hypothesis

Given that reoviruses disseminate with serotype-specific tropism, engage the same known proteinaceous receptors, yet interact with distinct glycans, I hypothesized that T1 reovirus engages host cell glycans and that this binding influences tropism in the murine host.

Significance

Receptor utilization has broad implications for viral disease, often influencing host range and pathogenesis. The reovirus reverse genetics system and mouse model of disease make it a useful model to manipulate both the host and pathogen to elucidate mechanisms of viral attachment and evaluate the effects of receptor engagement on disease. This work sheds light on more general principles of virus-glycan interactions and the function of receptor engagement in tropism and pathogenesis. Furthermore, reovirus is being developed as a vaccine vector and oncolytic agent (142-144). Cancer cells display altered glycan profiles (145). Thus, understanding reovirus-glycan interactions may enhance design of reovirus vectors for therapeutic applications.

CHAPTER II

IDENTIFICATION OF A CARBOHYDRATE BOUND BY SEROTYPE 1 REOVIRUS σ1

Introduction

Reoviruses engage cell-surface carbohydrates as first demonstrated in hemagglutination studies (137). The molecular and biophysical basis of T3 reovirus-sialic acid binding as well as the function of sialic acid engagement in disease were well established prior to my thesis research (7-9, 24, 139, 140, 146). However, before beginning this project, the interaction of T1 reovirus with cell-surface carbohydrates was not understood. Differences in hemagglutination behavior between T1 and T3 reoviruses suggested that these serotypes differentially interact with cell-surface carbohydrates. Additionally, one study showed that neuraminidase treatment to remove cell-surface sialic acid diminishes the capacity of strain T1L to infect M cells on Peyer's patch explants (141). Taken together, these observations suggest that T1 reovirus engages different sialylated glycans than does T3 reovirus. However, specific host glycans bound by any mammalian reovirus had not been defined. I sought to identify a specific glycan bound by T1 reovirus. The establishment of a precise carbohydrate that interacts with T1 reovirus would facilitate studies of the biophysical basis of σ1-glycan interactions and enhance studies to evaluate the function of glycan binding in pathogenesis. Moreover, understanding how

reoviruses interact with cell-surface glycans could improve their efficacy as oncolytic therapeutics.

I worked with Kerstin Reiss in the laboratory of Dr. Thilo Stehle at the University of Tübingen, Germany and Yan Liu in the laboratory of Dr. Ten Feizi, Imperial College of London, United Kingdom to identify a specific glycan bound by T1 reovirus. Data presented in this chapter reflect that collaboration. Kerstin Reiss generated the σ1 protein used in the glycan array that was performed by Yan Liu shown in Figure II-5. I designed and conducted all infectivity and binding experiments shown in the other figures.

Results

Establishing a cell-culture system

T3 reovirus-sialic acid interactions were investigated using murine erythroleukemia (MEL) cells, which are susceptible only to sialic-acid binding strains of T3 reovirus, and L929 (L) cells, which are permissive to sialic acid-binding and non-binding strains (7, 9, 139, 147). MEL cells are not susceptible to infection by T1 reovirus. Therefore, studies of T1 σ1-glycan interactions were hindered by the lack of a suitable cell-culture system. To establish an *in vitro* setup in which glycans bound by reovirus could be identified and residues in T1 σ1 required for functional carbohydrate engagement could be discerned, I tested HeLa cells, L cells, and murine embryonic fibroblasts (MEFs) for the capacity to support reovirus infection in the presence and absence of *A*. *ureafaciens*

neuraminidase, a broad spectrum sialidase that cleaves α2,3-, α2,6-, α2,8-, and α2,9-linked sialic acid from the cell surface (148). As expected, neuraminidase treatment of L cells did not alter T1L infectivity (Figure II-1A) but diminished the capacity of T1L to infect both MEFs (Figure II-1B) and HeLa cells (Figure II-1C). This finding indicates that sialylated glycan engagement is required for optimal T1 reovirus infectivity in some cell types. Moving forward, I used L cells and MEFs as murine cell types that display glycan independent and dependent infectivity, respectively.

The disparity displayed by L cells and MEFs in the dependence of T1 reovirus infectivity on sialic acid binding is likely a consequence of differences in expression of proteinaceous receptor JAM-A. L cells, which are susceptible to T1 reovirus infection in the absence of sialic acid engagement, express higher levels of cell-surface JAM-A than do MEFs, which are most susceptible to sialic-acid binding strains (Figure II-2). T1L may infect MEFs using an adhesion strengthening mechanism, similar to that used by T3 reovirus to infect cells (7), in which binding to glycan precedes binding to the relatively low abundance JAM-A receptor.

Lectin-based glycan identification

Experiments using neuraminidase indicate that a sialic-acid-bearing glycan is required for optimal reovirus infectivity of MEFs. One previous study demonstrated that the plant lectin, *Maackia amurensis* lectin (MAL-II), which binds α2,3-linked sialic acid, blocks the capacity of T1L ISVPs to adhere to M

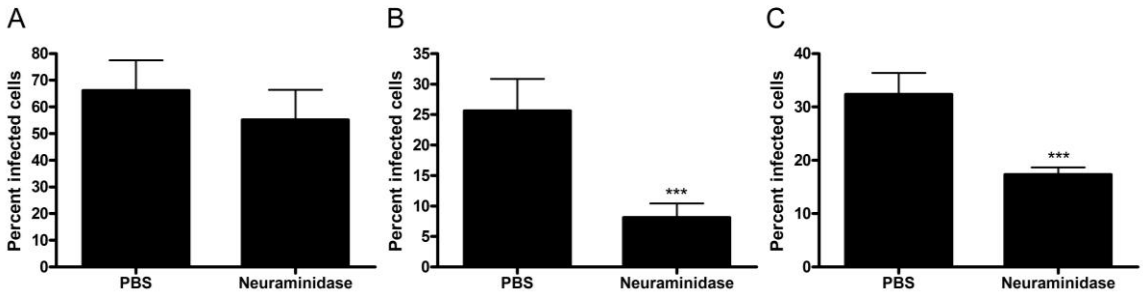

Figure II-1. The effect of neuraminidase treatment on T1L infectivity in various cell types. (**A**) L cells, (**B**) MEFs, or (**C**) HeLa cells were treated with *A. ureafaciens* neuraminidase for 1 h, followed by adsorption of T1L at MOIs of 10, 100, or 100 PFU/cell, respectively. Cells were washed twice with PBS, and fresh medium was added. After incubation at 37°C for 20 h, cells were fixed, and reovirus antigen was detected by indirect immunofluorescence. Nuclei were stained with DAPI. The percentage of infected cells in three fields of view per well was determined. The results are expressed as the mean percent infected cells per well in triplicate wells for two independent experiments. Error bars represent standard deviations. ***, $P < 0.001$, as determined by two-tailed Student's *t* test.

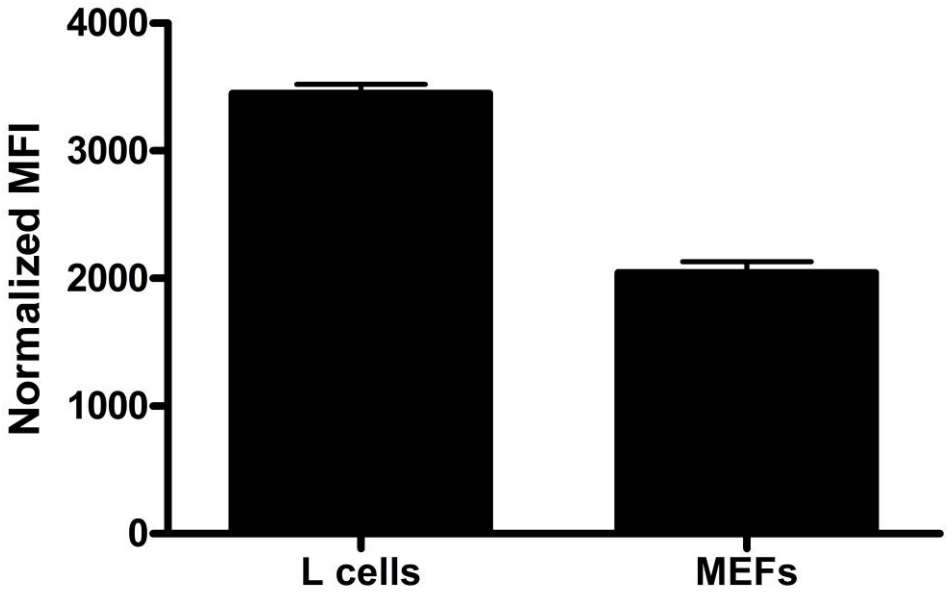

Figure II-2. JAM-A expression on L cells and MEFs. L cells or MEFs were stained with anti-JAM-A antibody followed by Alexa-488 labeled secondary antibody to assess cell-surface JAM-A expression. Fluorescence was detected by flow cytometry. Cells were gated on forward and side scatter, and the mean fluorescence intensity (MFI) of Alexa-488 was quantified. Results shown are from a representative experiment of three performed in duplicate.

cells on rabbit Peyer's patch explants (141). To determine the linkage-specificity of the sialylated glycan bound by T1 reovirus on the MEF cell surface, I tested the capacity of plant lectins to block T1L infectivity of MEFs. I employed α2,3-linked-sialic-acid-specific MAL-II and *Sambucus nigra* lectin (SNA), which binds α2,6-linked sialic acid and α2,3-linked sialic acid to a lesser degree. *Aleuria aurantia* lectin (AAL) binds α1,2-linked fucose and was used as a control. Incubation of MEFs with MAL-II or SNA decreased the infectivity of T1L relative to vehicle control, while AAL did not have an effect (Figure II-3). The lectins that blocked T1L infectivity of MEFs both interact with α2,3-linked sialic acids, suggesting that T1 reovirus interacts with α2,3-linked sialic-acid-bearing-glycans.

To complement this approach, I assessed the capacity of soluble 3' sialyllactose (3' SL), a simple molecule comprising a glucose bound to a galactose with an α2,3-linked sialic acid, to diminish T1 reovirus infectivity. Incubation of T1L with high doses of 3'SL had no effect on infectivity of MEFs (Figure II-4), suggesting that another glycan with an α2,3-linked sialic acid and not 3'SL is the functional receptor for T1 reovirus. Therefore, we needed to test a broader panel of candidate glycans to identify a functional binding partner for T1 σ1.

Glycan array screening

We used glycan array screening in collaboration with the Feizi and Stehle laboratories to identify precise glycans bound by T1 reovirus σ1. Two independent neoglycolipid arrays were used in this study. Sialylated glycans and

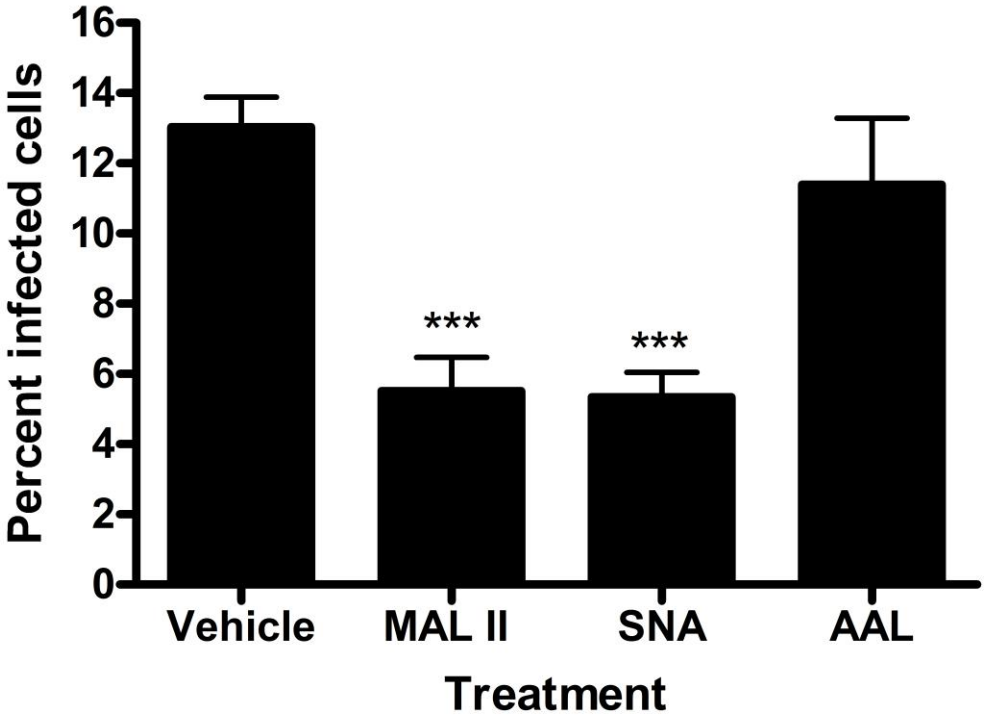

Figure II-3. The effect of soluble lectins on T1L infectivity in MEFs. T1L was pre-incubated with the lectins shown at a concentration of 10 μg/ml for 1 h prior to adsorption to MEFs at an MOI of 100 PFU/cell. Cells were washed twice with PBS, and fresh medium added. After incubation at 37^{o}C for 20 h, cells were fixed, and reovirus antigen was detected by indirect immunofluorescence. Nuclei were quantified by DAPI staining. The percent of infected cells in three fields of view per well was quantified. Results shown are from a representative experiment of 2 performed in triplicate wells. Error bars represent standard deviations. *** , $P < 0.001$, as determined by one-way ANOVA followed by a Bonferroni multiple-comparison post-test.

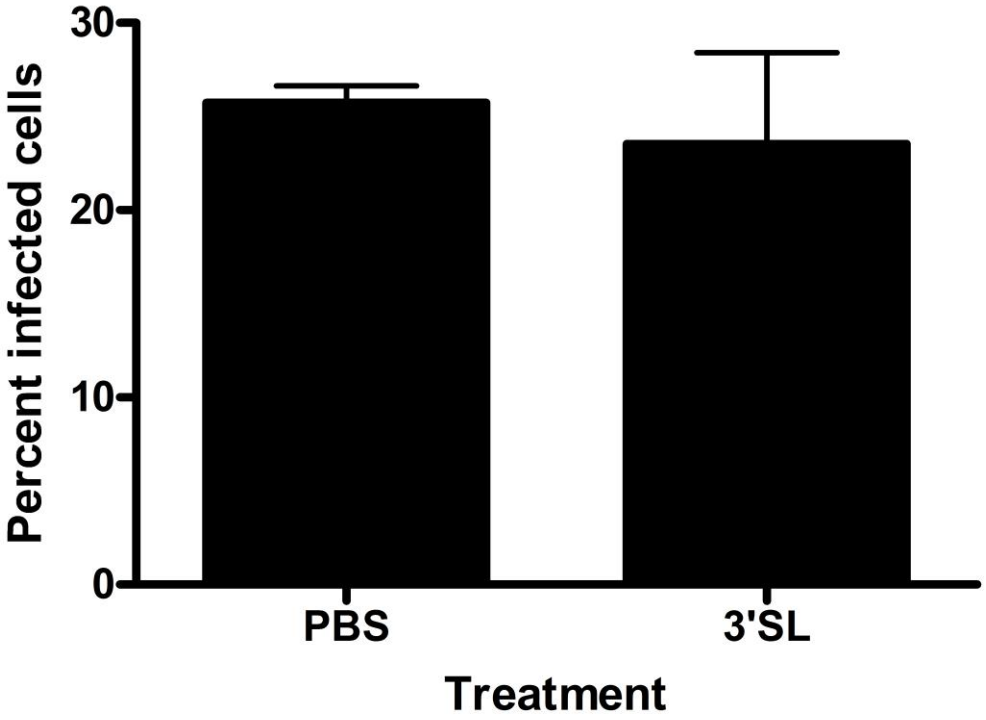

Figure II-4. The effect of soluble 3' sialyllactose on T1L infectivity in MEFs. T1L was incubated with 5 mM 3' sialyllactose for 1 h prior to adsorption to MEFs at an MOI of 100 PFU/cell. Cells were washed twice with PBS, and fresh medium was added. After incubation at 37^{o}C for 20 h, cells were fixed, and reovirus antigen was detected by indirect immunofluorescence. Nuclei were quantified by DAPI staining. The percent of infected cells in three fields of view per well was quantified. Results shown are from a representative experiment of two performed in triplicate wells. Error bars represent standard deviations. Differences are not significant as determined by two-tailed Student's *t* test.

non-sialylated control glycans were attached via lipid anchors to nitrocellulose membranes. His-tagged σ1 was adsorbed to these plates, and binding of σ1 to glycans was detected by immunofluorescence. Experiments using these arrays identified the GM2 glycan as a potential carbohydrate bound by T1 σ1. Related a-series gangliosides, GM3, GM1, and GD1a, yielded marginally detectable signals on the second glycan array performed for T1 σ1 (Figure II-5). Of note, T3 σ1 did not bind to GM2 on glycan arrays done in parallel (Liu and Feizi, unpublished). The GM2 glycan contains two terminal sugar moieties, an N-acetylgalactosamine (GalNAc) and a neuraminic acid (Neu5Ac), which are both bound to a central galactose via β1,4 and α2,3 linkages, respectively. This galactose is connected through a β1,4 linkage to a glucose molecule. In the full ganglioside, the glucose is connected to a ceramide tail that anchors the ganglioside in the lipid membrane. In the glycan form, only the sugar moieties, and not the ceramide, are present. Binding of T1 σ1 protein to the GM2 glycan was confirmed using NMR spectroscopy, which demonstrated that the Neu5Ac and GalNAc moieties interact with T1 σ1 in solution (10). I chose to use the GM2 glycan as opposed to the ganglioside for published experiments as the same glycan preparations were employed by our collaborators in the Stehle lab for crystallography studies. Moreover, the glycan is soluble in PBS, which is used as a common vehicle for reovirus infection experiments, whereas the ganglioside must be suspended in DMSO, which can be toxic at higher doses. Thus, use of the glycan allowed me to work with a larger range of concentrations.

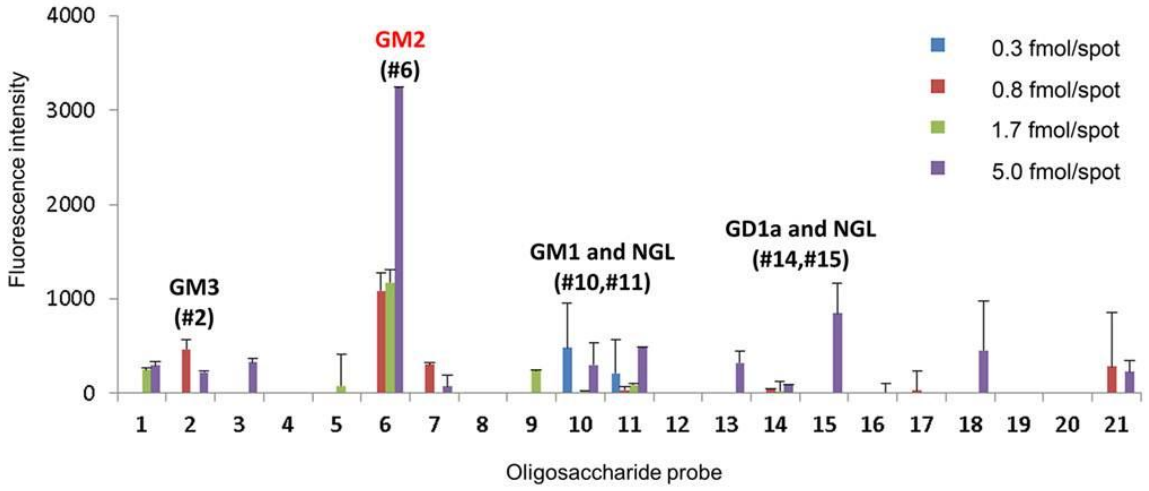

Figure II-5. Glycan array identification of GM2 as a candidate receptor. Glycan microarray analysis of recombinant T1L σ1 using 21 lipid-linked oligosaccharide probes. Each oligosaccharide probe was arrayed at four concentrations (as indicated) in duplicate. Numerical scores of the binding signals are means of duplicate spots (with error bars). A second array comprised of 124 lipid-linked oligosaccharide probes identified solely the GM2 glycan but had a higher signal-noise ratio.

Functional analysis of glycan array results

To determine whether GM2 is a functional receptor for T1 reovirus, I tested soluble GM2 for the capacity to inhibit infection of MEFs. Incubation of T1L with GM2 glycan diminished the infectivity of T1L in a dose-dependent manner (Figure II-6A). Related glycan GM3 blocked infectivity to a lesser degree and not in a dose-dependent fashion (Figure II-6B). To evaluate the serotype-specificity of GM2 as a reovirus receptor, I incubated T3D with soluble GM2 and quantified infectivity. Interestingly, soluble GM2 had no effect on the capacity of T3 reovirus to infect MEFs (Figure II-6C), suggesting that reovirus binding to this glycan is serotype-specific.

To establish whether soluble GM2 diminished T1L infectivity in MEFs due to a block in attachment, T1L was preincubated with soluble GM2, GM3, or GM1 glycans or the PBS vehicle control prior to adsorption at 4°C to prevent internalization. Binding was assessed using flow cytometry. The GM2 glycan decreased the capacity of T1L to adhere to MEFs, GM3 inhibited binding to a lesser degree, and GM1 had no effect (Figure II-7), suggesting that T1 reovirus directly binds to glycans on the cell surface.

Discussion

Prior to the initiation of these studies, hemagglutination experiments demonstrated that the reovirus-mediated agglutination of erythrocytes is

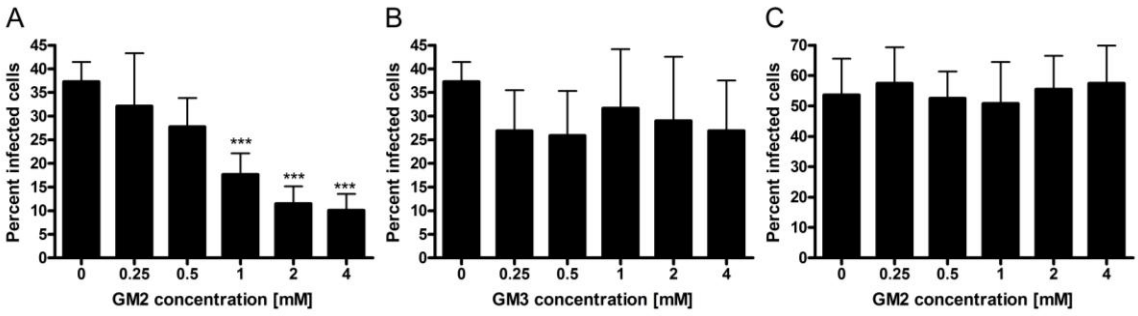

Figure II-6. The effect of soluble glycans on T1L infectivity in MEFs. (**A,B**) T1L or (**C**) T3D (10^7 PFU/well) was incubated with the GM2 (**A,C**) or GM3 (**B**) glycans at the concentrations shown for 1 h prior to adsorption to MEFs at an MOI of 100 PFU/cell. Cells were washed twice with PBS, and fresh medium was added. After incubation at 37°C for 20 h, cells were fixed, and reovirus antigen was detected by indirect immunofluorescence. Nuclei were quantified by DAPI staining. The results are expressed as the mean percent infected cells per field in triplicate wells for two independent experiments. Error bars represent standard deviations. ***, $P < 0.001$, as determined by one-way ANOVA followed by a Bonferroni multiple-comparison post-test.

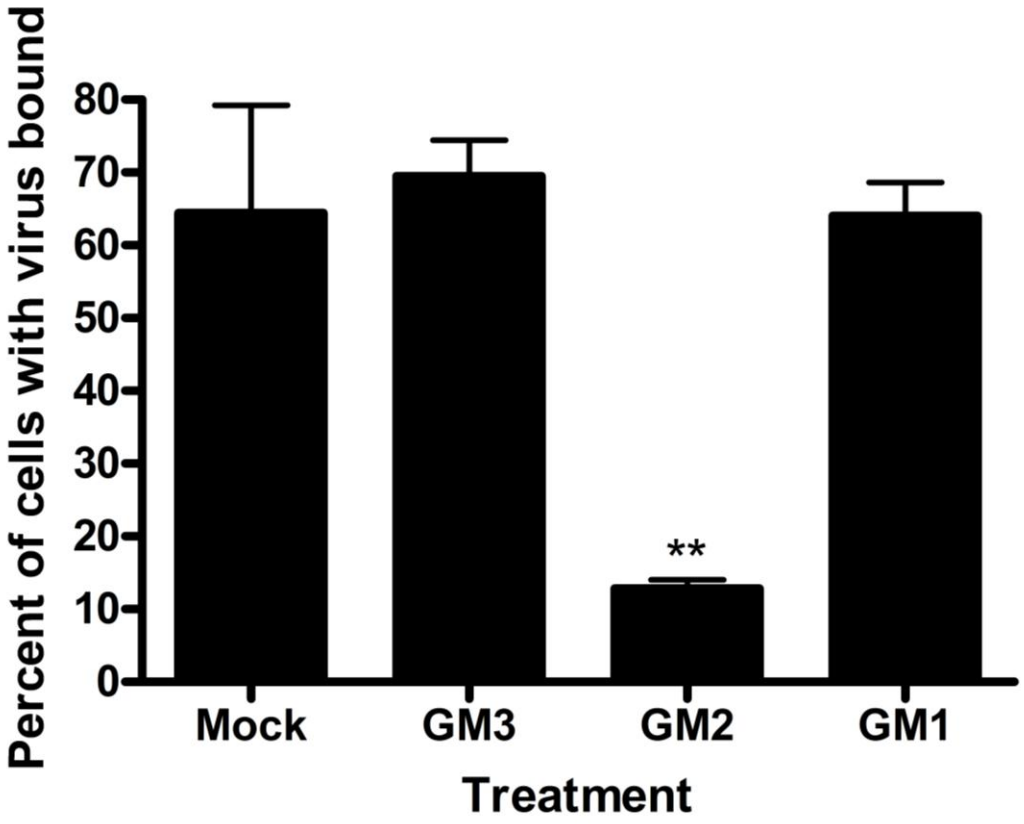

Figure II-7. The effect of soluble glycans on T1L attachment to MEFs. T1L virions were incubated with 2 mM of GM1, GM2, or GM3 at room temperature for 1 h prior to adsorption to MEFs at an MOI of 2 x 10^5 particles/cell. After incubation at 4^{o}C for 1 h, cells were washed twice with PBS, and binding was assessed by flow cytometry. The results shown are from a representative experiment of two performed in duplicate. **, $P < 0.01$, as determined by one-way ANOVA followed by a Bonferroni multiple-comparison post-test.

carbohydrate-dependent (137). Moreover, reovirus displays serotype-dependent hemagglutination profiles, suggesting that T1 and T3 reoviruses bind distinct glycans (8). T3 reovirus was known to bind α2,3-, α2,6-, and α2,8-linked sialic acid (9). However, lectins recognizing α2,3-linked sialic acid were shown to block T1L attachment to Peyer's patch explants (141), indicating that T1 also may engage carbohydrates containing α2,3-linked sialic acid.

Studies of virus-sialic acid interactions are slowly revealing that the interaction between a virus and a sialylated receptor may be more complex than the linkage-basis of the sialic acid alone. For example, human influenza viruses have long been appreciated to preferentially engage α2,6-linked sialic acid. One glycan array study investigating sialylated receptor binding by seasonal H3N2 influenza virus strains that circulated between 1968 and 2012 demonstrated that there was variation in the binding preferences on an annual basis. Of note, there was not a single sialylated carbohydrate present on the array that bound every yearly strain (53). These findings indicate that linkage-specificity is not the sole determinant of virus-sialic acid engagement.

In the experiments described in this chapter, glycan array screening identified the GM2 glycan as a candidate receptor for reovirus (Figure II-5). GM2 contains an α2,3-linked sialic acid; therefore, this finding is in line with additional observations that sialic acid binding is required for optimal T1L infectivity in MEFs (Figure II-1) and that lectins recognizing α2,3-linked sialic acid inhibit reovirus infection in MEFs (Figure II-3). Soluble GM2 inhibited the capacity of T1 to infect MEFs (Figure II-6A). However, the GM3 glycan (Figure II-6B), also known as

3’SL (Figure II-4), does not block T1L infectivity of MEFs. While T3 reovirus was known to interact with α2,3-linked sialic acid, specifically, 3’SL or the GM3 glycan (9), soluble GM2 did not diminish T3 infectivity of MEFs (Figure II-6C). Moreover, parallel glycan array screening revealed that T3 reovirus σ1 interacted with a-series gangliosides GM3, GM1, and GD1a, but no binding was detected to GM2 (Reiter, Stehle, Liu, and Feizi, unpublished observations). Taken together, these experiments demonstrate that the GM2 glycan is a biologically relevant entry mediator for T1 but not T3 reovirus in MEFs.

T1L attachment to cells was inhibited by the GM2 glycan (Figure II-7), suggesting that the block to infectivity results from diminished binding of the virus to the cell-surface. While the GM1 glycan had no effect on attachment, soluble GM3 diminished binding, albeit to a lesser degree than did GM2. The GM3 glycan serves as the precursor for GM2 and lacks the GalNAc moiety on that glycan but is otherwise identical. As GM2 blocks binding and infectivity, while GM3 diminishes binding only, we thought it likely that the T1 σ1 protein interacts with sialic acid and the GalNAc moiety to enhance specificity. This hypothesis was confirmed in structural studies presented in Chapter 3.

Reovirus is being evaluated in clinical trials as an oncolytic adjunct to conventional cancer therapy. Ganglioside expression, including GM2, is altered in many cancer cells compared with their untransformed counterparts (149) . Moreover, humanized anti-GM2 antibodies protect mice with small-cell lung cancer from metastases (150). It is possible that ganglioside overexpression in cancer cells alters susceptibility to reovirus infection. Thus, understanding the

precise ligands bound by reovirus could improve oncolytic vector targeting to certain tumors.

CHAPTER III

DEFINING RESIDUES REQUIRED FOR FUNCTIONAL T1 σ1-GM2 BINDING

Introduction

The identification of residues required for viral receptor binding enhances an understanding of the molecular basis of the virus-glycan interaction and facilitates *in vivo* studies to investigate the function of receptor-engagement in viral pathogenesis. While residues in the body domain of T3 reovirus σ1 required for sialic acid binding had been defined (8, 9, 24), sequences required for T1 σ1-glycan interactions were not known. Studies using reovirus σ1 protein expressed in insect cells using baculovirus vectors defined a region in the neck domain required for agglutination of human red blood cells. Additionally, purified T1 σ1 constructs lacking the head domain also are incapable of hemagglutination (8). These findings suggest that residues in the head and neck regions of T1 σ1 are required for glycan binding.

Several approaches can be used to successfully identify residues required for receptor binding, including alanine scanning mutagenesis, sequencing of field isolates differing in receptor engagement, and structure-guided mutagenesis. Investigators studying T3 reovirus-sialic-acid interactions capitalized on the existence of clinical isolates that differ in the requirement for sialic acid utilization to infect cells. T3 strains that do not bind sialic acid were serially passaged in MEL cells, which are susceptible to infection only by sialic-acid-binding T3 reovirus strains. Sequencing the resultant MEL cell-adapted strains revealed that

specific residues within the T3 σ1 body domain are required for functional glycan engagement (7, 24). The importance of these residues in T3 σ1-sialic acid binding was confirmed using crystallography and site-directed mutagenesis (9).

Advances in crystallography along with results from glycan array screening catalyzed studies conducted in parallel in the Stehle laboratory to determine the structure of T1 σ1 in complex with GM2. The success of the structural work, coupled with development of reverse genetics for reovirus (41, 42, 151), made structure-guided mutagenesis the most efficient approach for me to use to define residues in T1 σ1 required for functional GM2 binding. I sought to engineer mutant viruses that might be altered in engagement of the GM2 glycan. The finding that T1L requires interactions with sialylated glycans to efficiently infect MEFs but not L cells (Figure II-1) provided a cell-culture system in which I could evaluate T1 σ1-glycan engagement. I set out to engineer mutant viruses that displayed impaired hemagglutination capacity and infectivity in MEFs relative to T1L but infected L cells comparably to wildtype virus. Mutant viruses showing defects in replication assays using L cells would suggest alterations in overall viral fitness, most likely as a consequence of mutation-induced gross misfolding of the σ1 protein. Viruses capable of infecting L cells, yet impaired in GM2 engagement, would yield the most interpretable results *in vitro* and later *in vivo*.

To understand the molecular basis of T1 reovirus σ1-glycan interactions, I collaborated with graduate student Kerstin Reiss who was completing her Ph.D. training with Thilo Stehle at the University of Tübingen, Germany. Kerstin was interested in the structural basis of reovirus-receptor interactions. She generated

the crystallography figures shown in this chapter (Figures III-1-4). Together, Kerstin and I rationalized the structure-guided mutant design (Tables III-1 and III-2). Bärbel Blaum, a postdoctoral fellow in the Stehle laboratory, generated the NMR data shown in Figure III-13 after we collaboratively planned the experiment. I rescued the viruses using reverse genetics, generated virus stocks, and designed and conducted the infectivity, binding, and hemagglutination experiments shown in the other figures.

Results

Structure of the T1 σ1-GM2 complex

Recombinant hexahistidine-tagged T1L σ1 protein constructs were expressed in *E. coli* and purified for use in X-ray crystallography studies to identify the T1 σ1 glycan-binding site. Two constructs, $\sigma1_{long}$ and $\sigma1_{short}$, were designed using sequence alignment with T3D σ1, for which several crystal structures exist (9, 123, 152, 153). The first construct, $\sigma1_{long}$, comprised amino acids 261-470, which were predicted to fold into three β-spiral repeats and the C-terminal head domain. The second construct, $\sigma1_{short}$, comprised amino acids 300-470, which were predicted to form only the most C-terminal β-spiral and the head domain. Both σ1 constructs included the predicted carbohydrate-binding site (8). Crystals of $\sigma1_{short}$ and $\sigma1_{long}$ were formed using the single-drop-vapor-diffusion method. Once formed, crystals of $\sigma1_{long}$ were soaked in solution with GM2 to allow the glycan to bind. This approach yielded a 3.6 Å crystal structure of the T1 σ1-GM2 complex. The crystal structure of this complex was solved by molecular

replacement using a 2.6 Å crystal structure of His-tagged $\sigma1_{short}$ as a reference model during refinement.

The structure of the T1 σ1-GM2 complex revealed that the glycan-binding site is located within the head domain of σ1 (Figure III-1). All three monomers comprising the trimeric σ1 protein engage GM2 in an identical manner. Both the sialic acid (Neu5Ac) and GalNAc moieties of GM2 contact σ1 with the functional groups of sialic acid directly interacting with the protein. The carboxyl group of Neu5Ac forms a hydrogen bond with the side chain of Gln371, and the N-acetyl nitrogen and glycerol chain form hydrogen bonds with σ1 backbone residues. A methyl group of the N-acetyl side chain of sialic acid fits within a hydrophobic pocket flanked by Val354, Phe369, and Met372. While the majority of σ1 contacts are with sialic acid, the GalNAc enhances binding through Van der Waals interactions and likely contributes to the specificity of T1 σ1 for GM2 (Figure III-2). The finding that the majority of interactions between T1 σ1 and GM2 involve backbone elements and not side chains of the viral attachment protein is unprecendented in studies of virus-glycan binding (27) and necessitated confirmation using structure-guided mutagenesis to be certain that the binding site identified crystallographically was biologically relevant.

The T1 glycan-binding site is in a region of σ1 distinct from the binding sites of other known reovirus receptors (Figure III-3A). While JAM-A also binds the σ1 head domain (152) (Kirchner-Stettner and Stehle, unpublished), the binding sites for JAM-A and GM2 do not overlap (Figure III-3B). Moreover, analysis of the crystal structures of T1 σ1 in complex with GM2 and T3 σ1 in

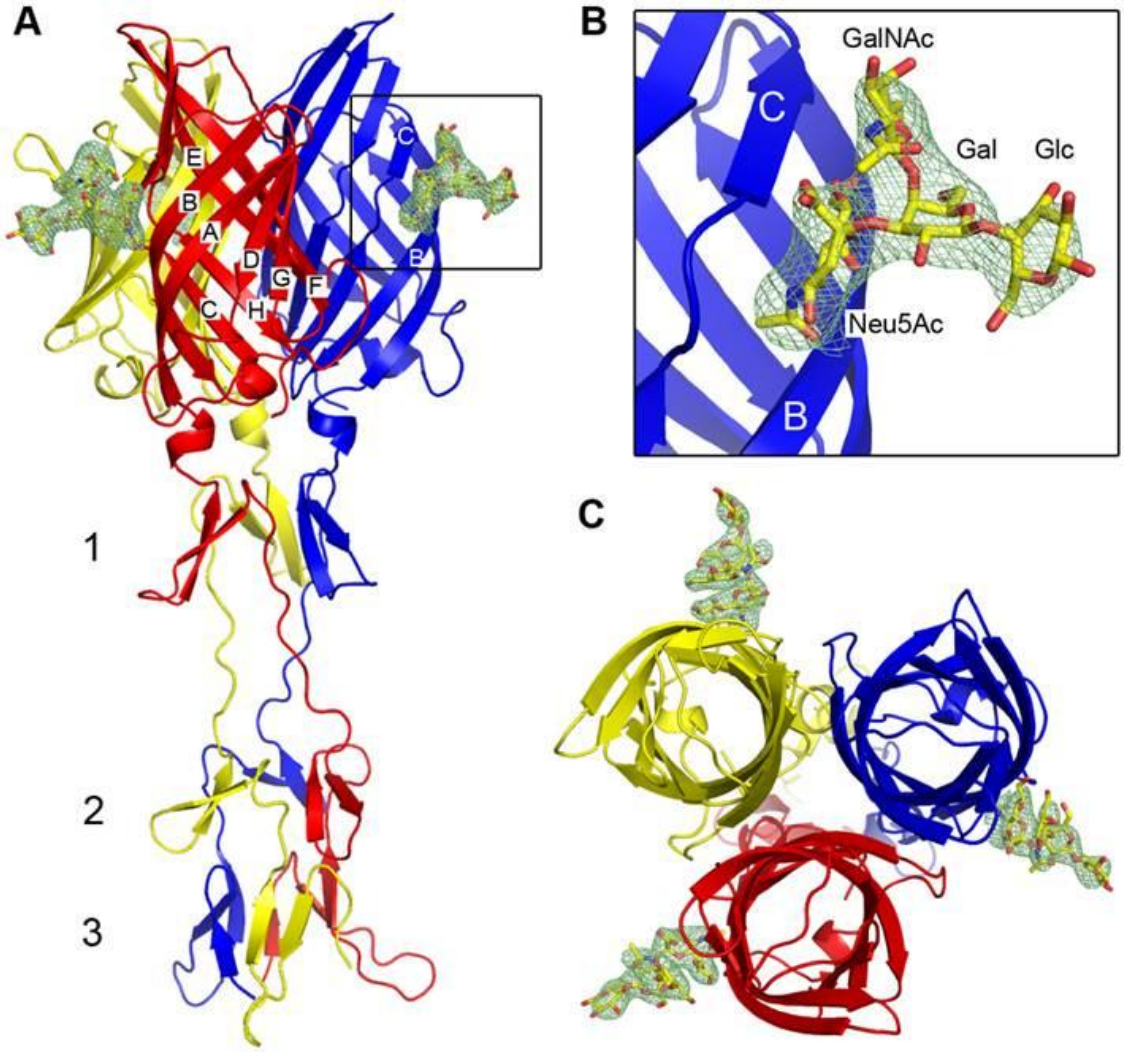

Figure III-1. Crystal structure of T1L σ1 in complex with the GM2 glycan. Ribbon tracing of the complex viewed from the side (**A**) with a close-up of the carbohydrate-binding site (**B**) and top-view of the complex (**C**). The three T1L σ1 monomers are depicted in blue, red, and yellow. β-spiral repeats 1, 2, and 3 and β-strands A-H are labeled. The GM2 oligosaccharide is shown in stick representation, with carbons, oxygens, and nitrogens colored yellow, red, and blue, respectively.

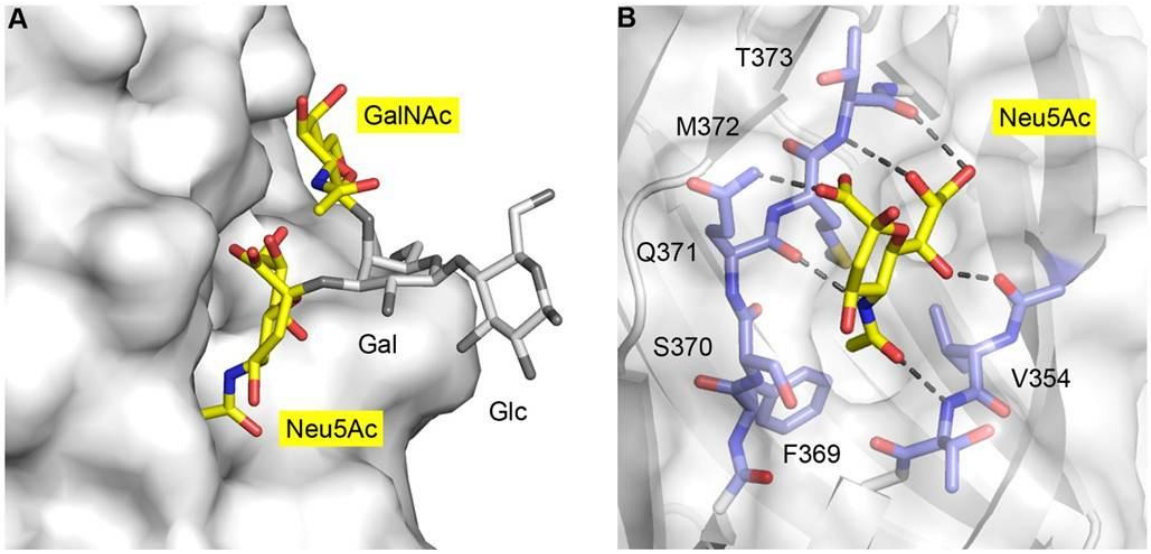

Figure III-2. The carbohydrate-binding site of T1L σ1. (**A**) Surface representation of T1L σ1 shown in light gray. The GM2 glycan is depicted in stick representation with the two terminal sugars, Neu5Ac and GalNAc, that contact T1L σ1 shown in color, and the Gal and Glc residues shown in gray. (**B**) Close-up view of the Neu5Ac-binding pocket, with contacting residues shown in stick representation in blue (carbons) and the protein surface shown in light gray. Neu5Ac is depicted in stick representation and colored as in Figure 1. Hydrogen bonds between T1L σ1 and Neu5Ac are represented with black dashes. The methyl group of the *N*-acetyl chain of Neu5Ac inserts into a hydrophobic pocket formed by residues Val354, Phe369, and Met372.

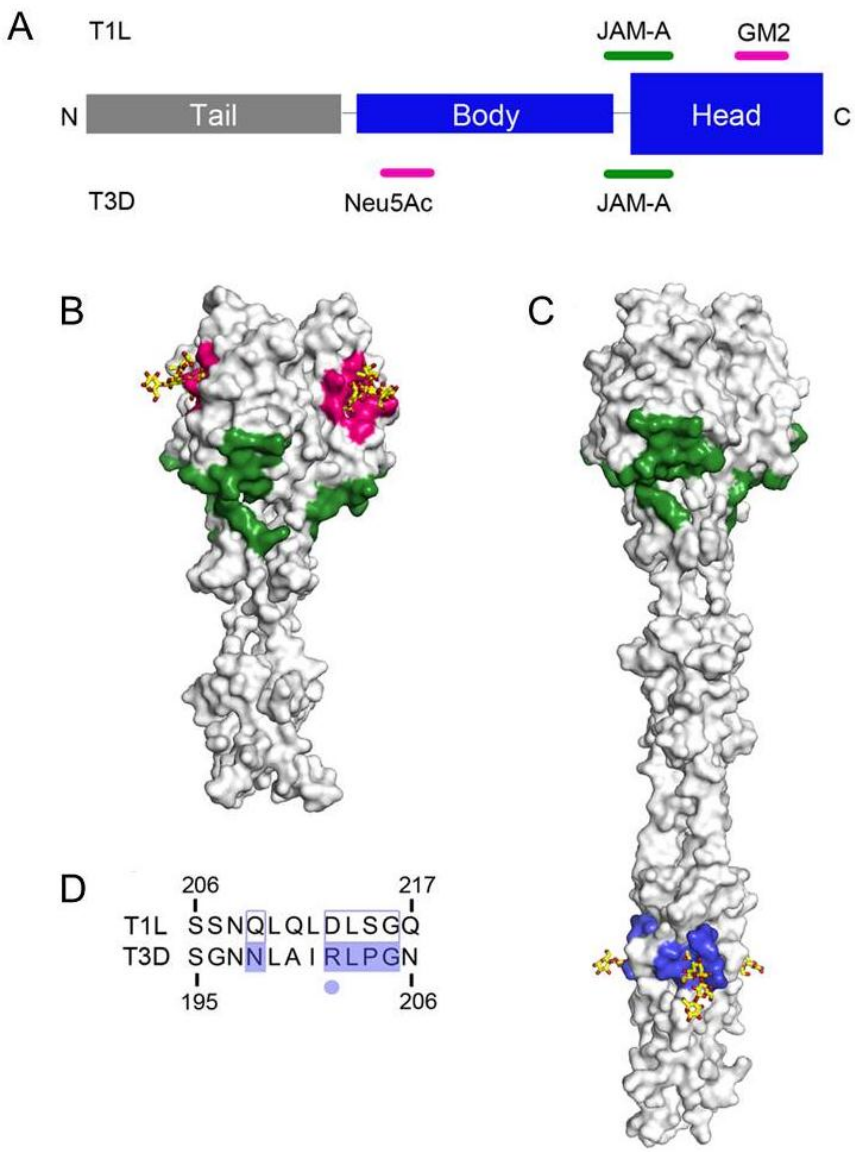

Figure III-3. Comparison of the σ1-receptor binding sites. (**A**) Schematic representation of σ1 domain organization. Binding sites in T1L and T3D σ1 for JAM-A and carbohydrate are depicted in green and pink, respectively. Surface representations of (**B**) T1L σ1 in complex with the GM2 glycan (PDB accession code 4GU3) and (**C**) T3D σ1 in complex with the GM3 glycan (also known as 3' sialyllactose) (PDB accession code 3S6X). The carbohydrates are shown in stick representation and colored as in Figure 1. The JAM-A-binding sites are highlighted in green, and the carbohydrate-binding sites in T1L and T3D σ1 are depicted in pink and purple, respectively. (**D**) Sequence alignment of the T3 carbohydrate-binding site in T1L and T3D σ1. Residues required for carbohydrate engagement in T3D σ1 are highlighted in blue. Residue Arg202, which forms a central interaction with Neu5Ac in T3D σ1, is marked with a blue dot.

complex with 3'SL, also known as the GM3 glycan, sheds light on the serotype specificity of reovirus carbohydrate-interactions, as both serotypes bind distinct glycans using different regions of the attachment protein. T3 σ1 binds sialic acid (9) using sequences within the body domain (Figure III-3C). While the T1 σ1 construct used in the Stehle lab crystallography studies did not include this region (Figure III-3B), sequence analysis suggests that the region of T1 σ1 corresponding to the T3 glycan-binding site could not bind sialic acid, as T1 σ1 lacks a key arginine residue required for the interaction (Figure III-3D). Alignment of the T1 and T3 σ1 structures suggests that the region in the T3 σ1 head domain corresponding to the T1 σ1 GM2-binding site could not bind GM2 due to steric hindrance (Figure III-4), thereby confirming results obtained using soluble GM2 to inhibit reovirus infection (Figure II-6A). These findings also provide a framework to engineer mutants with alterations in the T1 σ1 glycan-binding site.

Single-residue mutant design

Kerstin and I worked together to rationalize mutations in T1 σ1 that would disrupt the σ1-GM2 complex. Since single point mutations ablate the binding of T3 σ1 to sialic acid (7, 9, 24, 154), we designed a panel of T1 viruses that differed from wildtype by a single residue within the putative glycan-binding domain (Table III-1). Residues Val354, Ser370, Gln371, and Met372 were selected for mutational analysis as a consequence of their proximity to the T1 σ1 GM2-binding site. Val354 was replaced with phenylalanine and leucine residues

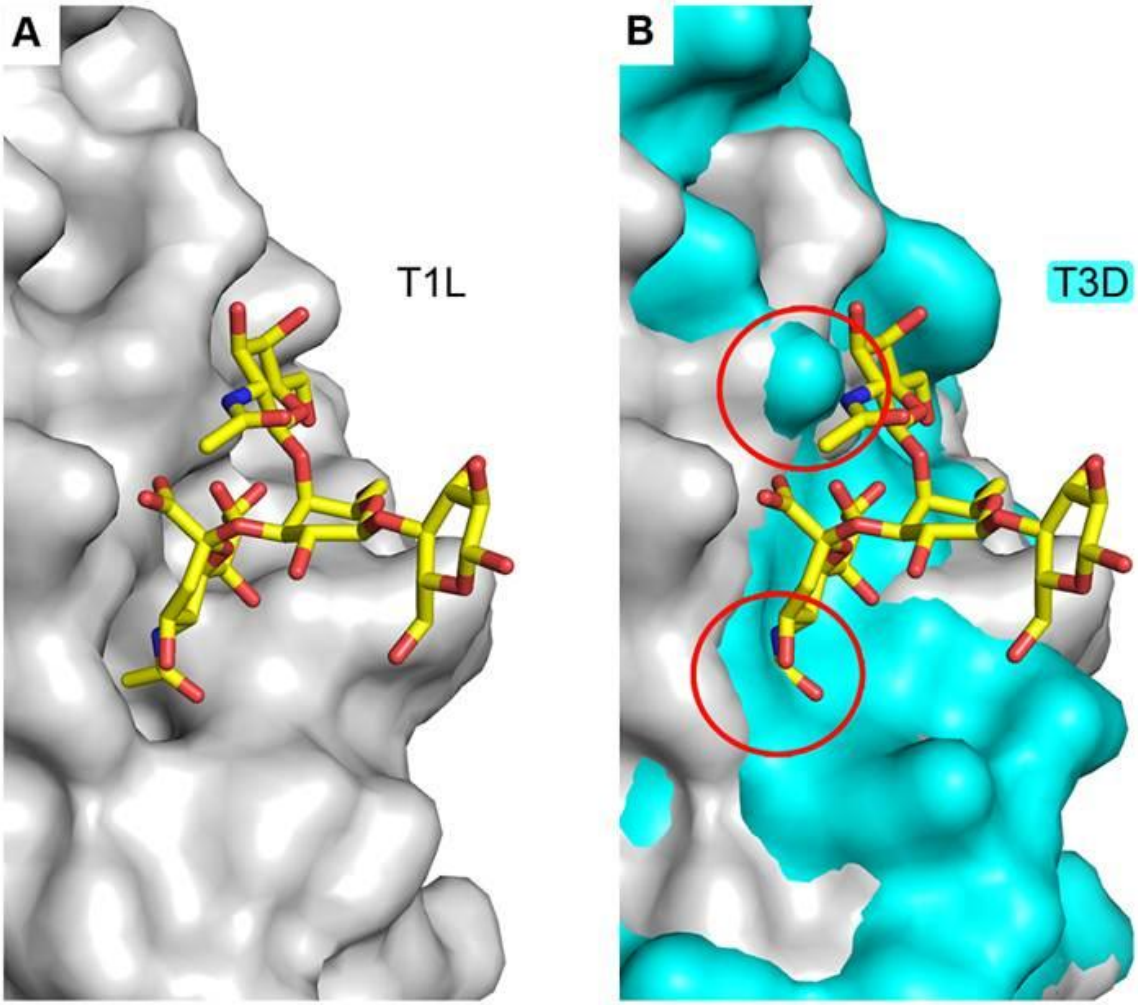

Figure III-4. The head domain of T3D σ1 does not bind Neu5Ac. (**A**) Surface representation of T1L σ1 depicted in gray. (**B**) Superposition of T1L (gray) and T3D (cyan) σ1. The GM2 glycan is shown in stick representation (colored as in Figure 2) in both panels. Clashes between the carbohydrate and T3D σ1 are highlighted with red circles in panel B. Both the Neu5Ac and GalNAc moieties of the GM2 glycan would clash with T3D σ1 residues.

T1L residue	Position	Mutation
V	354	F
V	354	L
S	370	P
Q	371	A
Q	371	E
M	372	F
M	372	L

Table III-1. Single-residue T1 σ1 mutant viruses. The position of the T1L residues (red) altered in the panel of single point mutants is shown. Some mutants contain residues found in the corresponding site in T3D (blue) and others represent changes (black) predicted to block GM2 binding.

that we hypothesized would block the sialic-acid-binding pocket through steric hindrance. The S370P, Q371A, and M372F mutants were engineered to replace the T1 σ1 residue with the corresponding residue in T3 σ1. The M372L substitution is a more conservative mutation than M372F and might not disrupt folding of the σ1 head. Point mutant Q371E was designed with an acidic residue to introduce a negative charge, which was predicted to repel the negatively charged sialic acid.

Characterization of the σ1 point mutants

I sought to identify T1 σ1 mutants that displayed impaired hemagglutination capacity and infectivity in MEFs. However, such alterations might be attributable to some unrelated defect in viral fitness other than diminished glycan binding. To eliminate the former possibility, I quantified viral replication in L cells, which do not require functional GM2 binding for infectivity and evaluated the capacity of a conformation-specific monoclonal antibody to block infection. L cells were adsorbed with wildtype or mutant viruses, and viral yields were quantified by plaque assay 24, 48, and 72 hours post-inoculation. Mutants V354L, S370P, Q371E, M372F, and M372L replicated similarly to wildtype virus in L cells, while V354F and Q371A showed a slight, albeit insignificant, impairment at 24 hours (Figure III-5). To establish whether the mutant σ1 proteins are properly folded, I tested T1 σ1 conformation-specific monoclonal antibody 5C6 for the capacity to neutralize infection by wildtype and mutant viruses in L cells. Escape mutants for this antibody display sequences

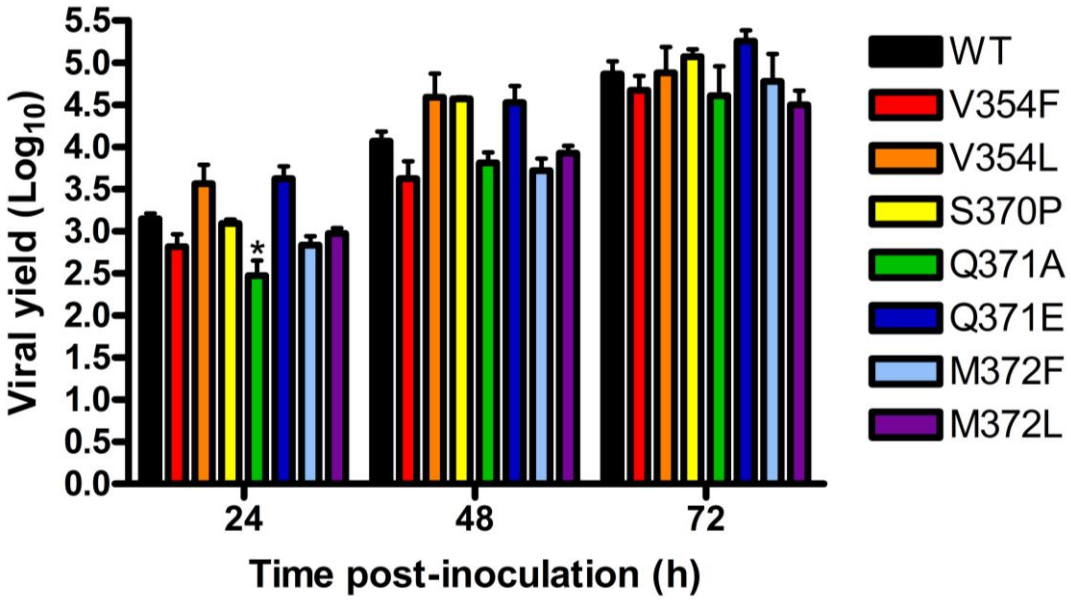

Figure III-5. Replication of the single-residue T1 σ1 mutant viruses in L cells. L cells were adsorbed with the strains shown at an MOI of 0.1 PFU/cell at room temperature for 1 h. Cells were washed with PBS, and fresh medium was added. Cells were frozen at 0, 24, 48, and 72 h post-adsorption, and viral titer was quantified by plaque assay. Results are expressed as the mean $\log_{10}$ viral yield from a representative experiment of two independent experiments, each performed in triplicate. Error bars represent standard deviation. *, $P < 0.05$, as determined by two-way ANOVA followed by Bonferroni's multiple comparison test.

changes at Gln417 and Gly447 in T1 σ1 (155). These residues are located on the upper portion of the T1 σ1 head domain, near the intersubunit interface and distinct from the glycan-binding site (Figure III-6A). 5C6 is a conformation-specific monoclonal antibody that likely binds a trimeric form of the T1 σ1 head domain. Recognition and neutralization by 5C6 indicates the presence of properly folded and assembled trimeric T1 σ1 head. Preincubation with mAb 5C6 diminished the capacity of wildtype and all mutant viruses to infect L cells (Figure III-6B), suggesting that the head domain of the mutants is properly folded.

To test whether these mutant viruses have an altered capacity to infect cells that are maximally susceptible to glycan-binding reovirus strains, I quantified infectivity using MEFs. MEFs were inoculated with wildtype and mutant viruses at an MOI of 1 FFU/cell as determined in assays using L cells. The V354F, S370P, Q371A, and Q371E mutants displayed a significant defect in infectivity in MEFs, suggesting that these residues influence glycan engagement. Infectivity of the V354L, M372F, and M372L mutants did not differ statistically from that of wildtype virus (Figure III-7). I also used hemagglutination assays as a proxy for glycan binding (137) and found that all of the mutants had a defect in the capacity to agglutinate human erythrocytes, with V354F, V354L, S370P, Q371A, and Q371E showing the greatest impairment (Figure III-8). However, hemagglutination capacity by these mutants is diminished but not ablated, as is the case for T3 mutants defective in glycan binding (9). This observation raises the possibility that the T1 σ1 single-residue mutants may retain glycan-binding

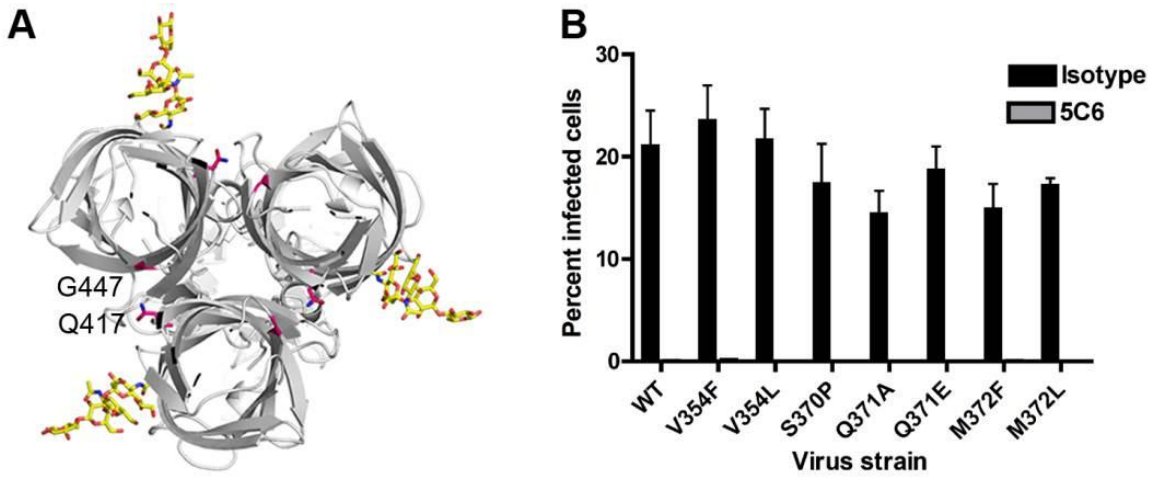

Figure III-6. Single-residue T1 σ1 mutant viruses are neutralized by mAb 5C6. (**A**) Top-view of T1L σ1 (gray) in complex with the GM2 glycan (yellow). Residues Gln417 and Gly447 (Helander and Nibert REF), which are altered in mAb 5C6-resistant mutants and likely form part of the 5C6 epitope, are shown in stick representation in pink. (**B**) Wildtype and mutant viruses were incubated with conformation-specific T1L σ1-specific mAb 5C6 at room temperature for 1 h, and the virus-antibody mixture was adsorbed to L cells at room temperature for 1 h. Cells were washed twice with PBS, and fresh medium was added. After incubation at 37°C for 20 h, cells were fixed, and reovirus antigen was detected by indirect immunofluorescence. Nuclei were stained with DAPI. The percentage of infected cells in three fields of view per well was determined. Results are expressed as the mean infectivity per well from three independent experiments, each performed in triplicate. Error bars represent standard error of the mean. ***, $P < 0.001$, as determined by two-way ANOVA followed by Bonferroni's multiple comparison test.

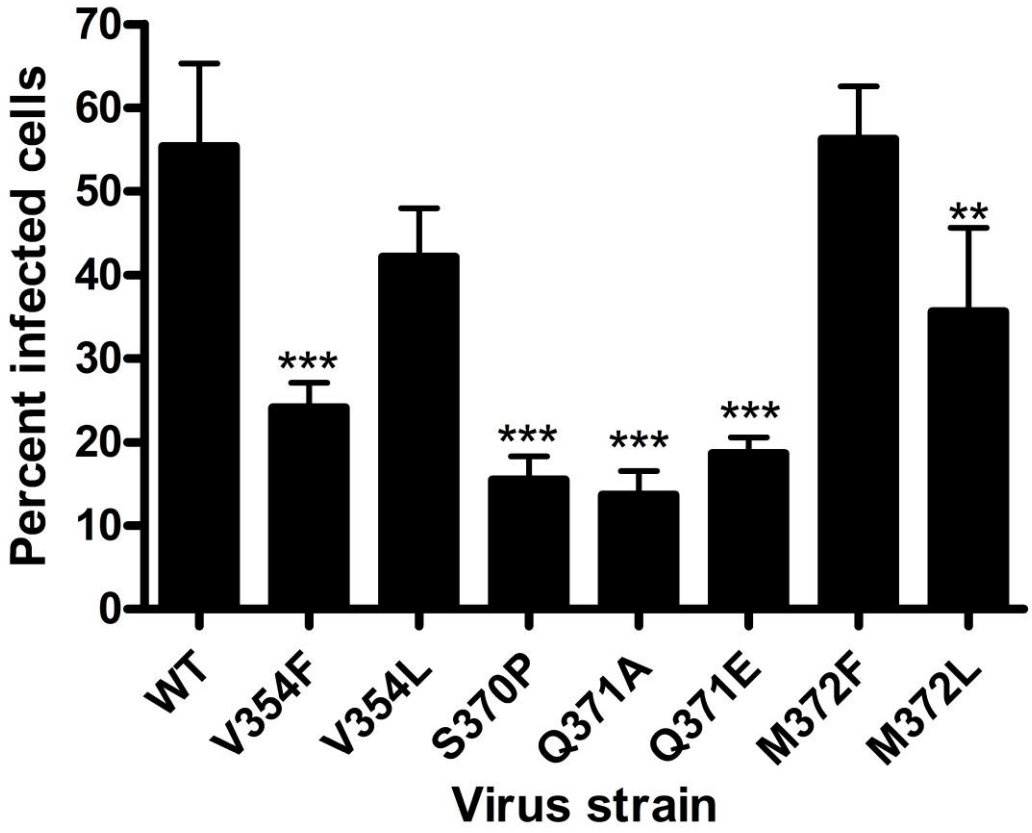

Figure III-7. Infectivity of single-residue T1 σ1 mutant viruses in MEFs. Monolayers of MEFs were adsorbed with the strains shown at an MOI of 1 FFU/field (as titered on L cells) at room temperature for 1 h. Cells were washed twice with PBS, and fresh medium was added. After incubation at 37°C for 20 h, cells were fixed, and reovirus antigen was detected by indirect immunofluorescence. Nuclei were stained with DAPI. The percentage of infected cells in three fields of view per well was determined. The results are expressed as the percent infected cells from a representative experiment of three experiments, each performed in triplicate. Error bars represent standard deviations. ***, $P < 0.01$, as determined by one-way ANOVA followed by Bonferroni's multiple comparison test.

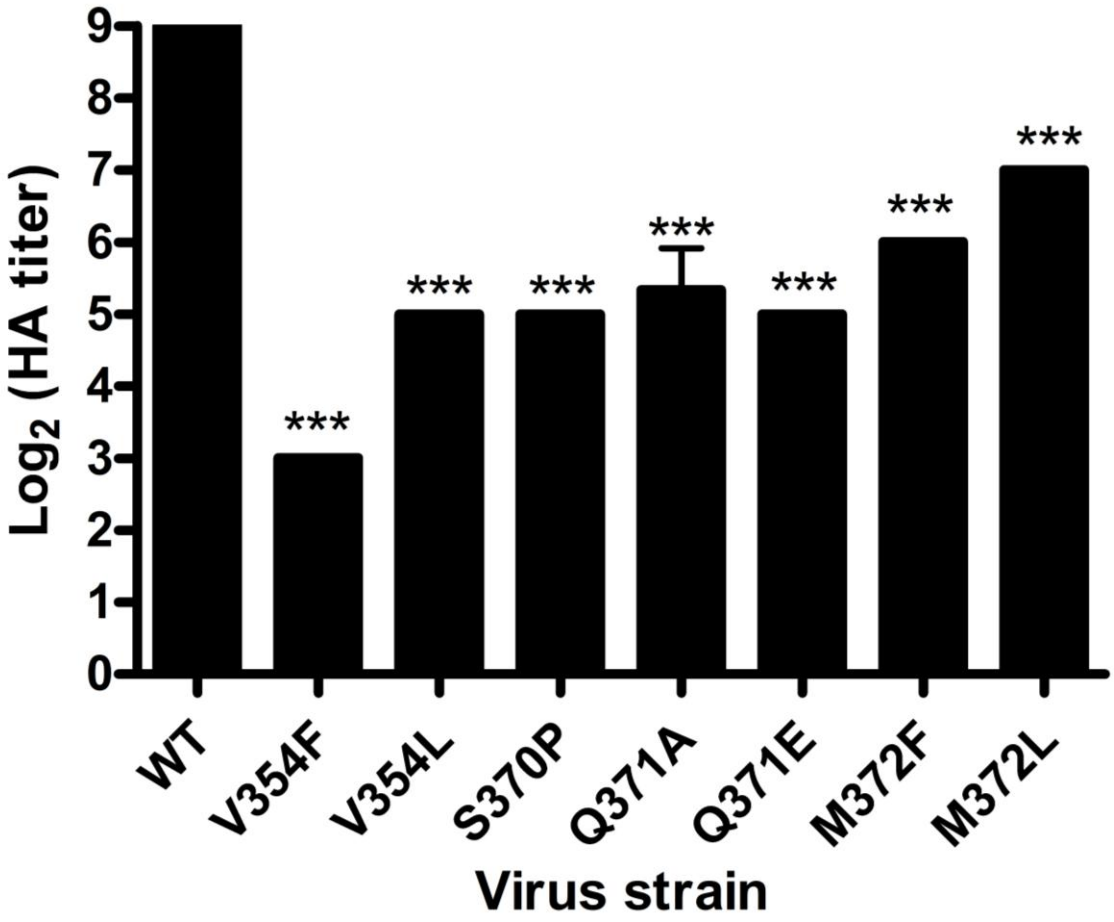

Figure III-8. Hemagglutination by single-residue T1 σ1 mutant viruses. Purified virions of the strains shown (10^{11} particles/well) were serially diluted 1:2 in PBS in 96-well U-bottom plates. Human erythrocytes were washed several times with PBS, resuspended to a concentration of 1% (vol/vol) in PBS, added to virus-containing wells, and incubated at 4°C for 3 h. Results are expressed as $\log_2$ (HA titer) from three independent experiments. HA titer is defined as 10^{11} particles divided by the number of particles/HA unit. One HA unit is the particle number sufficient to produce hemagglutination. *** $P < 0.001$, as determined by one-way ANOVA followed by Bonferroni's multiple comparison test.

activity. Therefore, I engineered a second panel of multiple-residue mutants with the goal of identifying a virus that does not bind GM2. Moreover, I planned to use such a virus for *in vivo* studies, and the introduction of multiple mutations in σ1 would make it more difficult for the virus to potentially revert to wildtype in mice.

Design of multiple-residue mutants

Using site-directed mutagenesis, I, along with the consultative assistance of Kerstin Reiss, designed a panel of viruses containing multiple mutations within the GM2-binding site (Table III-2). The S370P/Q371E mutant combined two of the most effective single-residue mutants that displayed impaired hemagglutination and infection of MEFs but infected L cells comparable to wildtype virus. The S370P/Q371A mutant was designed to exchange two native T1 σ1 residues to those in T3 σ1. The S370P/Q371A/M372F virus added an additional residue from T3 σ1. The S370P/Q371A/M372F/T374G mutant exchanged much of one of the β strands in T1 σ1 that interact with GM2 with the corresponding T3 residues. The T374G mutation was added because the M372F single-residue mutant virus had a slight replication defect in L cells, and T3D contains a glycine at the position corresponding to residue 374. We hypothesized that addition of this glycine residue would provide more room for the bulky phenylalanine residue and hopefully restore full replication capacity in L cells. Similarly, the full β-strand exchange mutant, F369L/S370P/Q371A/M372F/T374G, also would provide additional space for the proline at the amino-terminal end of the β strand and render the protein even

Multiple-residue mutants
S370P/Q371E
S370P/Q371A
S370P/Q371A/M372F
F369L/S370P/Q371A/M372F/T374G
S370P/Q371A/M372F/T374G

Table III-2. Multiple-residue T1 σ1 mutant viruses. The position of the T1L residues (red) altered in the panel of single point mutants is shown. Some mutants contain residues found in the corresponding site in T3D (blue) and others represent changes (black) predicted to block GM2 binding.

more like T3 σ1. All of the mutants were rescued by reverse genetics and working stocks of virus were prepared using L cells.

Characterization of the multiple-residue mutants

Viral infectivity experiments revealed that most of the multiple-residue mutant viruses replicated similarly to wildtype T1L in L cells (Figure III-9). However, when grown in parallel, titers of purified stocks of F369L/S370P/Q371A/M372F/T374G were repeatedly 100- to 1000-fold lower than those of T1L and the other mutants. This finding suggests that this virus has defects in viral replication independent of GM2 engagement. To specifically assess folding of the σ1 head, I evaluated the capacity of conformation-specific monoclonal antibody 5C6 to block wildtype and mutant virus infectivity, as was done for the single-residue mutants. T1L, S370P/Q371A, S370P/Q371E, S370P/Q371A/M372F, and S370P/Q371A/M372F/T374G were neutralized by the antibody (Figure III-10). The F369L/S370P/Q371A/M372F/T374G mutant was not completely neutralized by 5C6, suggesting that the head domain is not properly folded. Closer inspection of the crystal structure revealed that Phe369 is involved in an aromatic stacking interaction with Trp461 on the neighboring β strand. Disruption of that phenylalanine likely disrupts this interaction and consequentially alters the overall conformation of the σ1 head domain (Kerstin Reiss, personal communication).

To test whether the mutants have impaired sialic acid binding, I quantified

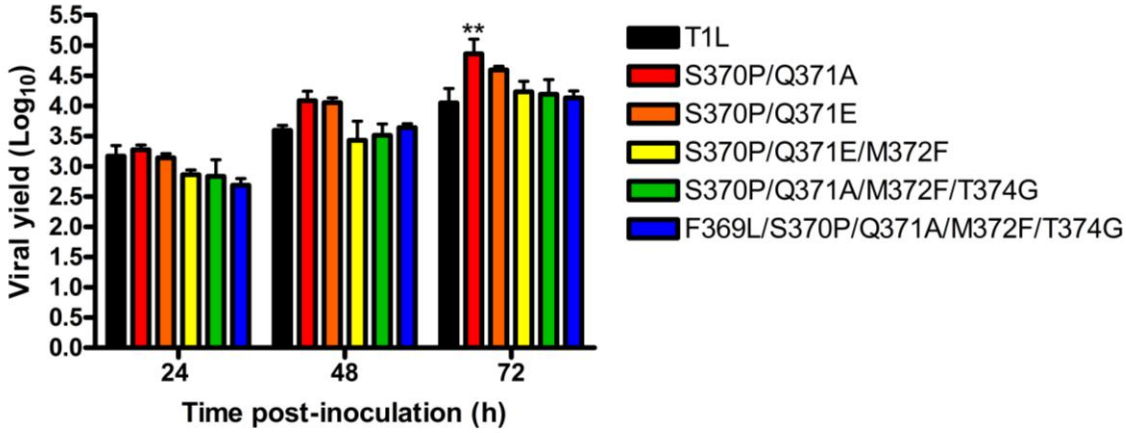

Figure III-9. Replication of the multiple-residue T1 σ1 mutant viruses in L cells. L cells were adsorbed with the strains shown at an MOI of 0.1 PFU/cell at room temperature for 1 h. Cells were washed with PBS, and fresh medium was added. Cells were frozen at 0, 24, 48, and 72 h post-adsorption, and viral titer was quantified by plaque assay. Results are expressed as the mean $\log_{10}$ viral yield from a representative experiment of two independent experiments, each performed in triplicate. Error bars represent standard deviation. ** *PI* < 0.01 as determined by two-way ANOVA followed by Bonferroni's multiple comparison test.

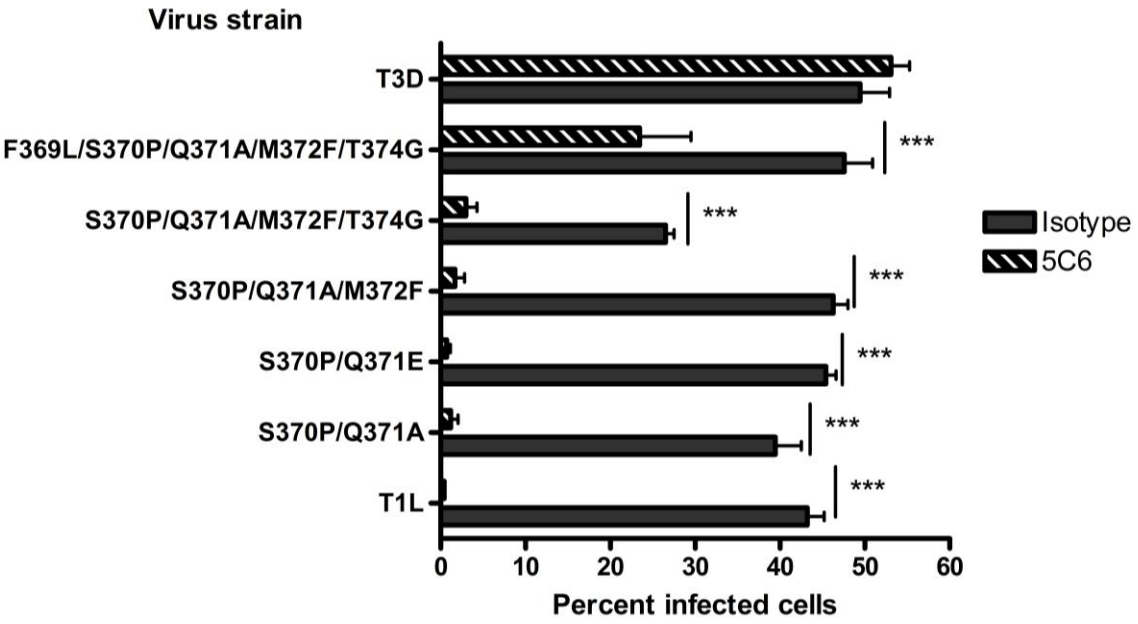

Figure III-10. Multiple-residue T1 σ1 mutant viruses are neutralized by mAb 5C6. T1L, T3D, and multiple-residue T1 σ1 mutant viruses were incubated with T1L σ1-conformation-specific mAb 5C6 at room temperature for 1 h, and the virus-antibody mixture was adsorbed to L cells for 1 h. Cells were washed twice with PBS, and fresh medium was added. After incubation at 37°C for 20 h, cells were fixed, and stained with Alexa-647-labeled polyclonal reovirus antisera. The percentage of infected cells was quantified using flow cytometry. The data shown are a representative experiment of two independent experiments each performed in triplicate. Error bars represent standard deviation. ***, $P < 0.001$, as determined by two-way ANOVA followed by Bonferroni's multiple comparison test.

hemagglutination titers of the wildtype and mutant viruses using human erythrocytes. The S370P/Q371A, S370P/Q371E, S370P/Q371A/M372F, and S370P/Q371A/M372F/T374G mutants displayed significantly diminished hemagglutination titers relative to wildtype (Figure III-11). However, like the single-residue mutants, the multiple-residue mutants retained a degree of hemagglutination capacity. Moreover, the magnitude of the hemagglutination titer difference between wildtype and mutant viruses was the same for the single- and multiple-residue mutants. The F369L/S370P/Q371A/M372F/T374G mutant lacked the capacity to agglutinate human erythrocytes. However, this mutant was removed from further study due to the defects observed in infectivity experiments using L cells and difficulties preparing high-titer stocks. The S370P/Q371E mutant was selected for further characterization.

The S370P/Q371E virus as well as the S370P and Q371E single-residue mutants replicated well in L cells (Figure III-5) and were neutralized by conformation-specific monoclonal antibody 5C6 (Figure III-6). Stocks of these double and single mutants consistently produced titers approximating those of wildtype T1L. The S370P/Q371E mutant was selected over the S370P/Q371A mutant because the Q371A single mutant had a slight defect in replication in L cells and, more importantly, steric hindrance caused by the introduction of a proline at residue 370 coupled with a negative charge associated with the introduction of a glutamic acid at residue 371 was thought more likely to repel GM2 binding compared with an alanine at 371. It is possible that any of the multiple-residue mutants would have been equally compromised in GM2-binding

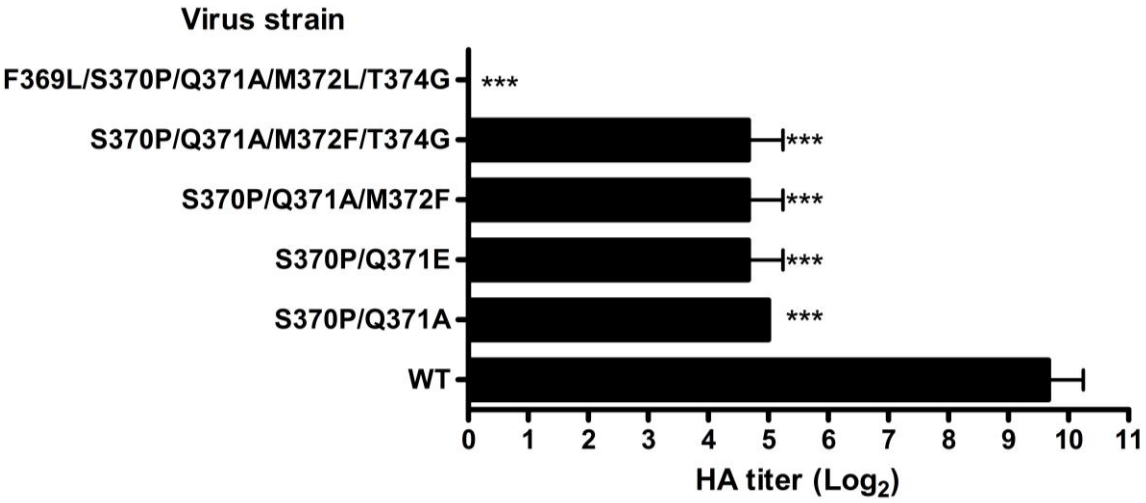

Figure III-11. Hemagglutination by σ1 mutant viruses. Purified virions of the strains shown (10^{11} particles/well) were serially diluted 1:2 in PBS in 96-well U-bottom plates. Human erythrocytes were washed several times with PBS, resuspended to a concentration of 1% (vol/vol) in PBS, added to virus-containing wells, and incubated at 4°C for 3 h. Results are expressed as $\log_2$ (HA titer) from three independent experiments. ***, $P < 0.001$, as determined by one-way ANOVA followed by Bonferroni's multiple comparison test.

capacity relative to S370P/Q371E, but only one virus was selected for *in vivo* experiments. Further characterization using saturation-transfer difference nuclear magnetic resonance (STD-NMR) demonstrated that the S370P/Q371E mutant is incapable of binding GM2, but if this had not been the case, I would have returned to this mutant panel and further characterized additional mutant viruses.

The S370P/Q371E double mutant, like the S370P and Q371E single mutants, displayed impaired hemagglutination capacity compared with wildtype T1L. However, unlike T3 sialic acid-binding mutants, which do not have the capacity to agglutinate erythrocytes (9) the T1 σ1 mutants altered in GM2-binding still produce hemagglutination (Figures III-8 and III-11), albeit at reduced levels compared with wildtype virus. While T1 reovirus mediated-agglutination of human erythrocytes is known to be glycan-dependent (137), the influence of neuraminidase treatment on T1 reovirus-induced hemagglutination had not been reported. Neuraminidase treatment ablates T3 reovirus mediated-hemaggulatination (156). Therefore, I performed a hemagglutination inhibition (HAI) assay using 4 hemagglutination units, where 1 hemagglutination unit is defined as the minimal number of viral particles required to produce hemagglutination. Strains T1L or S370P/Q371E were incubated with erythrocytes that had been treated with either *A. ureafaciens* neuraminidase to remove cell-surface sialic acid or PBS as a vehicle control. T1L-mediated hemagglutination was impaired following neuraminidase treatment, while S370P/Q371E agglutination capacity was not affected (Figure III-12A). This finding suggests that T1L, but not S370P/Q371E, binds sialic acid to agglutinate human

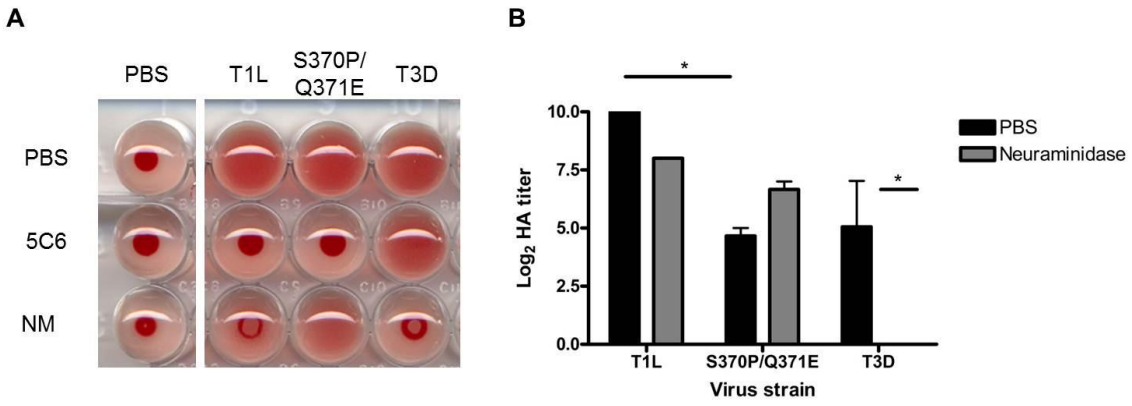

Figure III-12. Neuraminidase diminishes hemagglutination capacity of T1L but not S370P/Q371E. (**A**) Human erythrocytes were washed with PBS, resuspended at a concentration of 1% (vol/vol), and treated with PBS (vehicle control), T1L σ1-conformation-specific mAb 5C6, or 200mU of *A. ureafaciens* neuraminidase (NM) at room temperature for 1 h prior to adsorption with 4 HA units of the virus strains shown in 96-well U-bottom plates. Erythrocytes were incubated with virions at 4^{o}C for 3 h. The data shown are a representative of three independent experiments. (**B**) Human erythrocytes were washed with PBS, resuspended at a concentration of 1% (vol/vol), and treated with PBS (vehicle control) or 200 mU of *A. ureafaciens* neuraminidase at room temperature for 1 hour prior to distribution into wells of 96-well U-bottom plates containing 10^{11} purified virions of T1L or S370P/Q371E serially diluted 1:2 in PBS. Plates were incubated at 4°C for 3 h. Results are expressed as $\log_2$ HA titer from three independent experiments. Error bars represent standard deviation (S.D.) * p <0.05, as determined by two-way ANOVA followed by Bonferroni's multiple comparison test.

erythrocytes. Furthermore, the residual hemagglutination capacity of S370P/Q371E is likely due to interactions with non-sialylated receptors on the erythrocyte surface.

One caveat of performing a standard HAI assay with two different virus strains is that 4 HA units, standard in these assays, represents different concentrations of viral particles for T1L and S370P/Q371E because the wildtype virus agglutinates erythrocytes more efficiently than does the mutant. Therefore, to further evaluate the influence of neuraminidase on T1 reovirus hemagglutination, I performed a standard hemagglutination assay and quantified HA titer using erythrocytes that had been pre-treated with either *A. ureafaciens* neuraminidase or PBS. Neuraminidase treatment abolishes the hemagglutination capacity of T3 reovirus as expected (156). However, neuraminidase treatment only diminishes the capacity of T1 reovirus to agglutinate human erythrocytes. Moreover, the capacity of T1L to agglutinate neuraminidase-treated erythrocytes approximated the capacity of S370P/Q371E to agglutinate PBS-treated erythrocytes. The hemagglutination capacity of S370P/Q371E was not further reduced by treatment of the erythrocytes with neuraminidase (Figure III-12B). Taken together, these findings suggest that T1L binds to sialylated glycans on erythrocytes, while S370P/Q371E does not.

To determine whether the S370P/Q371E mutation is incapable of engaging GM2, I collaborated with Bärbel Blaum in the Stehle lab to assess the binding of wildtype T1L, S370P, Q371E, and S370P/Q371E σ1 proteins to GM2 in solution using NMR spectroscopy. This approach is well suited to study low-

affinity interactions between a large molecule, such as σ1, and a small ligand, such as the GM2 glycan (157, 158). As anticipated, T1L σ1 engaged GM2 in solution, consistent with our previous results (10). The GM2 protons specifically in the GalNAc and sialic acid moieties interact with σ1, mimicking the binding contacts in the crystal structure. While the S370P and Q371E single-residue mutant σ1 proteins minimally interacted with the GM2 glycan in solution, we did not detect binding of the S370P/Q371E double-mutant σ1 protein to the GM2 glycan (Figure III-13).

To determine whether the S370P/Q371E mutant virus has altered capacity to infect cells in a carbohydrate-dependent manner, I quantified infectivity using MEFs, which require GM2 for optimal infection. MEFs were inoculated with T1L or S370P/Q371E at a range of MOIs as determined in assays using L cells. S370P/Q371E displayed diminished capacity to infect MEFs compared with T1L at all MOIs tested (Figure III-14). This finding suggets that S370P/Q371E does not interact with GM2 on the MEF cell-surface and consequentially infects these cells less efficiently than T1L.

To establish whether the difference in infectivity displayed by wildtype and mutant viruses in MEFs resulted from compromised viral attachment, T1L and S370P/Q371E were adsorbed to MEFs and L cells at 4°C to prevent internalization, and the percentage of cells with bound virus was quantified using flow cytometry. Both T1L and S370P/Q371E bound equally well to L cells, but

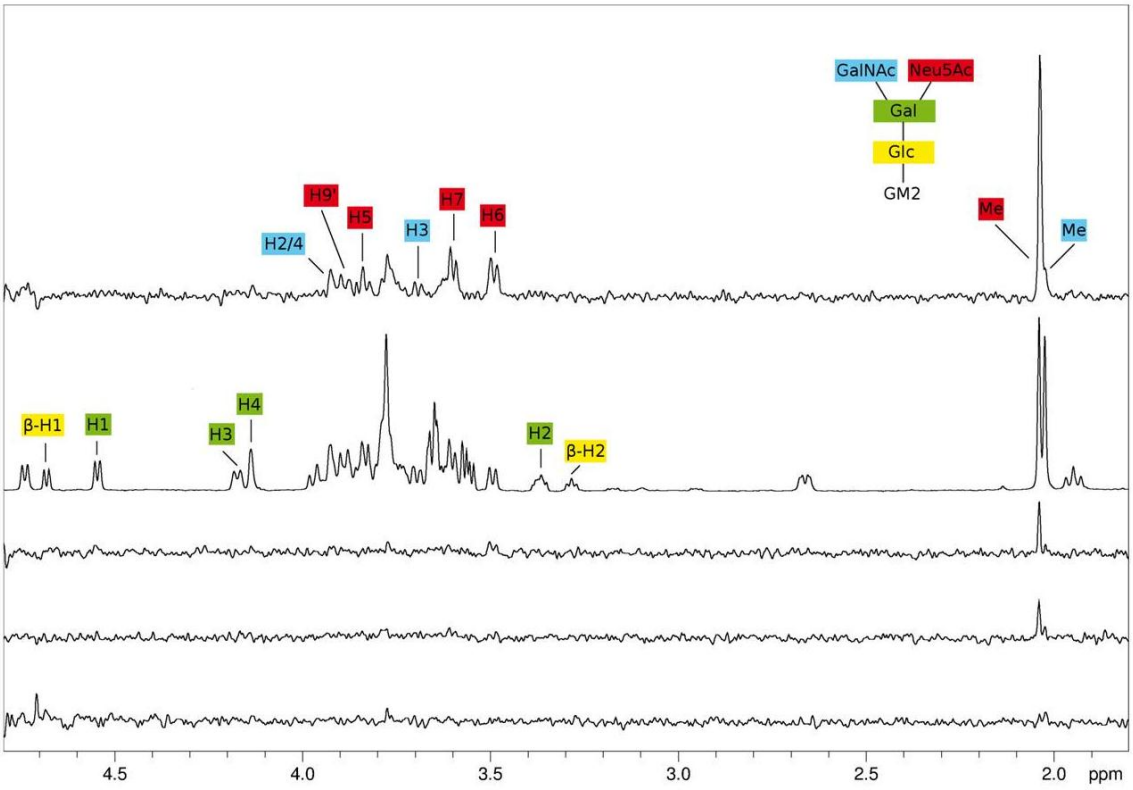

Figure III-13. Binding of T1L and S370P/Q371E to the GM2 glycan. STD NMR spectroscopy demonstrates that the WT T1L σ1 binds to the GM2 glycan in solution. Single S370P and Q371E mutants and the double S370P/Q371E mutant σ1 proteins bind minimally or not at all, respectively. From top to bottom: STD spectrum of T1L σ1 and GM2 glycan, GM2 glycan alone, S370P mutant σ1 and GM2, Q371E mutant σ1 and GM2, and S370P/Q371E double mutant σ1 and GM2. Resonances that can be unambiguously assigned to individual protons are labeled and color-coded according to the sugar moieties within the GM2 glycan: glucose (Glc), yellow; galactose (Gal), green; neuraminic acid (red); and N-acetylgalactosamine (GalNAc), blue.

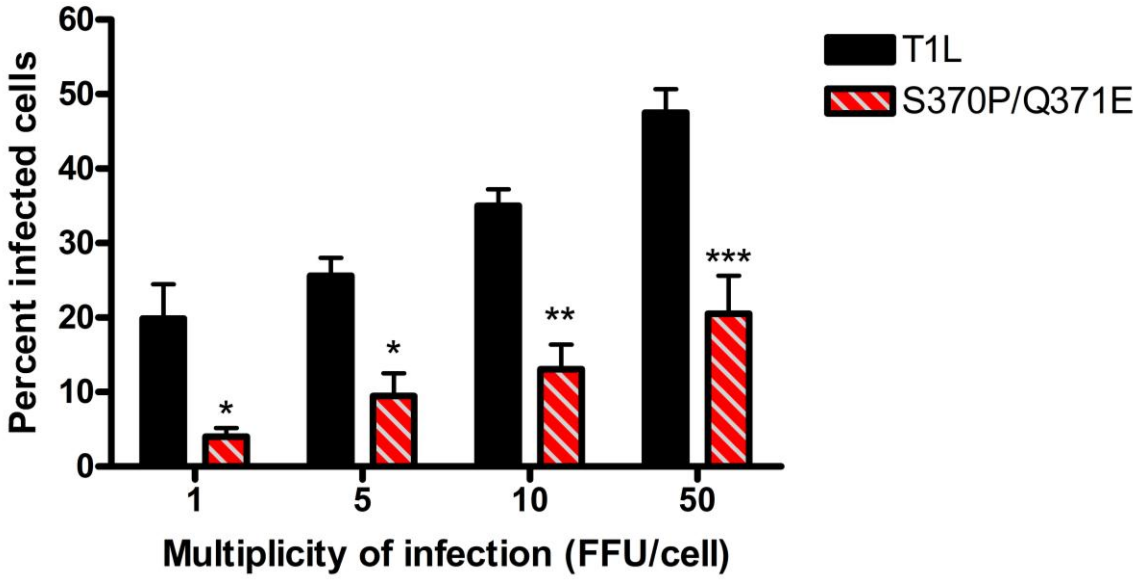

Figure III-14. Infectivity of T1L and S370P/Q371E in MEFs. Monolayers of MEFs were adsorbed with the strains shown at an MOI of 1 FFU/field (as titered on L cells) at room temperature for 1 h. Cells were washed twice with PBS, and fresh medium was added. After incubation at 37°C for 20 h, cells were fixed, and reovirus antigen was detected by indirect immunofluorescence. Nuclei were stained with DAPI. The percentage of infected cells in three fields of view per well was determined. The results are expressed as the percent infected cells from the combined means of three independent experiments each performed in triplicate wells. Error bars represent standard error of the mean. * P <0.05, ** P < 0.01, *** P < 0.001, as determined by two-way ANOVA followed by Bonferroni's multiple comparison test.

S370P/Q371E adhered less efficiently to MEFs in comparison to T1L (Figure III-15). Thus, S370P/Q371E has a defect in attachment to and infectivity of host cells that require glycan engagement for optimal infection.

Discussion

Studies reported in this chapter defined the σ1-GM2 binding site and identified residues required for functional GM2 engagement. Using NMR spectroscopy and crystallography, we determined that the head domain of T1 σ1 contacts the sialic acid and GalNAc moieties of GM2 (Figures III-1, III-2, and III-13). Structure-guided, site-directed mutagenesis revealed that residues Val354, Ser370, and Gln371 are required for functional glycan binding. Mutation of single or multiple residues within the glycan-binding site diminishes hemagglutination and infectivity in MEFs. Additionally, a T1 reovirus engineered with both S370P and Q371E mutations in σ1 is incapable of binding GM2 (Figure III-13) and displays diminished capacity to attach to the MEF cell-surface (Figure III-15).

The crystal structure of the T1 σ1-GM2 complex revealed that the carbohydrate-binding site is located within the head domain of the attachment protein. Yet, GM2 and JAM-A bind distinct regions of the T1 σ1 head domain, making it possible for both receptors to be bound simultaneously (Figures III-2 and III-3). Reovirus engagement of host cells is likely a multistep process in which interactions with glycans function in adhesion strengthening (7). In support of this idea, the NMR data (Figure III-13) coupled with the high doses of GM2 required to block T1 reovirus infection (Figure II-6) suggest that the virus binds

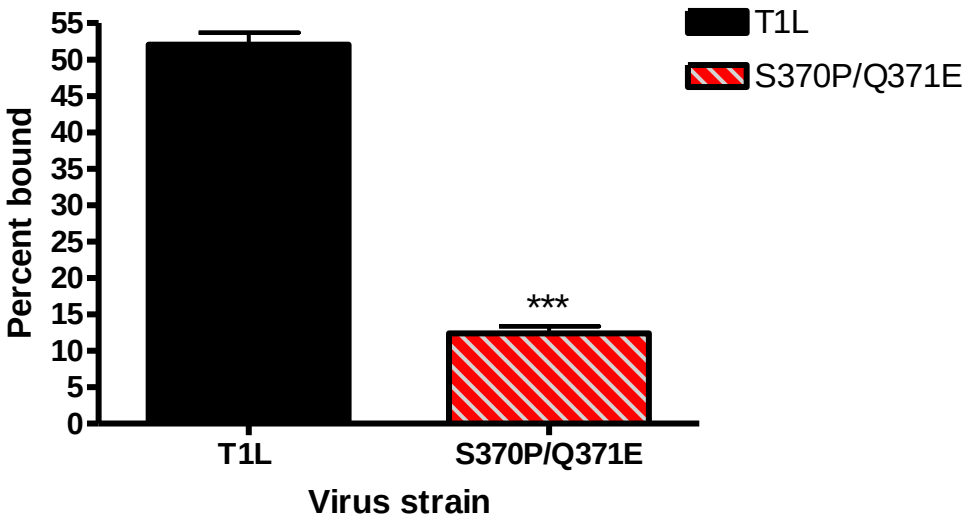

Figure III-15. The capacity of T1L and S370P/Q371E to bind MEFs. MEFs were adsorbed with the virus strains shown at an MOI of 5 x 10^4 particles per cell at 4°C for 1 h. Cells were washed twice with PBS and stained with Alexa-647-labeled reovirus antiserum. The percentage of cells with bound virus was quantified using flow cytometry. Results are a representative experiment of three independent experiments, each performed in triplicate. *** $P < 0.001$ as determined by two-tailed student's *t* test.

GM2 with relatively low affinity compared with the high-affinity binding of reovirus to JAM-A. Additionally, glycan binding is required for T1 reovirus infection of MEFs, which express modest levels of JAM-A, and dispensable for infection of L cells, which express significantly higher JAM-A levels (Figure II-2).

T1 and T3 reovirus bind sialylated carbohydrates using entirely different domains of σ1. Steric hindrance would prevent the T3 σ1 protein from engaging GM2 in the region corresponding to the glycan-binding domain of T1 σ1. This observation is in accordance with my finding that GM2 blocks T1 but not T3 reovirus infection of MEFs (Figure II-6). While the crystal structure of T1 σ1 does not contain the region corresponding to the T3 σ1 sialic acid-binding site, sequence analysis suggests that the body domain of T1 σ1 is unlikely to engage sialic acid. T1 σ1 contains an aspartate at the location in which T3 σ1 contains an arginine residue (Figure III-3D) that contacts sialic acid. Mutation of this arginine at residue 202 in the T3 σ1 body domain disrupts the bidentate salt bridge between the arginine side chain and the sialic acid carboxylate and renders the virus incapable of binding sialylated glycan (9). We predict that the negatively charged aspartate residue would repel sialic acid and thereby prevent the body domain of T1 σ1 from engaging the negatively charged sialic acid.

The crystal structure of the T1 σ1-GM2 binding site demonstrates that the sialic acid (Neu5Ac) and GalNAc contact the protein. The majority of the contacts are contributed by Neu5Ac through hydrogen bonds with the backbone of T1 σ1, while the GalNAc docks onto a shallow pocket using van der Waals interactions. This finding was unexpected, as side chains are commonly involved in virus

attachment protein-carbohydrate interactions (27). To provide biological evidence to support these structural findings, I engineered mutants using reverse genetics and identified residues required for glycan engagement on host cells. The single-residue mutant viruses displayed impaired hemagglutination capacity (Figure III-8) and infectivity in MEFs (Figure III-7), with substitutions of Val354, Ser370, and Gln371 having the greatest effects. Residue V354 flanks a hydrophobic pocket into which the methyl group of the *N*-acetyl chain of Neu5Ac inserts. The S370P substitution introduces a protruding and rigid ring structure, which is expected to cause steric hindrance within the glycan-binding pocket. Gln371 likely forms a hydrogen bond with the carboxyl group of Neu5Ac. In the point mutants Q371E and Q371A, this hydrogen bond would be lost, resulting in reduced affinity for ligand and, in the case of Q371E, electrostatic repulsion. Taken together, these findings indicate that V354, S370, and Q371 are required for functional GM2 engagement.

The single point mutants retained some capacity to agglutinate red blood cells, suggesting that either these mutants retained some sialic-acid-binding capacity or engagement of alternative receptors contributes to hemagglutination capacity. I therefore generated a panel of multiple-residue mutants in an attempt to further compromise glycan binding. These mutants did not display a further decrease in hemagglutination capacity or infectivity in MEFs compared with the single-residue mutants (Figures III-8 and III-11). We used NMR spectroscopy to determine whether the mutants retained residual GM2 binding capacity. The S370P and Q371E single mutants display minimal, if any, interaction with GM2 in

solution, while the S370P/Q371E double mutant does not interact with the glycan at all (Figure III-13). Thus, introduction of multiple mutations in the T1 σ1 glycan-binding site only slightly diminishes glycan-binding, if at all, relative to the single-residue mutants.

From these data, I conclude that cell-surface structures in addition to glycans contribute to T1 reovirus-mediated agglutination of human erythrocytes. Hemagglutination by T1 reovirus is carbohydrate-dependent, as sodium periodate decreased hemagglutination capacity (137). While neuraminidase treatment abolishes T3-mediated agglutination of human erythrocytes (156) (Figure III-12), such treatment diminishes the HA titer of T1L to levels approximating those of the glycan-binding-site mutants (Figure III-12). Type O erythrocytes were used in these studies, yet reovirus agglutinates erythrocytes from all blood groups (159), suggesting that human blood group antigens are not required for erythrocyte agglutination. Of note, reovirus receptor JAM-A is expressed on erythrocytes (160) and may mediate hemagglutination, although this possibility has not been formally tested.

These studies with T1 reovirus support a general principle observed for other viruses, including influenza virus (47, 161-163), polyomaviruses (51, 74), and T3 reovirus (7, 9, 24), that few mutations are required to disrupt virus-sialic acid interactions. Viruses containing mutations in the sialyloligosaccharide-binding site are valuable tools to determine the function of sialylated glycan binding in tropism and pathogenesis. A T1 reovirus containing S370P and Q371E mutations cannot bind GM2 and was selected for *in vivo* studies to investigate

the contribution of GM2 engagement to reovirus-mediated disease. This work is described in Chapter IV.

CHAPTER IV

THE FUNCTION OF GM2 BINDING IN SEROTYPE 1 REOVIRUS PATHOGENESIS

Introduction

Reovirus disseminates with serotype-specific tropism in neonatal mice, but the basis for serotype-specific neurologic disease is not known. T1 reovirus infects ependymal cells and causes hydrocephalus (16, 105, 106), whereas T3 reovirus infects neurons and causes lethal encephalitis (140, 164). Reassortant viruses containing a T1 S1 gene cause hydrocephalus whereas viruses containing a T3 S1 gene cause encephalitis (114). This observation suggests that differences in receptor engagement contribute to serotype-specific tropism.

JAM-A serves as a receptor for T1 and T3 reoviruses (11, 125, 152, 165) and is required for hematogenous reovirus spread (12) (Lai and Dermody, unpublished). However, JAM-A is dispensable for reovirus infection in the brain and, therefore, cannot account for serotype-specific patterns of reovirus-induced neurologic disease (12). T3 reoviruses differing only in the capacity to bind sialic acid display striking differences in tropism particularly within the bile duct epithelium (139) and CNS (140). When I began this project, the contribution of T1 σ1-glycan interactions to disease was not known. This knowledge gap precluded a precise understanding of reovirus tropism and the basis of serotype-specific disease phenotypes. While the tissue distribution of GM2 is not known, this glycan is a component of the mammalian nervous system (166-169), suggesting

that reovirus engagement of GM2 influences serotype-specific neurologic disease. Through genetic manipulation of reovirus and the murine host, I investigated the effect of GM2 engagement by T1 reovirus on systemic viral dissemination and hydrocephalus, the cardinal T1 reovirus disease manifestation.

Using structure-guided mutagenesis, I engineered a T1L mutant virus containing S370P and Q371E mutations in σ1. The σ1-S370P/Q371E protein does not interact with GM2 in solution (Figure III-13). Moreover, this mutant virus displays diminished hemagglutination capacity and impaired binding to and infection of MEFs (Figure III-14), which are optimally susceptible to sialic acid-binding reovirus strains (Figure II-1). The S370P/Q371E mutant replicates efficiently in L cells, which are equally susceptible to strains that differ in sialic-acid-binding capacity. I used mice that lack expression of the GM2 glycan in a few experiments to complement studies using the S370P/Q371E mutant virus.

I collaborated with Dr. Daniel Colvin at the Vanderbilt Small Animal Imaging Core to use magnetic resonance imaging (MRI) to quantify the severity of hydrocephalus after reovirus infection. Daniel designed a program in MatLab that I used to quantify the ventricular volume (Figure IV-6). I worked with Dr. Ty Abel, a Vanderbilt neuropathologist, to evaluate histological changes in brain tissue of reovirus-infected animals. He obtained images presented in Figure IV-4. I also worked with Dr. Kelli Boyd, a Vanderbilt veterinary pathologist, to evaluate regions of the brain targeted by reovirus. She obtained the images presented in Figure IV-3.

Results

Analysis of viral load and disease using viruses that differ in the capacity to bind GM2

To define the function of T1 σ1-GM2 interactions in viral dissemination and disease, I inoculated two-to-three day old wildtype C57Bl/6 mice perorally with 10^2 PFU of either wildtype T1L or the σ1-S370P/Q371E mutant virus. The intestine, mesenteric lymph nodes (MLN), spleen, liver, heart, and brain were excised 4, 8, and 12 days post-inoculation, and viral titer was quantified by plaque assay. Wildtype and mutant viruses produced comparable titers in the intestine, MLN, spleen, liver, and heart. However, T1L produced slightly higher titers in the brain compared with S370P/Q371E, although these differences were not statistically significant (Figure IV-1). The magnitude of this difference in viral loads in the brain is similar to that observed between T3 reoviruses differing in sialic-acid-binding capacity (139, 140).

To determine whether the lower viral titer in the brain following inoculation with S370P/Q371E was a result of diminished dissemination to the brain or replication at that site, wildtype mice were inoculated intracranially with 10^2 PFU of either T1L or S370P/Q371E. Brain homogenates were titered by plaque assay 4, 8, and 12 days post-inoculation (Figure IV-2A). Concordant with differences in viral titer after peroral inoculation, T1L produced higher titers in the brain compared with S370P/Q371E, reaching statistical significance on day 8 post-inoculation. These findings suggest that T1 σ1-glycan interactions are required for optimal replication within the murine brain.

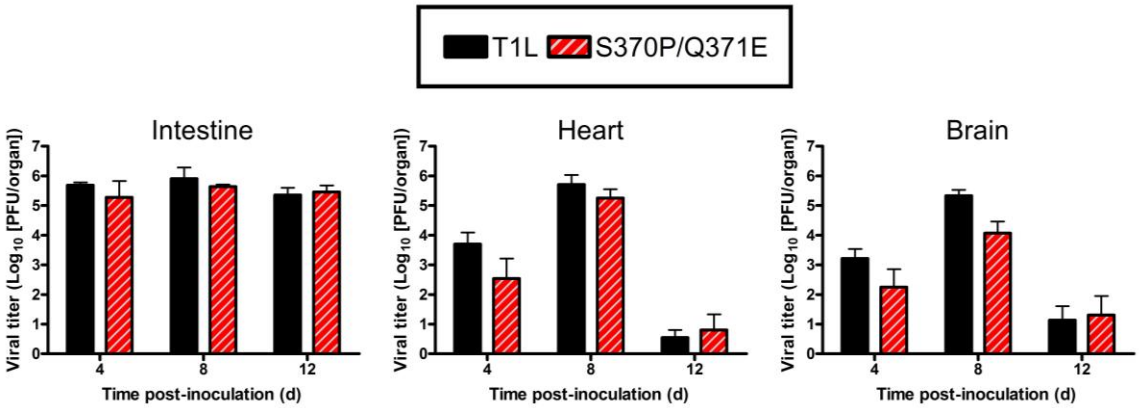

Figure IV-1. Viral titers in various organs following peroral inoculation with either T1L or S370P/Q371E. Newborn C57BL/6 mice were inoculated perorally with 10^2 PFU of either T1L or S370P/Q371E. At days 4, 8, and 12 post-inoculation, mice were euthanized, and the intestine, heart, and brain were excised and homogenized. Viral titers in organ homogenates were quantified by plaque assay. Results are expressed as mean viral titers for 4 to 10 mice per virus strain per timepoint. Error bars represent standard error of the mean. Values were not statistically significant as quantified by a two-way ANOVA followed by Bonferroni's multiple-comparison test.

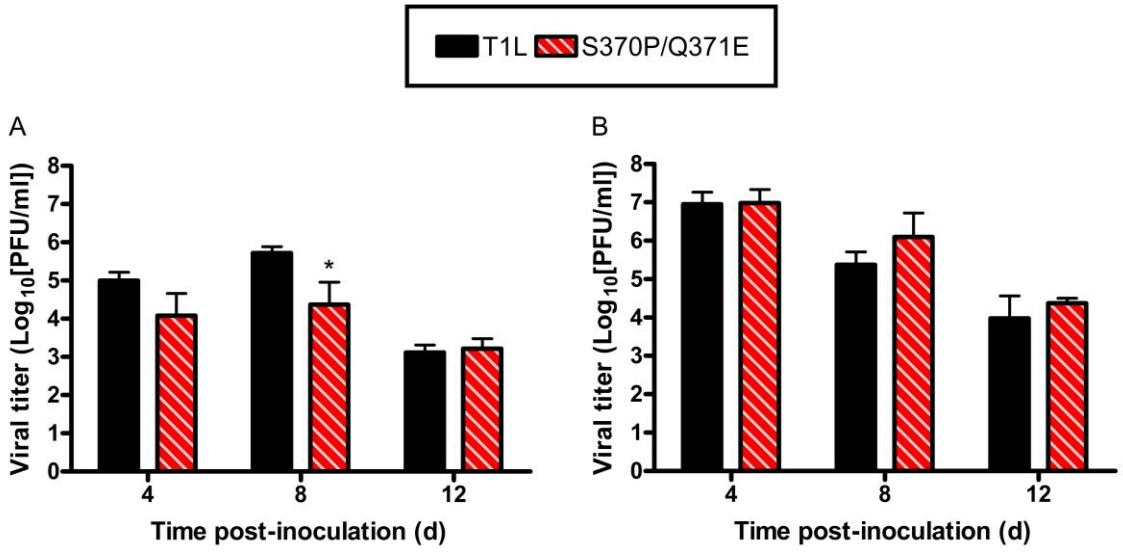

Figure IV-2. Viral titers in the brain following intracranial inoculation with either T1L or S370P/Q371E. Newborn mice were inoculated intracranially with 10^2 (A) or 10^8 (B) PFU of either T1L or S370P/Q371E. At days 4, 8, and 12 post-inoculation, mice were euthanized, and brains were excised and homogenized. Viral titers in brain homogenates were determined by plaque assay. Results are expressed as mean viral titers for 4 to 11 mice per virus per timepoint. Error bars represent SEM. * $P < 0.05$ as determined two-way ANOVA followed by Bonferroni's multiple-comparison test.

I next sought to assess the contribution of glycan-binding capacity to T1 reovirus-mediated hydrocephalus. Higher doses of T1L are required to uniformly induce hydrocephalus (16, 17, 114, 116). Moreover, previous experiments used Balb/c or NIH Swiss Webster mice, which tend to be more susceptible to reovirus in comparison to C57Bl/6 mice (Boehme and Dermody, unpublished). Therefore, I increased the viral dose for studies of hydrocephalus induction. Wildtype mice were inoculated with 10^8 PFU of T1L or S370P/Q371E intracranially, and viral titers in brain homogenates were quantified 4, 8, and 12 days post-inoculation by plaque assay (Figure IV-2B). No significant differences in titer were observed, suggesting equivalent replication capacity of T1L and S370P/Q371E in the brain following intracranial inoculation at high doses (Figure IV-2B).

Since the overall viral titer in the brain was equilibrated following high-dose inoculation, we used histology to determine whether T1L and S370P/Q371E differ in tropism. Mice were inoculated in the right cerebral hemisphere with 10^8 PFU of T1L or S370P/Q371E and euthanized 4 and 12 days post-inoculation. The left hemisphere was excised and stained for reovirus antigen. Major differences in cells targeted by wildtype and mutant virus were not detected. However, evaluation of the samples by a pathologist blinded to the conditions of the experiment revealed that S370P/Q371E displayed less dissemination to the contralateral hemisphere compared with T1L at 4 days post-inoculation (Figure IV-3). Although reovirus antigen was detected, hydrocephalus was not evident. Conversely, at 12 days post-inoculation reovirus antigen could no longer be detected in the brain, yet signs of pathologic injury were present.

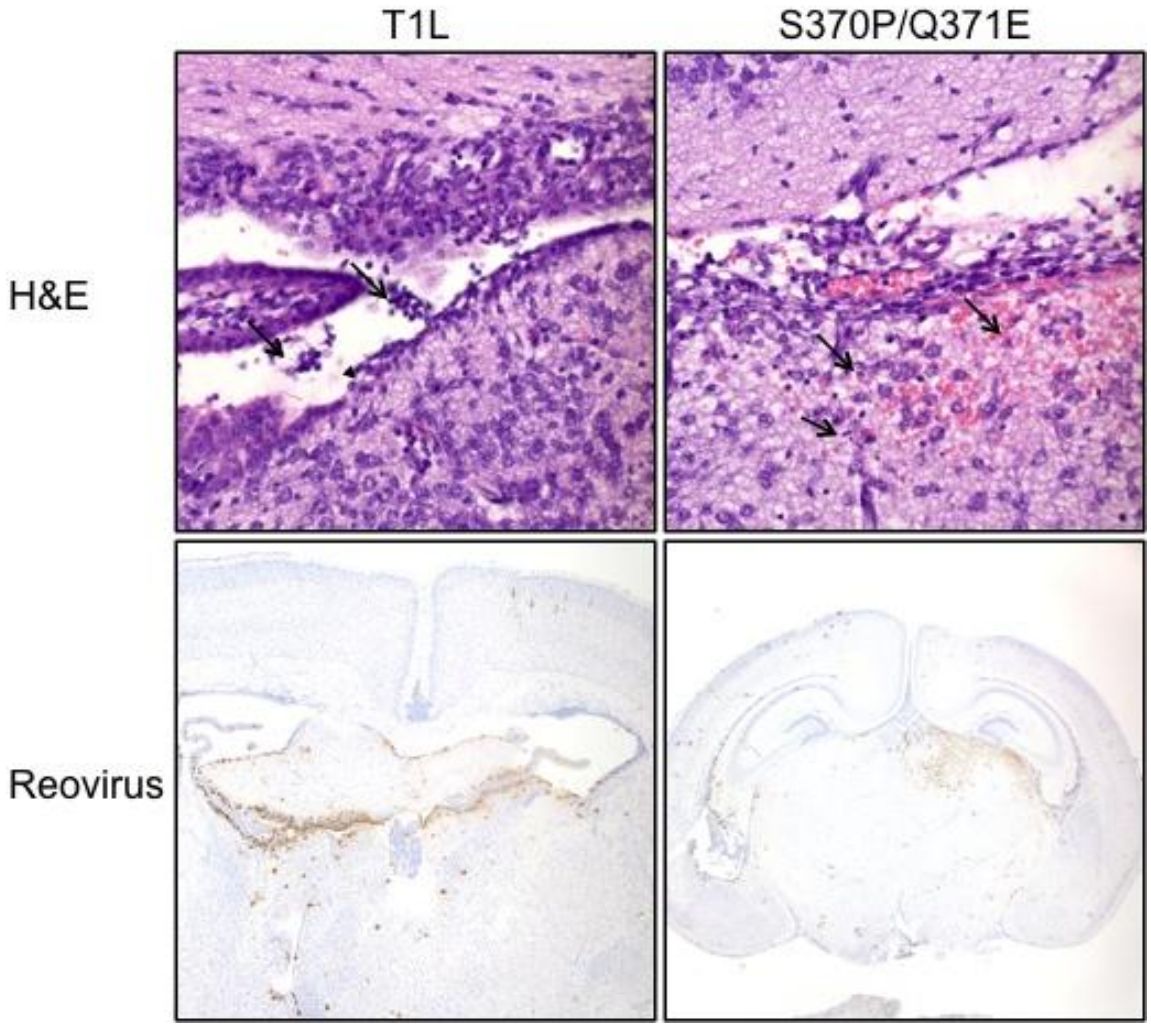

Figure IV-3. Reovirus histology four days following intracranial inoculation with either T1L or S370P/Q371E.
Newborn mice were inoculated intracranially with PBS or 10^8 PFU of T1L or S370P/Q371E. Four days-post-inoculation, mice were euthanized, and brains were excised, fixed, and paraffin embedded. Samples were stained with H&E (top) to examine tissue pathology. In the T1L sample, arrowheads indicate areas ependymal cell denuding. Arrows point toward sloughed cells in the ventricles, which may contribute to hydrocephalus. In the S370P/Q371E brain, focal malacia in the periventricular neurophil is observed. Arrows indicate regions of apoptotic neurons and glia with mild hemorrhage. Samples were stained with reovirus (bottom) antisera to detect viral antigen. Viral antigen is dispersed in the T1L-infected brain, but more localized to the inoculation site in the S370P/Q371E-infected brain.

Histological evaluation of brains from wildtype mice inoculated with T1L showed a disorganized choroid plexus with greater cell density within the ventricle compared with mice inoculated with PBS as a control. Moreover, cells in the PBS-inoculated mice are evenly spaced with pale, monomorphous nuclei, and abundant cytoplasm. Conversely, cells in the choroid plexus of the T1L-inoculated mice are jumbled and display high nuclear to cytoplasm ratios. Brain samples from wildtype mice inoculated with S370P/Q371E showed evidence of disease but displayed more normal epithelial borders and lower cell density within the choroid plexus relative to that seen in T1L-infected animals (Figure IV-4A). The sections were stained with Ki-67, which recognizes a nuclear protein expressed during the cell cycle, and is used as a marker for cellular proliferation (170, 171). Immunohistochemical analysis showed greater proliferation within the ventricle, evidenced by enhanced Ki-67 staining in the brains of wildtype mice inoculated with T1L compared with that observed in brains of mice inoculated with S370P/Q371E. Differences in apoptosis induction, evidenced by staining for activated caspase-3, were minimal (Figure IV-4B).

To test whether GM2-binding capacity contributes to hydrocephalus, wildtype mice were inoculated intracranially with either T1L or S370P/Q371E. Hydrocephalus was assessed using MRI 21 days post-inoculation (Figure IV-5). Wildtype mice inoculated with T1L developed much more substantial hydrocephalus than those infected with S370P/Q371E. Quantification of the ventricular volume (Figure IV-6) confirmed that T1L induces a greater degree of hydrocephalus compared with S370P/Q371E in which ventricular volume did not

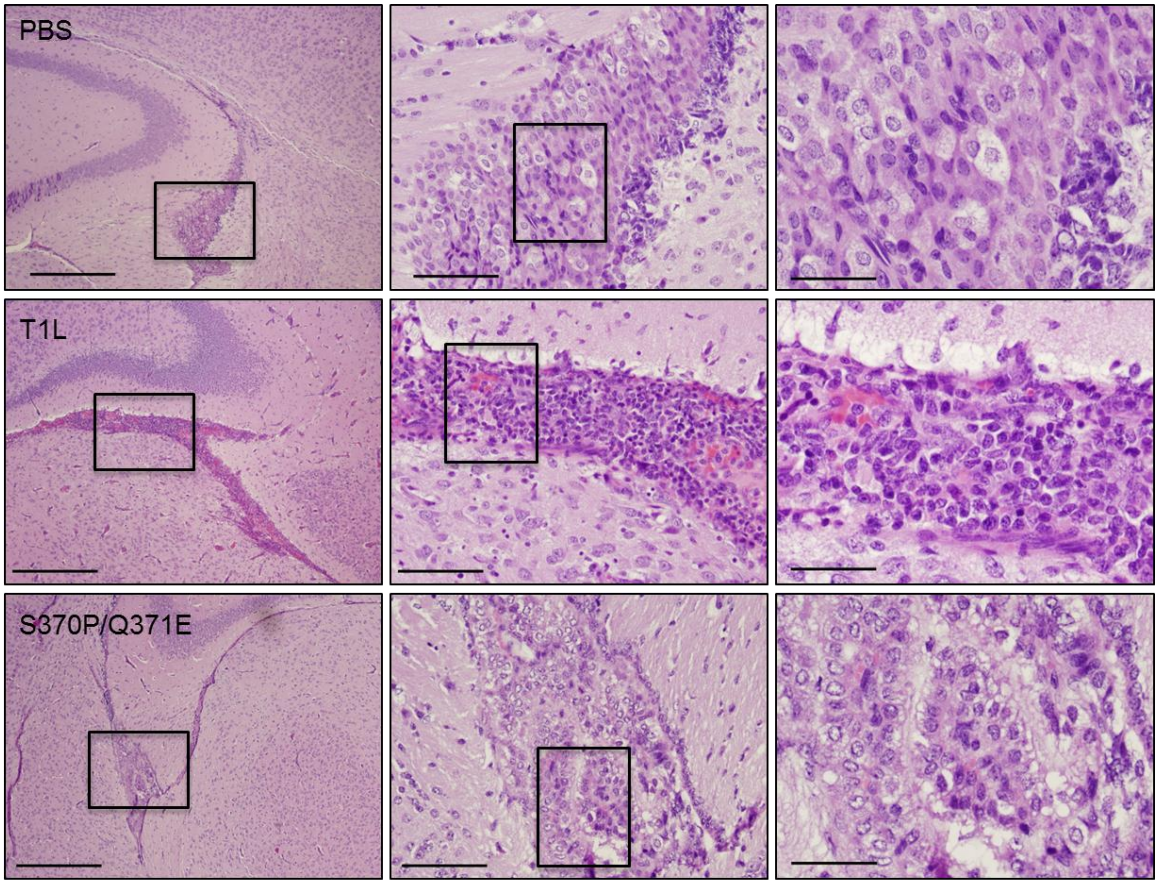
PBS
T1L
S370P/Q371E
4X
20X
40X

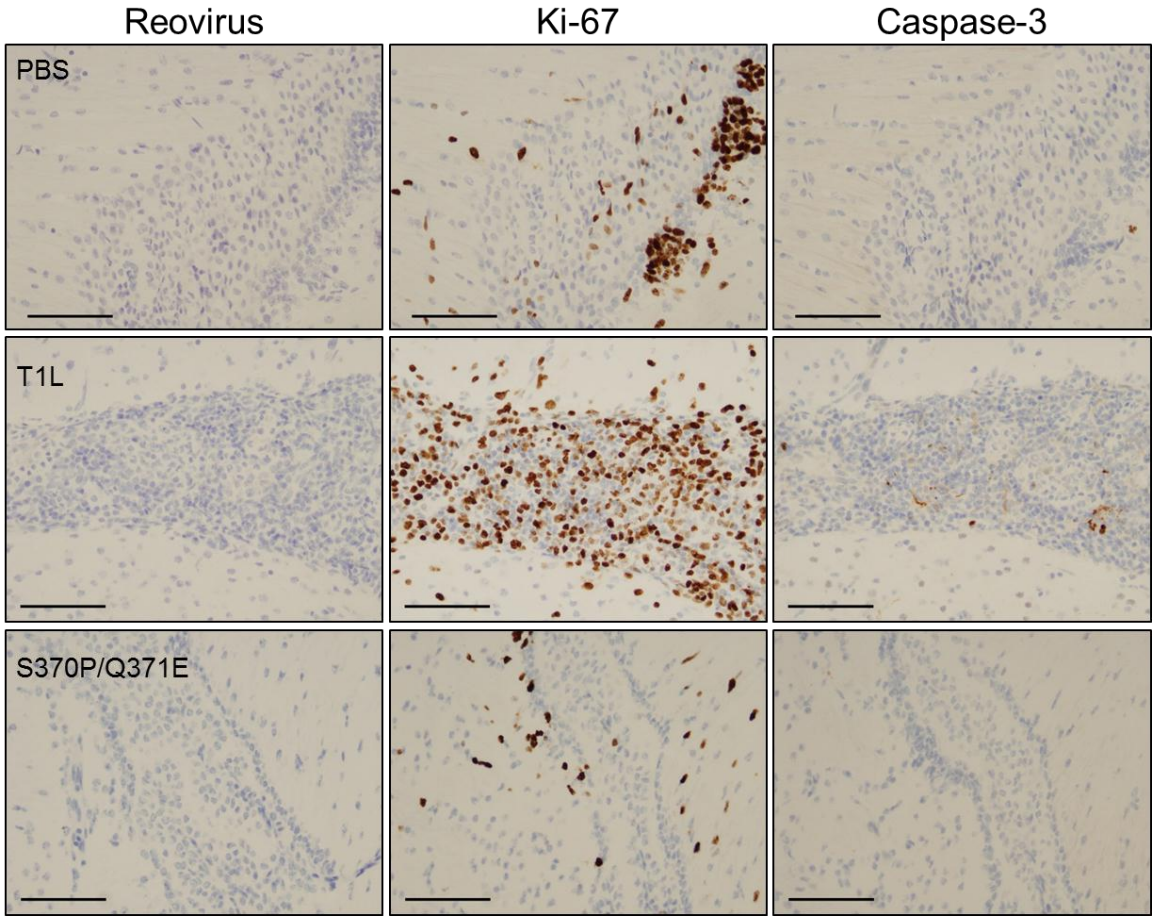
Reovirus
Ki-67
Caspase-3
PBS
T1L
S370P/Q371E

Figure IV-4. Brain histology twelve days following intracranial inoculation with either T1L or S370P/Q371E. Newborn mice were inoculated intracranially with PBS or 10^8 PFU of T1L or S370P/Q371E. Twelve days-post-inoculation, mice were euthanized, and brains were excised, fixed, and paraffin embedded. Samples were stained with H&E (**A**) to examine tissue pathology. Brain tissue of a mock (PBS) infected mouse displays a normal choroid plexus while the brain tissue of mice infected with wildtype virus (T1L) display a disorganized choroid plexus marked with enhanced cellular density within the capillary structure. The brain tissue of the mice infected with the mutant virus (S370P/Q371E) more closely resembles that of the PBS-inoculated mice. (**B**) Brain tissue was stained for reovirus antigen (left panel), Ki-67 as a marker for proliferation (middle panel), and caspase-3 (right panel). Reovirus antigen is not detectable in the choroid plexus at this time. The Ki-67 staining shows that T1L infected mice display enhanced proliferation within the capillary structure of the choroid plexus compared with mock and S370P/Q371E inoculated mice. The brown staining in the PBS-inoculated mice is outside of the capillary structure and likely represents a neural stem cell population. Caspase-3 staining is minimal.

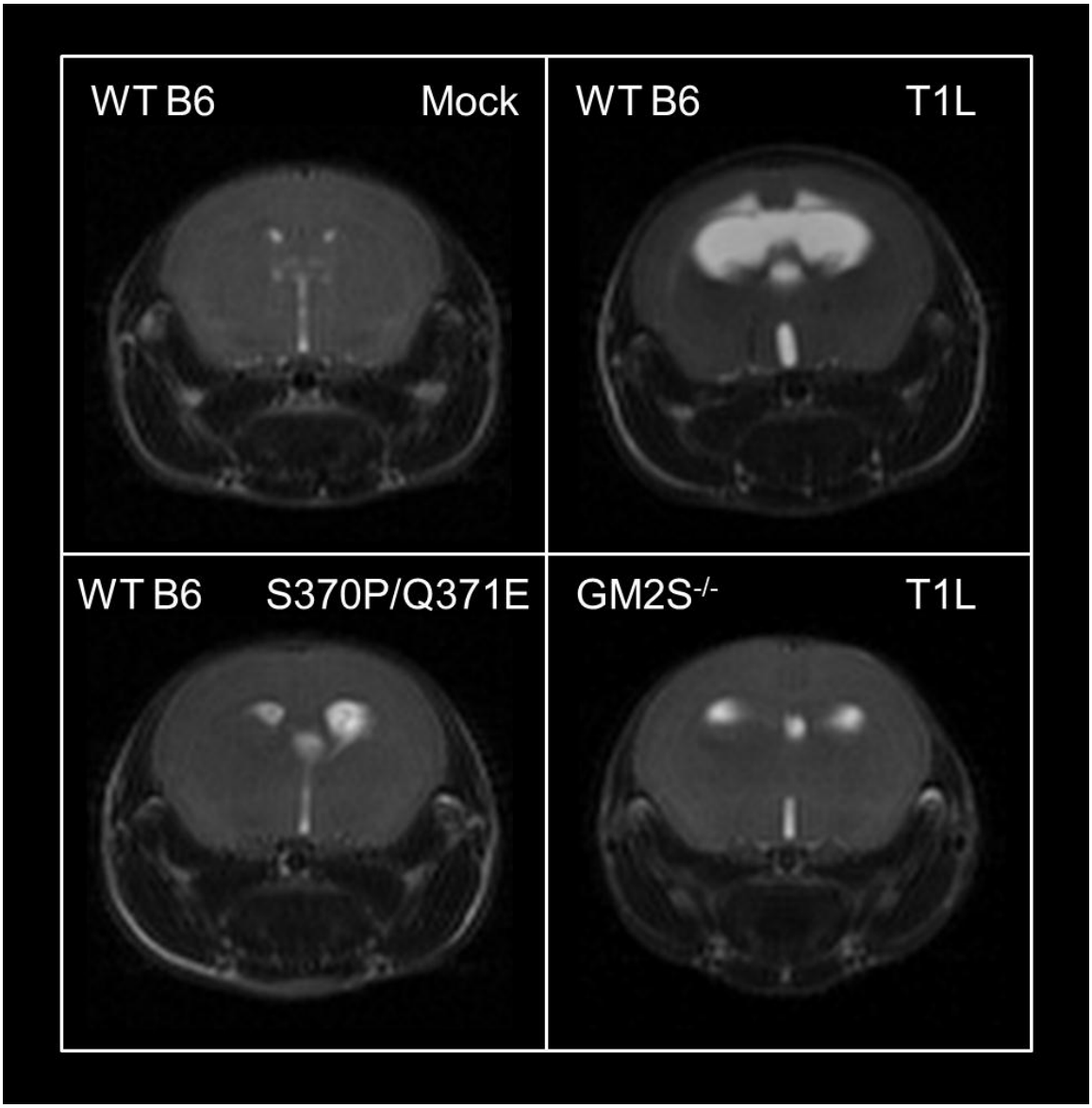

Figure IV-5. Glycan binding capacity influences hydrocephalus induction. Wildtype and GM2$^{-/-}$ mice were inoculated intracranially with 10^8 PFU of T1L or S370P/Q371E. Twenty-one days post-inoculation, T2-weighted magnetic resonance images were obtained. Coronal images of representative wildtype mice inoculated with PBS (top left), wildtype mice inoculated with T1L (top right), wildtype mice inoculated with S370P/Q371E (bottom left), and GM2$^{-/-}$ mice inoculated with T1L (bottom right) are shown. Cerebrospinal fluid appears white, indicating inflammation of the ventricles. Images were obtained from mice with the medium ventricular volume (n = 4-10 mice per group).

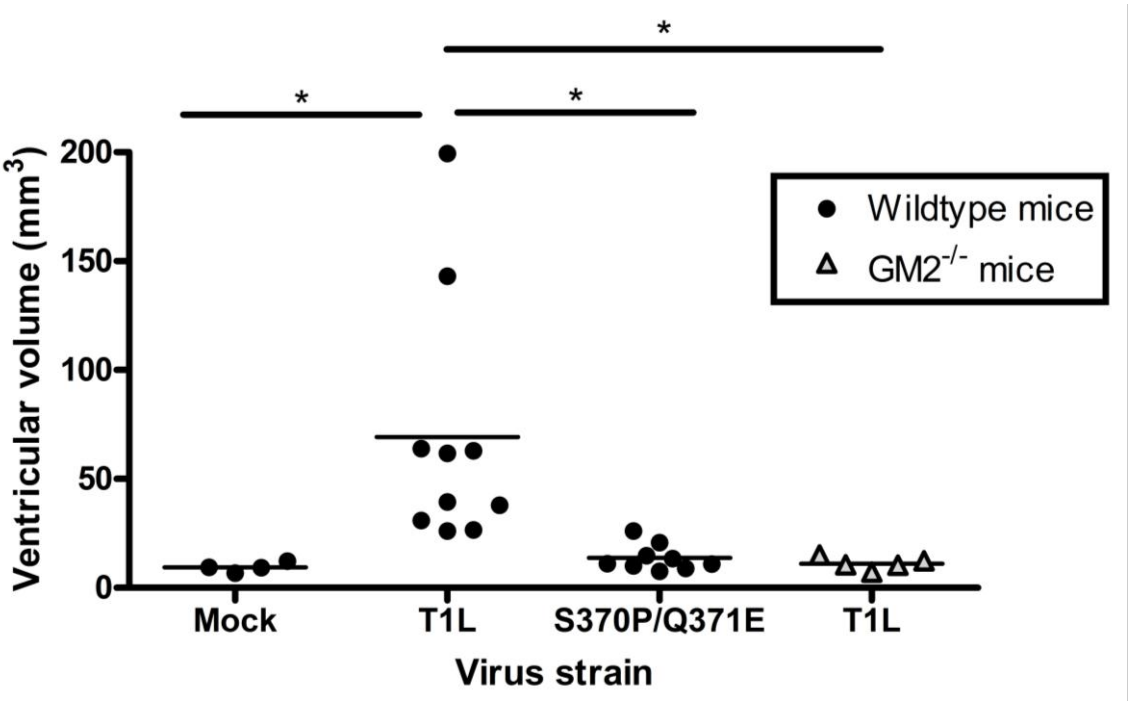

Figure IV-6. Glycan binding capacity influences ventricular volume. Ventricular volume was quantified from MRI images of reovirus-infected mice as described in the Figure 4 legend using Matlab. Each symbol represents the ventricular volume from a single mouse. Mean ventricular volume is indicated with a horizontal bar. *, $P < 0.05$ as quantified by a one-way ANOVA followed by Bonferroni's correction for multiple tests.

differ appreciably from mock-infected animals. This observation suggests that the capacity to bind GM2 enhances reovirus-mediated hydrocephalus.

Analysis of reovirus-induced hydrocephalus in mice lacking GM2 expression

To complement studies evaluating hydrocephalus induction by viruses that differ in the capacity to engage GM2, I analyzed the magnitude of hydrocephalus using mice that differ in expression of the GM2 glycan. I obtained mice that lack functional copies of the *galgt1* and *galgt2* genes on a C57Bl/6 background. The *galgt1* and *galgt2* genes encode the enzymes required to express the GM2 glycan on gangliosides and glycoproteins, respectively (172). Thus, *galgt1 x galgt2* double-knockout mice, herein referred to as $GM2^{-/-}$ mice, lack GM2 glycan expression on both gangliosides and glycoproteins (172, 173). These mice express GM3 but do not express gangliosides for which GM2 is a progenitor, such as GM1.

To test whether GM2 binding contributes to hydrocephalus, wildtype and $GM2^{-/-}$ mice were inoculated intracranially with T1L, and hydrocephalus was assessed using MRI 21 days post-inoculation. The severity of T1L mediated hydrocephalus, evidenced by visual examination of the MRIs (Figure IV-5) and quantification of the ventricular volume, (Figure IV-6) was more severe in wildtype mice than in $GM2^{-/-}$ mice. Taken together, these studies demonstrate that disruption of the σ1-GM2 interaction through manipulation of the viral GM2-binding site or host GM2 expression diminishes the severity of hydrocephalus caused by T1 reovirus.

The effect of GM2 binding capacity on viral dissemination and transmission

The glycan-binding site is conserved in the T1 reovirus strains for which sequence information is available (Figure IV-7). Therefore, I considered the possibility that glycan-binding capacity confers a fitness advantage such as enhancing dissemination within a host or spread between hosts. To determine whether glycan binding enhances dissemination, I co-inoculated two-to-three-day-old C57Bl/6 mice perorally with 10^2 PFU of T1L and 10^2 PFU of S370P/Q371E. Mice were euthanized 8 days post-inoculation and the intestine and brain were resected and homogenized. Organ homogenates were subject to plaque assay using L cells, and individual plaques from the intestine and brain of six mice were picked and passaged once in L cells prior to sequencing. T1L predominated in three of the six brains, while S370P/Q371E predominated in the remaining three brains (Figure IV-8A). A similar trend was observed in the intestine where T1L predominated in two of the six mice, and S370P/Q371E predominated in the remaining four mice (Figure IV-8B). Combined analysis of the virus stocks grown from the selected plaques demonstrates that both wildtype and mutant viruses are present in roughly equal proportion (Figure IV-8C). These findings suggest that glycan binding capacity does not influence reovirus dissemination within a host.

To determine whether GM2-binding capacity influences viral spread between hosts, I inoculated two newborn mice with 10^4 PFU of either T1L or S370P/Q371E and returned the infected animals to a cage with uninfected

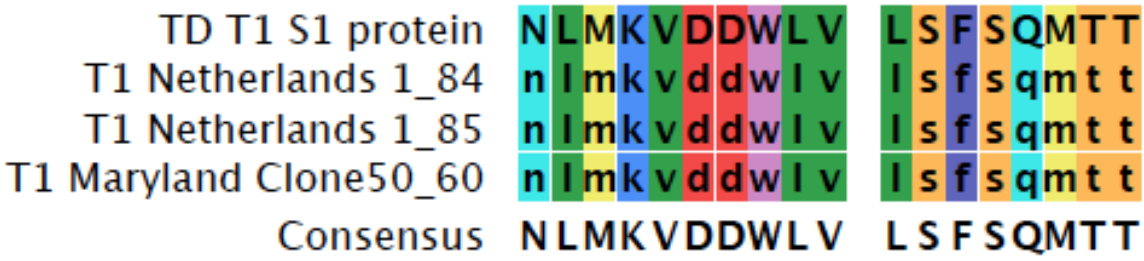

Figure IV-7. The GM2-binding site is conserved in T1 clinical isolates of T1 reovirus.

Sequence alignment of prototype strain T1L and three T1 reovirus clinical isolates reveals that the residues required for functional GM2 engagement (Val354, Ser370, and Gln371) are conserved in T1 reovirus strains.

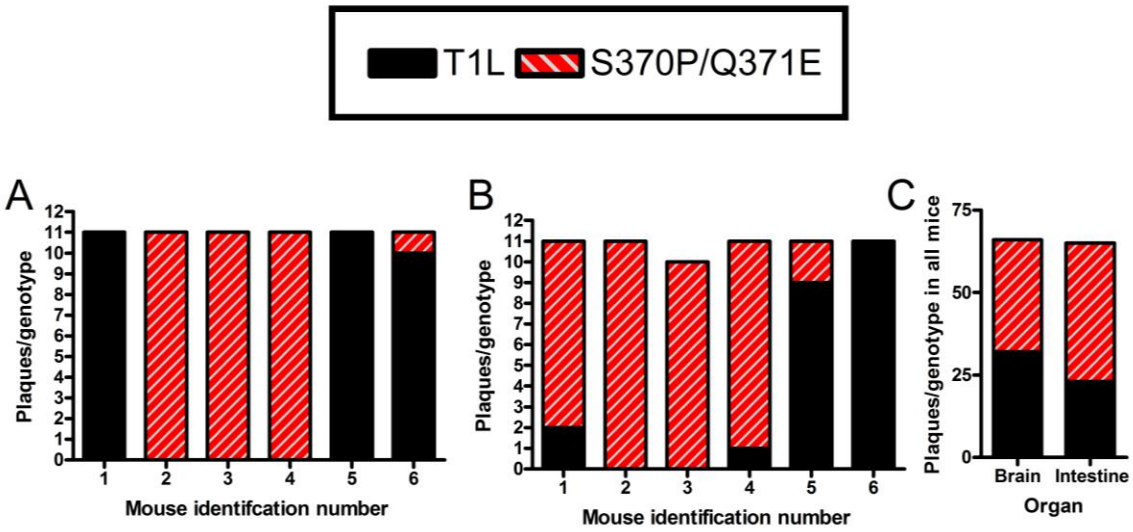

Figure IV-8. T1L and S370P/Q371E replicate comparably within a host. Newborn C57BL/6 mice were inoculated with 10^2 PFU of both T1L and S370P/Q371E. Eight-days post-inoculation, mice were euthanized, and intestine and brain were resected and homogenized. Homogenates were subject to plaque assay using L cells, 10-11 plaques per organ per mouse were picked randomly and passaged once on L cells. RNA was extracted from these viral stocks and subject to Sanger sequencing for the T1 S1 gene. The number of viral isolates from each strain in the (**A**) brain and (**B**) intestine per mouse are shown. The overall total number of plaques per strain in all mice combined is shown in (**C**). Differences between T1L and S370P/Q371E are not statistically significant as determined by ANOVA followed by Bonferroni's correction for multiple tests.

littermates. Eight days later, the mice were euthanized, and intestine, heart, and brain were excised and homogenized. Viral titer in organ homogenates prepared from inoculated and uninoculated mice was quantified by plaque assay. Both wildtype and S370P/Q371E viruses were transmitted to uninoculated littermates with equivalent efficiency (Figure IV-9), suggesting that GM2 engagement does not alter host-to-host transmission, at least in the setting of mice housed in the conditions used for this experiment.

Discussion

The main finding of this study is that wildtype T1L induces more severe hydrocephalus in wildtype mice than does the S370P/Q371E mutant virus. Concordantly, T1L induces less severe hydrocephalus in $GM2^{-/-}$ mice compared to wildtype mice (Figures IV-5 and IV-6). Previous studies of reovirus-induced hydrocephalus report cytoplasmic inclusion formation in the ependymal cells and choroid plexus and denuding of the ependymal layer (16, 106, 108). Reparative processes were reported to be evident including proliferation of astroglia and capillaries at sites of ependymal damage 10-12 days post-inoculation. This tissue grew into the ventricular cavities and obstructed the flow of cerebrospinal fluid (108). The ependymal layer does not regenerate in mammals of any age. However, reactive gliosis is sometimes observed to disrupt the existing ependymal cells during the damage response (174). Histological evaluation of samples from my study support these previous observations (Figure IV-4). Reovirus titer 12 days post-inoculation had subsided to levels undetectable by

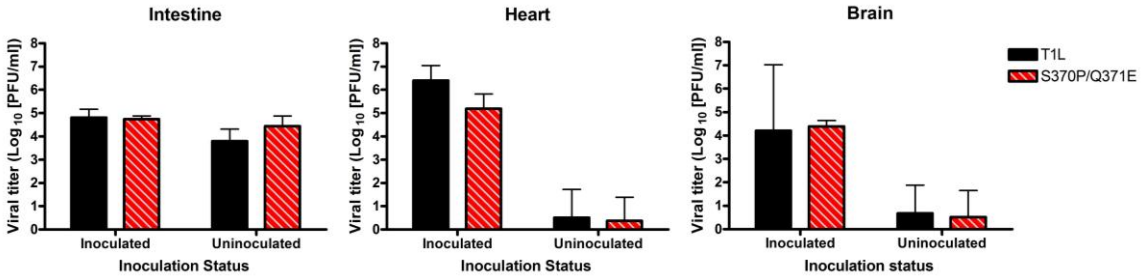

Figure IV-9. GM2 engagement does not appear to alter littermate transmission of T1 reovirus to uninoculated littermates.
In each cage, two newborn C57BL/6 mice were inoculated with 10^4 PFU of either T1L and S370P/Q371E and returned to their naïve littermates. Eight days later, mice were euthanized, and intestine, heart, and brain were excised and homogenized. Viral titers in organ homogenates from inoculated and uninoculated animals were quantified by plaque assay. No significant differences were observed between T1L and S370P/Q371E. Data represent 4-6 inoculated mice per virus and 18-21 uninoculated littermates.

immunohistochemistry. However, histopathological analysis showed a disorganized choroid plexus and enhanced cellular density within the ventricle of mice inoculated with wildtype virus. This phenotype was less severe in mice inoculated with the S370P/Q371E mutant virus. Accordingly, brain samples of wildtype mice inoculated with T1L showed enhanced Ki-67 staining (Figure IV-4), which is indicative of cellular proliferation. T1 reovirus also induces dilation of the lateral ventricles (16, 106, 108). This finding was recapitulated in wildtype mice inoculated with T1L, but disease was much less severe in mice inoculated with the GM2-binidng mutant and in mice that did not express the GM2 glycan. Taken together, these observations indicate that glycan binding is required for hydrocephalus caused by T1 reovirus.

While infection of mice with viruses that differ in the capacity to engage GM2 resulted in differences in disease, these viruses only differed modestly in viral replication efficiency (Figures IV-1 and IV-2). Titers produced by wildtype and mutant virus were comparable in the intestine and heart following peroral inoculation. T1L reached higher titers in the brain following peroral inoculation compared with the S370P/Q371E mutant. This result, coupled with the finding that T1L also reached higher titers in the brain than S370P/Q371E following intracranial inoculation, suggest that T1 σ1-GM2 interactions influence replication in the brain, but not dissemination to that site. Interestingly, histological analysis revealed that T1L spreads more efficiently than does S370P/Q371E to the contralateral hemisphere following intracranial inoculation (Figure IV-3).

Ideally, I would have inoculated $GM2^{-/-}$ and wildtype mice with T1L to determine whether expression of the GM2 glycan influences viral replication efficiency in organs targeted by reovirus. Unfortunately, the $GM2^{-/-}$ mice are not as healthy as their wildtype counterparts. Following 18 months of breeding (I lost many litters during parturition or nursing), I had five knockout pups that were used in the hydrocephalus study. Additional mice were not available for use in viral infectivity experiments. Nonetheless, these mice were a valuable resource and phenocopied results gathered using the S370P/Q371E mutant virus, thereby strengthening the overall conclusions of the study.

Viral titers in the brain were equilibrated at the doses used to assess hydrocephalus (Figure IV-2B), yet differences in disease manifestations were observed. The brain is comprised of several cell types, and it is possible that certain cell types, such as ependymal cells or choroid plexus cells, display altered glycan-dependent susceptibility to T1 reovirus. As these cells constitute only a small fraction of the total brain tissue, a viral plaque assay would not be sufficiently sensitive to detect differences in replication at such discrete sites. Differences in infectivity were not observed by immunohistochemistry, but the limit of detection of reovirus antigen by this technique is less than that of viral plaque assays. Therefore, it would be useful to determine whether explanted cultures of ependymal cells, choroid plexus epithelial cells, or both display GM2-dependent infectivity. Ependymal cells are difficult to cultivate and often do not survive for intervals sufficient to allow reovirus infection studies (Chappell and Dermody, unpublished). However, an immortalized ependymoma cell line,

XBD1425, is available (175). Additionally, a choroid plexus cell line, Z310, polarizes and expresses tight-junction markers (176). It would be informative to infect these cells with wildtype T1L and S370P/Q371E to determine whether GM2 binding capacity influences infectivity in these biologically relevant cell types. If so, it would be useful to establish whether the capacity of T1L to infect these cells is altered following neuraminidase treatment or incubation with soluble GM2. These studies would enhance a mechanistic understanding of T1 reovirus-induced hydrocephalus.

Glycan-binding capacity does not appear to influence viral spread within a host. Both T1L and S370P/Q371E spread efficiently from the intestine to sites of secondary replication following peroral inoculation with either virus (Figure IV-1). Additionally, co-infection experiments (Figure IV-8) suggest that glycan binding does not confer an advantage in viral spread. Following co-inoculation with T1L and S370P/Q371E both strains reached the brain in equivalent proportion. T1 reovirus spreads hematogenously, in contrast to T3 reovirus, which disseminates via hematogenous and neural routes (12, 177, 178). Proteinaceous receptor JAM-A is a key determinant of hematogenous spread (12) (Lai and Dermody, unpublished) and, thus, the finding that virus-GM2 interactions do not influence dissemination is not surprising and further supports the conclusion that JAM-A binding is sufficient for hematogenous dissemination.

The GM2-binding site is conserved in four sequenced isolates of T1 reovirus (Figure IV-7), suggesting that glycan binding confers some type of fitness advantage. The co-infection (Figure IV-8) and littermate transmission

experiments (Figure IV-9) demonstrate that GM2 engagement does not enhance spread within or between newborn mice under the conditions of my experimental protocol. It is possible that these conditions do not accurately reflect how reovirus is transmitted between hosts in nature. The day 8 time-point was selected because T1L produces peak titers at that time point following peroral inoculation. It would be informative to investigate early time points after inoculation to determine whether GM2-binding capacity enhances host-to-host spread during early rounds of viral replication. Such differences might not be evident by day 8 post-inoculation. Another possibility is that sequence data is available for too few strains of T1 reovirus. There are more sequences of T3 reovirus available, and analysis of these sequences indicates the presence of polymorphisms in the sialic-acid-binding site of T3 σ1 that disrupt glycan binding (7, 24, 179). It is possible that evaluation of additional strains of T1 reovirus would demonstrate polymorphisms in the GM2 binding-site of T1 σ1.

Differences in reovirus-mediated serotype-specific neurologic disease segregate with the S1 gene and are thought to be attributable to differences in receptor engagement. Results from this study, coupled with previous reports (139, 140), support this hypothesis. My findings demonstrate that T1L induces more severe hydrocephalus than does S370P/Q371E, which is deficient in glycan binding. Additionally, hydrocephalus was less severe following T1L infection of mice lacking the GM2 glycan compared with that induced in wildtype mice. T3 reoviruses differing only in the capacity to engage sialic acid differ in the

capacity to infect neurons and cause lethal encephalitis (140). Thus, glycan binding contributes to reovirus serotype-specific tropism and pathogenesis.

CHAPTER V

SUMMARY AND FUTURE DIRECTIONS

Summary

Viruses must bind to receptors expressed on the host cell-surface to initiate an infectious cycle. Consequentially, receptor expression governs the susceptibility of cells to viral infection and serves as a key determinant of pathogenesis. Viruses commonly engage multiple receptors to facilitate productive attachment and entry (1, 2, 4, 7, 11). However, the function of individual receptors in tropism and disease is not completely understood. To fill this knowledge gap, I designed and conducted experiments to identify a carbohydrate receptor for T1 reovirus (Chapter 2), define residues required for functional glycan engagement (Chapter 3), and determine the contribution of glycan-binding to T1 reovirus disease (Chapter 4). These experiments demonstrated that the T1 σ1 head domain interacts with the sialic acid and GalNAc moieties of the GM2 glycan. Moreover, reovirus engagement of GM2 is a determinant of hydrocephalus severity in neonatal mice.

The lack of an *in vitro* system had hindered studies of T1 reovirus-glycan interactions. A cell-culture system had been established for T3 reovirus-sialic acid interactions, as MEL cells are susceptible to only sialic-acid-binding T3

reovirus strains, whereas L cells support infection by all reovirus strains (7, 24). However, T1 reovirus cannot infect MEL cells. My work established a cell-culture system in which T1-sialic acid interactions could be evaluated *in vitro* as infection of MEFs by T1 reovirus is sensitive to neuraminidase (Figure II-1). This difference in the requirement for sialic acid engagement is likely due to differences in the expression of proteinaceous receptor JAM-A, as MEFs express less JAM-A than do L cells (Figure II-2). Levels of JAM-A on the L cell surface are likely sufficient to permit efficient attachment in the absence of sialic-acid-mediated adhesion strengthening.

Two independent glycan arrays identified the GM2 glycan as a specific sialylated carbohydrate bound by T1 reovirus (Figure II-5). Biological confirmation of this array data demonstrated that soluble GM2, but not related glycan GM3, blocks T1 reovirus infection of MEFs in a dose-dependent manner (Figure II-6). Soluble GM2 also blocks attachment (Figure II-7), suggesting that the decreased T1L infectivity in MEFs in the presence of soluble GM2 is the result of diminished viral binding to the cell surface. Moreover, soluble GM2 does not decrease the capacity of T3 reovirus to infect MEFs, suggesting that GM2 is a serotype-specific glycan receptor (Figure II-6C).

A combination of crystal structure determination, subsequent structure-guided mutagenesis, and experiments using mutant viruses with substitutions in the glycan-binding pocket, demonstrated that the T1 GM2-binding site is located within the σ1 head domain (Figures III-1 and III-2). NMR spectroscopy (Figure III-13) and X-ray crystallography (Figures III-1 and III-2) experiments established

that the sialic acid and GalNAc moieties of GM2 interact with T1 σ1. Residues Val354, Ser370, and Gln371 are required for σ1-GM2 engagement as V354F, S370P, Q371A, and Q371E mutations diminish hemagglutination capacity and infectivity of MEFs (Figures III-8 and III-7).

A S370P/Q371E mutant virus was selected for use in *in vivo* studies to establish the function of GM2 engagement in reovirus disease. This double-residue mutant virus replicates with wildtype efficiency in L cells (Figure III-9) and is neutralized by a T1 σ1 conformation-specific antibody (Figure III-10) yet displays impaired hemagglutination capacity and infectivity in MEFs relative to T1L. Unlike wildtype T1L, the T1 σ1-S370P/Q371E mutant protein does not interact with GM2 in solution as assessed by NMR spectroscopy (Figure III-13).

Analysis of wildtype T1L and S370P/Q371E viruses *in vivo* revealed that T1 reovirus-GM2 engagement is not required for viral dissemination, at least in newborn mice. Following peroral inoculation, both wildtype and mutant viruses replicate within the primary site of replication and disseminate with comparable efficiency to all organs sampled except the brain (Figure IV-1). The S370P/Q371E produces slightly lower viral titers in the brain following peroral inoculation. Additionally, S370P/Q371E produces lower titers than T1L in the brain following intracranial inoculation, suggesting that the GM2-binding mutant displays impaired capacity to replicate at that site (Figure IV-2). When higher doses of T1L and S370P/Q371E were delivered intracranially to assess hydrocephalus induction, the viruses produced equivalent titers (Figure IV-2),

although S370P/Q371E did not disseminate to the contralateral hemisphere as efficiently as did T1L (Figure IV-3).

Most remarkably in my studies, I found that T1 reovirus σ1-GM2 interactions contribute to serotype-specific disease. Hydrocephalus is more severe in wildtype mice inoculated with T1L compared with the disease induced in wildtype mice inoculated with S370P/Q371E. T1L also induced more severe hydrocephalus in wildtype mice compared with those lacking expression of the GM2 glycan, thereby mimicking the phenotype of limited hydrocephalus induced by S370P/Q371E in wildtype mice (Figures IV-5 and IV-6). These observations provide strong evidence that GM2-binding capacity is a T1 reovirus virulence determinant.

Virus-sialic acid interactions

Like other viruses, reoviruses engage sialyloligosaccharides to facilitate attachment and entry. Lessons learned from these experiments enhance our understanding of more general principles of virus-sialic acid interactions. Virus-sialic-acid binding was thought to rely mainly on the linkage type of the sialic acid, but this study and others (48, 53, 180) have recently demonstrated that this paradigm is overly simplistic. T3 reovirus binds α2,3-, α2,6-, and α2,8-linked sialic acid (9). However, while the GM2 glycan contains an α2,3-linked sialic acid, it does not diminish T3 infectivity in MEFs (Figure II-6) and was not identified on the glycan array as a potential ligand for T3 σ1 (Reiter, Stehle, Liu, and Feizi,

unpublished). Instead, the GM3 glycan was identified as a potential T3 σ1 ligand by glycan array. While preliminary experiments (data not shown) suggest that the GM3 glycan diminishes T3 infectivity on some cell types, this glycan did exhibit a dose-dependent decrease in T1 infectivity (Figure II-6). This finding is similar to observations made in studies of polyomaviruses, as BKPyV binds GD3, while SV40 binds GM1 (51), both of which contain α2,3-linked sialic acid. In this same vein, glycan array screening of seasonal H3N2 influenza virus strains did not identify a single moiety that bound all 45 strains tested (53). Moreover, the preference of the H3N2 influenza viruses for certain ligands appears to have changed over time. Binding preferenecs could be divided into six phases. Isolates from the late 1960s and early 1970s preferentially bind short and branched sialylated glycans, whereas more contemporary strains from the late 1980s to 2012 preferentially bind sialic acids attached to long polylactosamine chains with high avidity (53). Thus, while these human influenza viruses bind glycans containing α2,6-linked sialic acid, the sialic acid linkage type is insufficient to explain strain-specific binding preferences.

This study and others also shed light on the diversity of the molecular and structural basis of virus-sialic acid interactions. Studies of adenovirus (36), influenza virus (181-183), polyomavirus (51), rotavirus (22), and T1 (10) and T3 (9) reovirus demonstrate that in general, viruses primarily engage the sialic acid moiety using a modest number of contacts. Additional residues confer specificity for a given glycan. Mutation of very few residues is sufficient to alter virus-sialyloligosaccharide engagement (7, 9, 51, 74, 157). However, my study

demonstrates that interactions between the backbone of the viral attachment protein and the sialylated glycan can dictate virus-glycan biniding, which had not been observed previously (27).

While influenza virus, reovirus, and rotavirus all contain stalk-like attachment proteins, they engage glycans in distinct ways. The carbohydrate-binding site is conserved in all influenza subtypes and located in a shallow groove in HA1 (181). The orientation of Neu5Ac and its interactions with HA1 also are mostly conserved among all influenza virus strains (181-184). The glycosidic bond between sialic acid and galactose can be in the cis or trans conformation to accommodate different HA molecules (56).

Rotavirus attachment is mediated by the VP8* domain of the VP4 protein on the virion surface. Rotaviruses engage sialylated and non-sialylated glycans using the same site in VP8* (22). The crystal structure of rotavirus strain HAL 1166 VP8* in complex with human blood group antigen A (HBGA A) demonstrates that VP8* displays subtle modifications in its binding site that render it incapable of binding sialic acid and instead allow binding to HBGA A. The change in specificity is due to the insertion of a single amino acid, Asn187, in the binding pocket that reorients a neighboring tyrosine, Tyr188, such that its side chain would clash with sialic acid. At the same time, the reoriented tyrosine can now form hydrophobic contacts with HBGA A (22). As the remaining residues in the binding site are largely conserved among sialic acid-binding and non-sialic-acid-binding rotaviruses, this analysis demonstrates the substantial

effect on glycan specificity of an exceedingly subtle change in the receptor-binding pocket.

The reovirus serotypes have evolved distinct glycan-binding regions in the attachment proteins depending on viral serotype. The T1 σ1 head domain contacts GM2, whereas the body domain of T3 σ1 contacts sialylated glycans. This pattern is reminiscent of the glycan-binding properties of polyomaviruses, in which gangliosides bind loop structures on the attachment protein VP1. These loops are one of the few regions not conserved between strains and in turn dictate strain-dependent receptor specificity (51). Thus, it appears that viruses can engage similar receptors using similar binding sites as is seen for influenza virus, engage disparate glycans using the same site, as is seen for rotavirus, or engage different glycans using distinct sites on the attachment protein as is observed for reoviruses and polyomaviruses.

Glycan-binding capacity can alter viral disease outcome. For example, North American strains of Eastern equine encephalitis virus binds heparan sulfate unlike other clinical isolates. This virus is neurovirulent in humans and mice, yet, causes limited signs of febrile illness in humans. Studies in which the heparan sulfate binding site was disrupted revealed that the capacity to engage heparan sulfate leads to increased neurologic disease but decreased cytokine production and fever (19). This study and others (139, 140) demonstrate that sialylated glycan engagement contributes to serotype-specific reovirus disease. GM2 is a serotype-specific glycan bound by T1 reovirus σ1. Ablation of T1 reovirus-GM2 interactions by altering virus or host attenuates hydrocephalus in

mice (Figures IV-5 and IV-6). Studies of T3 reoviruses differing in the capacity to engage α2,3-, α2,6-, and α2,8-linked sialylated glycans demonstrate that sialic acid-binding T3 reoviruses infect neurons more efficiently and cause a more robust encephalitis than do non-sialic-acid-binding strains (140). Taken together, such studies suggest that glycan-binding is a determinant of serotype-specific disease.

Future Directions

Identify specific glycan receptors for T3 reovirus

While GM2 is a glycan engaged by T1 reovirus σ1, the precise glycan ligands bound by T3 reovirus σ1 are unknown. Glycan array screening identified potential glycan receptors of T3 σ1 including GM3, GM1, and GD1a, as well as several others (Reiss, Reiter, Stehle, Liu, and Feizi, unpublished). However, the biological relevance of these candidate receptors should validated using infectivity and cell-binding assays as I did for T1 reovirus.

Reovirus cell-type specific glycans

A comprehensive understanding of the role of glycan binding in reovirus tropism has been hindered by a lack of information about the specific glycans present on tissues targeted by reovirus. While we identified the GM2 glycan as a biologically relevant attachment mediator for T1 reovirus, tissue-specific expression of GM2 and other gangliosides is not well characterized. Analysis of

gangliosides was historically done by extracting glycolipids from cell and tissue homogenates and analyzing the glycan profile using thin-layer-chromatography (185). I attempted to use a GM2-specific antibody for immunohistochemistry analysis to determine whether T1 reovirus targets regions of the brain where GM2 is expressed. However, this antibody had not been previously used for immunohistochemistry, and I worked with the Vanderbilt Shared Pathology Resource Core to develop a staining protocol. However, despite several attempts, the staining was not specific when tested using wildtype and $GM2^{-/-}$ mice, and therefore, this antibody could not be used to assess the relationship between GM2 expression and reovirus targeting in the brain (data not shown).

New approaches are available to define the glycome expressed on specific cells and tissues. Mass spectrometry (186), microarray technology (187), and shotgun glycomics enable definition of glycan-expression profiles. In shotgun glycomics, glycolipids and glycoproteins are extracted from organs, tissues, or cells. The identity and composition of these glycans is determined by high throughput liquid chromatography (HPLC), and glycans are added to glycan arrays in equal concentrations. This approach (188, 189) could provide a framework for studying organ- and cell-type-specific glycan utilization by viruses, as recently demonstrated for swine influenza virus (189). This technology could be applied to the murine brain, and specifically ependymal and choroid plexus cells, to establish whether GM2 is a biologically relevant glycan engaged by T1 reovirus σ1 on those cell types. Such technology also could be used to define the glycans specifically engaged by T3 reovirus on neurons.

Defining the sufficiency of GM2 engagement in T1 reovirus tissue tropism

T1 and T3 reovirus engage sialyloligosaccharides using distinct domains of the attachment protein. However, it is not clear whether differential glycan-binding capacity is sufficient to potentiate serotype-specific reovirus-mediated disease. It would be informative to use viruses containing T1 and T3 σ1 with reciprocal exchanges of the glycan-binding sites. Specifically, the viruses should be on the T1 background to eliminate additional variables and contain a T1 or T3 S1 gene. The σ1 proteins on these viruses would comprise either the T1-GM2-binding site, the T3-sialic acid binding site, both the T1 and T3 glycan-binding sites, or neither binding site (Figure V-1). The capacity of soluble GM2 and GM3 to block infection of MEFs by these viruses as well as their capacity to agglutinate human and bovine erythrocytes could be used as *in vitro* correlates of serotype-specific glycan utilization. I propose that such viruses should be inoculated intracranially into newborn mice to assess hydrocephalus and encephalitis induction. If glycan-binding capacity is sufficient to induce serotype-specific tropism and disease, then viruses containing the GM2-binding site will cause hydrocephalus, irrespective of the rest of the S1 gene. Conversely, viruses containing a T3-sialic acid-binding site would have the capacity to infect neurons and cause encephalitis.

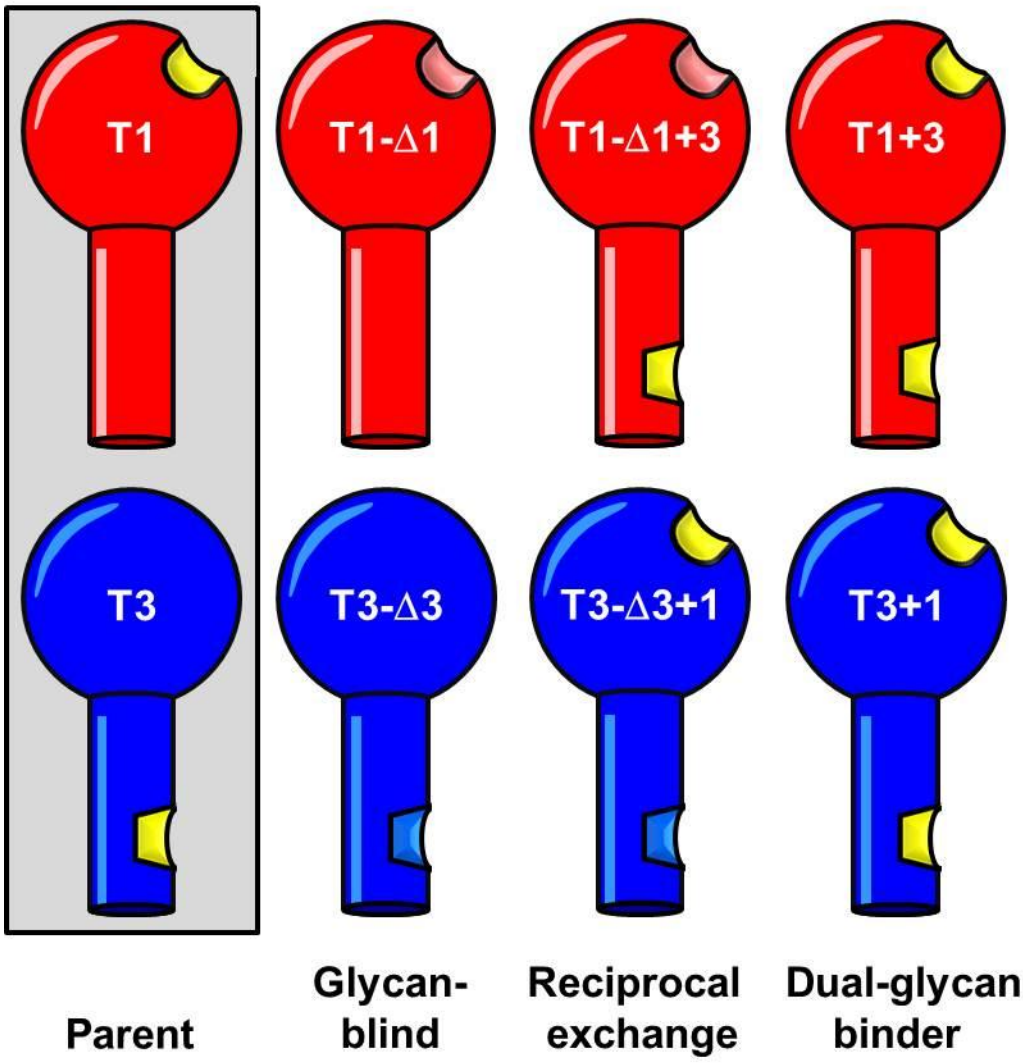

Figure V-1. Schematic of glycan-binding site chimeric σ1 proteins for studies of glycan utilization. Parent T1 (red) and T3 (blue) σ1 proteins (shaded) can be engineered on an otherwise T1 reovirus background to (i) lack binding to all glycan receptors (T1-Δ1, such as S370P/Q371E and T3-Δ3), (ii) lack binding to the parent receptor but gain binding to the glycan receptor of the heterologous serotype (T1-Δ1+3 and T3-Δ3+1), and (iii) bind both the T1 (GM2) and T3 glycans (T1+3 and T3+1). Glycan-binding domains are shown in yellow, ablated glycan-binding domains are shaded. (Figure adapted from Sutherland and Dermody, unpublished).

Understanding the contribution of other reovirus receptors to hydrocephalus

While wildtype mice infected with S370P/Q371E and GM2$^{-/-}$ mice infected with T1L developed less severe hydrocephalus than did wildtype mice (Figure IV-5), all mice developed some disease compared with control mice inoculated with PBS. This observation suggests that glycan-binding capacity contributes to hydrocephalus, but it is not the sole determinant of disease induction. Therefore, experiments should be conducted to test whether other known reovirus receptors contribute to hydrocephalus in mice. A function for the other known reovirus receptors, JAM-A and NgR1, in T1-mediated hydrocephalus has not been formally evaluated. It would be informative to inoculate JAM-A$^{-/-}$ and NgR1$^{-/-}$ mice with T1L and S370P/Q371E and assess ventricular volume by MRI to determine whether these receptors are required for hydrocephalus induction. The precedent for multiple receptors contributing to reovirus infection comes from studies of T3 reovirus infection of cortical neurons *in vitro*. While JAM-A is dispensable for infection of primary neurons in culture (12), fewer wildtype neurons are infected following inoculation with a sialic acid-binding mutant compared with wildtype virus. Additionally, T3 infectivity is diminished in NgR1$^{-/-}$ neurons compared with wildtype neurons and nearly ablated in NgR1$^{-/-}$ neurons infected with a T3 reovirus that cannot bind sialic acid. Collectively, these findings indicate that both NgR1 and sialic acid engagement are required for optimal infection of neurons (15).

The contribution of reovirus infection to human disease

Reovirus is infrequently associated with human disease. However, my findings raise the possibility that reovirus infection might be associated with hydrocephalus in human infants. The causes of congenital hydrocephalus in humans are not completely understood, but some prescription drugs (190) and viruses (191, 192) are thought to be potential triggers. In support of this hypothesis, analysis of brain samples from persons seropositive for mumps demonstrated that 65 percent of the mumps-infected brains displayed evidence of ependymitis (193). Additionally, a case-control study suggested that prenatal infection with cytomegalovirus was more prevalent in infants with hydrocephalus compared with healthy controls (191). However this study needs to be repeated with a larger sample size to assess statistical significance.

Most humans are seropositive for reovirus by five years of age (194), but the associations of reovirus infection with human disease are not well defined. T3 reovirus has been isolated from children with febrile and diarrheal illnesses (195). Additionally, T1 reovirus has been isolated from the brain of an infant who had died from hepatitis and encephalitis (196). However, reovirus strains also have been isolated from asymptomatic children (99). Therefore, it is not clear whether reovirus causes illness in humans. Viral etiology of disease in humans is difficult to definitively demonstrate compared with experimental animals. However, one study found that only a few of the twenty-seven healthy, young-adult volunteers inoculated with reovirus intranasally developed a mild febrile illness, and it was not clear whether reovirus was responsible for the symptoms (197).

It is plausible that T1 reovirus, like other viruses (191, 193), might be associated with congenital infection and hydrocephalus in humans. In support of this idea, T1 reovirus binds human ependymal cells *in vitro* (105) and causes hydrocephalus in newborn mice. It would be worthwhile to perform a case-control study of infants born with congenital hydrocephalus and those with no neurologic disease. As reovirus does not cause disease in adults, it is likely that the mother would be asymptomatic. Additionally, it may be informative to quantify IgG and IgM antibody titers in the serum of children with congenital hydrocephalus, healthy controls, and their mothers to determine whether reovirus antibody titers are higher in cases than controls. If true, this finding would suggest that reovirus infection contributes to congenital hydrocephalus in humans.

Therapeutic targeting of virus-sialic acid interactions

Sialic-acid-binding viruses include important human pathogens, such as adenovirus, influenza virus, and rotavirus, as well as viruses with therapeutic applications, such as adenovirus and reovirus, which are being tested as gene-delivery vectors and oncolytics. Therefore, manipulating these virus-sialic acid interactions may enhance therapeutic design and efficacy. For example, influenza virus attachment and release necessitate interactions with sialic acid and are potent antiviral targets. Structure-based therapeutic design led to the generation of oseltamivir (Tamiflu®) and zanamivir (Relenza®), which are sialic acid derivatives that inhibit influenza virus NA and block release of progeny virions(54, 55). Additionally, DAS181 (Fludase®) is a fusion of an epithelial

anchoring domain and a sialidase, which removes α2,3- and α2,6-linked sialic acid from the respiratory epithelium (198, 199). DAS181 is effective against influenza A and B strains *in vitro* (198), protects mice from lethal challenge with H1N1 (198), and protects mice post-exposure from H5N1 (199). Phase II clinical trials demonstrated that DAS181 reduced viral shedding in humans (200). Thus, both virus and host can provide antiviral targets for disruption of virus-sialic acid interactions. Knowledge gained from studies of virus-glycan binding may be particularly useful to retarget viruses either for use as gene delivery vehicles or oncolytics.

Reoviruses are naturally cytotoxic and preferentially infect transformed cells (201-204). Targeting of transformed cells coupled with the relative avirulence of these viruses in humans beyond the first few weeks of life makes reovirus an attractive candidate for oncolytic therapy. Phase I-II clinical trials have shown that reovirus strain T3 Dearing (Reolysin®) is safe and non-toxic even at high doses (142-144). T3 Dearing is now being tested in phase III clinical trials for the treatment of head and neck cancer (205).

It is not yet clear why reoviruses infect tumor cells more efficiently than untransformed cells, but it is possible that distribution, accessibility, and density of cellular receptors contribute to this process. Interestingly, the sialylation pattern in transformed cells is altered compared with that in untransformed cells (149). The abundance of sialic acid is increased in transformed cells owing to overexpression of sialyltransferases (145). Understanding reovirus-glycan interactions could improve tumor targeting. In this regard, a T3 Dearing virus

lacking the σ1 head domain is less toxic in the host yet retains its oncolytic potential (206). This truncated T3 reovirus cannot bind JAM-A, indicating that the virus must adhere to cells using only sialic acid or a receptor that has not been identified. It is possible that the altered glycan profile of cancer cells allows all three sialic-acid-binding sites of the T3 σ1 trimer to be occupied, thereby enhancing the avidity through the multivalency of the virus. In support of this idea, human glioblastoma cells grown in standard culture conditions require JAM-A binding for reovirus infection, but in spheroid cultures of these glioblastoma cells, which more closely resemble tumors in humans, reovirus infection is independent of JAM-A expression (207), suggesting that other factors, such as sialylated glycans, mediate attachment of reovirus to tumor cells.

Structural studies of reovirus σ1-sialic acid interactions (9, 10) coupled with structure-guided mutagenesis (41, 151) can facilitate the generation of strains with increased affinity for sialic acids that may have enhanced tumor specificity and oncolytic potential. Some tumor cells overexpress gangliosides such as GM2 (145, 149). Humanized antibodies directed against GM2 prevent the formation of organ metastases in mice with small-cell lung cancer (150). It is possible that ganglioside overexpression in tumor cells alters the susceptibility of certain cancers to reovirus infection. T1 reovirus has not been tested for oncolytic capacity, but these observations about glycan expression on tumors provide sufficient rationale to initiate such experiments. Another possible approach would be to engineer an oncolytic T3 reovirus that contains the T1-GM2-binding site. Such a virus might have enhanced targeting to GM2-expressing tumor cells.

Thus, understanding the molecular basis of reovirus-glycan interactions might improve the design of effective oncolytics.

Conclusions

Work presented in this thesis enhances an understanding of the molecular basis of T1 σ1-carbohydrate interactions, defines the function of GM2 engagement in T1 reovirus-mediated hydrocephalus, and illuminates more general principles of virus-glycan interactions. Yet, perhaps the greatest contribution to the field comes in new questions raised by this research. Using knowledge gained from these studies, it is now possible to elucidate the function of glycan binding in reovirus serotype-specific neurologic disease and determine how multiple reovirus attachment mediators work in concert to infect cells within the CNS. Additionally, as glycomics technology continues to improve, it will be fascinating to define cell- and tissue-specific glycan utilization by T1 reovirus and other viruses to establish how intricate glycan-binding preferences displayed by viruses function in tropism and pathogenesis. Reovirus also is being evaluated in clinical trials as an adjunct to conventional chemotherapy for the treatment of cancer. Since certain cancer cells display altered glycan profiles (145), it is possible that manipulation of reovirus-glycan engagement will enhance therapeutic efficacy.

CHAPTER VI

MATERIALS AND METHODS

Cells

Spinner adapted murine L cells were grown in suspension culture in Joklik's minimum essential medium (Lonza) supplemented to contain 5% fetal bovine serum (FBS) (Gibco), 2 mM L-glutamine, 100 U/mL penicillin, 100 µg/mL streptomycin (Invitrogen), and 25 ng/mL amphotericin B (Sigma-Aldrich). MEFs were generated from C57/BL6 mice at embryonic day 13.5 as described (113, 208). MEFs were maintained in Dulbecco's modified Eagle's minimum essential medium (DMEM) (Gibco) supplemented to contain 10% FBS, 2 mM L-glutamine, 100 U/ml penicillin, 100 µg/mL streptomycin, 1X MEM nonessential amino acids (Sigma-Aldrich), 20 mM HEPES, and 0.1 mM 2-mercaptoethanol (Sigma-Aldrich). Cells at passages 3-6 were used in this study. HeLa S3 cells were maintained in DMEM supplemented to contain 10% FBS, 2mM L-glutamine, 100 U/mL penicillin, 100 µg/ml streptomycin, and 25 ng/mL amphotericin B.

Viruses and Plasmid-Based Reovirus Rescue

Viruses were generated using plasmid-based reverse genetics (41, 151). BHK-T7 cells (5×10^5) were seeded in 60 mm tissue-culture dishes (Corning) and allowed to incubate at 37°C overnight. OptiMEM (Invitrogen) (0.75 ml) was mixed with 53.25 µl TransIT-LT1 transfection reagent (Mirus) and incubated at RT

for 20 min. Plasmid constructs representing cloned gene segments from the T1L genome, pT7S1 T1L, pT7S2 T1L, pT7L3S3 T1L, pT7S4 T1L, pT7M1 T1L, pT7L1M2 T1L, and pT7L2M3 T1L were mixed into the OptiMEM/TransIT-LT solution. Equal amounts of each plasmid were added for a total of 17.75 μg DNA. The plasmid-transfection solution was added to BHK-T7 cells and incubated for 3-5 days. Following two freeze-thaw cycles, recombinant viruses were isolated by plaque purification using L-cell monolayers (117). Purified virions were generated using second-passage L cell-lysate stocks. Viral particles were vertrel-extracted from infected cell lysates and layered onto 1.2 to 1.4 g/cm^3 CsCl gradients and centrifuged at 62,000 x g for 18 h. Bands were collected and dialyzed exhaustively in virion-storage buffer as described (178, 209). To generate mutant viruses, resides V354, S370, Q371, and M372 in the S1 gene plasmid were altered by QuickChange (Stratagene) site-directed mutagenesis. S1 gene sequences were confirmed using the OneStep RTPCR kit (Qiagen), gene-specific primers, and viral dsRNA extracted from infected L cells (Trizol, Invitrogen). Primer sequences are provided in Table VI-1. Sanger sequencing was performed using purified PCR products (Gene Hunter and Vanderbilt Sequencing Core). Genotypes were confirmed by electrophoresis of viral particles in 4-to-20% gradient sodium dodecyl sulfate polyacrylamide gels stained with ethidium bromide and visualized by UV illumination(210). Particle concentrations were determined using the conversion 1 AU_{260} = 2.1 x 10^{12} particles (117). Viral titers were quantified by plaque assay(117) or fluorescent focus assay (11).

Primer and Direction	Direction	Sequence 5' → 3'
BAC-1	Forward	AACCATCTCGCAAATAAATA
BAC-2	Reverse	ACGCACAGAATCTAGCGCTT
S1F	Forward	GGATGCATCTCTCATTACAGAGATACG
S1R	Reverse	GCCGAGGGTTCGCGCTAGATTC
V354F	Forward	CACCCACAATTGAGTTGGAGAGCAAATTTCACTTTGAATTTGA
V354F	Reverse	TCAAATTCAAAGTGAAATTTGCTCTCCAACTCAATTGTGGGTG
V354L	Forward	ACCCACAATTGAGTTGGAGAGCAAATCTCACTTTGAATTTG
V354L	Reverse	CAAATTCAAAGTGAGATTTGCTCTCCAACTCAATTGTGGGT
S370P	Forward	GGTTGGTGTTGAGCTTTCCTCAGATGACGACTAAC
S370P	Reverse	GTTAGTCGTCATCTGAGGAAAGCTCAACACCAACC
Q371A	Forward	GGTGTTGAGCTTTTCTGCGATGACGACTAACTC
Q371A	Reverse	GAGTTAGTCGTCATCGCAGAAAAGCTCAACACC
Q371E	Forward	GGTGTTGAGCTTTTCTGAGATGACGACTAACTC
Q371E	Reverse	GAGTTAGTCGTCATCTCAGAAAAGCTCAACACC
M372F	Forward	GGTGTTGAGCTTTTCTCAGTTCACGACTAACTCAATAATGGC
M372F	Reverse	GCCATTATTGAGTTAGTCGTGAACTGAGAAAAGCTCAACACC
M372L	Forward	GGTGTTGAGCTTTTCTCAGTTGACGACTAACTCAATAATG
M372L	Reverse	CATTATTGAGTTAGTCGTCAACTGAGAAAAGCTCAACACC
S370P/Q371A	Forward	GTTGGTGTTGAGCTTTCCTGCGATGACGACTAACTC
S370P/Q371A	Reverse	GAGTTAGTCGTCATCGCAGGAAAGCTCAACACCAAC
S370P/Q371E	Forward	GGTTGGTGTTGAGCTTTCCTGAGATGACGACTAACTC
S370P/Q371E	Reverse	GAGTTAGTCGTCATCTCAGGAAAGCTCAACACCAACC
S370P/Q371A/M372F	Forward	GATTGGTTGGTGTTGAGCTTTCCTGCGTTCACGACTAACTCAATAATGGCAG
S370P/Q371A/M372F	Reverse	CTGCCATTATTGAGTTAGTCGTGAACGCAGGAAAGCTCAACACCAACCAATC
S370P/Q371A/M372F/T374G	Forward	GATTGGTTGGTGTTGAGCTTTCCTGCGTTCACGGGTAACTCAATAATGGCAGATGGG
S370P/Q371A/M372F/T374G	Reverse	CCCATCTGCCATTATTGAGTTACCCGTGAACGCAGGAAAGCTCAACACCAACCAATC
F369L/S370P/Q371A/M372F/T374G	Forward	GATGATTGGTTGGTGTTGAGCTTGCCTGCGTTCGATGGTAACTCAATAATGGCAGATGGG
F369L/S370P/Q371A/M372F/T374G	Reverse	CCCATCTGCCATTATTGAGTTACCATCGAACGCAGGCAAGCTCAACACCAACCAATCATC

Table VI-1. Primers used in these studies. The sequences of the primers used for wildtype and mutant virus generation and sequencing are shown.

Antibodies

Polyclonal immunoglobulin G (IgG) raised against T1L and T3D was used to stain for reovirus antigen (211). Alexa-488 conjugated goat anti-rabbit antibody (Invitrogen) was used as a secondary antibody. Monoclonal rat anti-mouse JAM-A (Abcam, clone H202-106) was used to stain for JAM-A expression followed by goat anti-rat secondary antibody conjugated to Alexa-488 (Invitrogen). Conformation-sensitive neutralizing mAb 5C6 specific for T1L (155) was used in neutralization assays as described (212). Ki-67 (Vanderbilt University Histology Core) was used as a marker for cell proliferation. Anti-caspase 3 (Vanderbilt University Histology Core) was used as a marker for apoptosis. Polyclonal rabbit ganglioside GM2-specific antiserum (EMD Millipore) was used to stain for GM2.

Infectivity Studies

L cells (10^5) or MEFs (5×10^4) were incubated in 24-well plates (Costar) at 37°C overnight. To evaluate the importance of sialic acid engagement in T1L infection, cell monolayers were treated with 100 mU/ml of *A. ureafaciens* neuraminidase diluted in PBS (MP Biomedicals, LLC) or PBS alone (mock) at RT for 1 h prior to virus adsorption at an MOI of 1 PFU/cell in L cells or 100 PFU/cell (as titered in L cells) in MEFs. Following incubation at RT for 1 h, the inoculum was removed, and cells were washed twice with PBS and incubated at 37°C for 20 h. Cells were fixed in methanol and visualized by indirect immunofluorescence (11) with the addition of a DAPI stain to quantify cell nuclei. Cells were blocked in

PBS supplemented to contain 5% bovine serum albumin (BSA) (Sigma). Infected cells were detected by staining with reovirus polyclonal antiserum diluted 1:1000 and secondary Alexa-488 goat anti-rabbit Ig 1:1000 (Invitrogen). Nuclei were quantified using DAPI (1:1000). All antibodies were diluted in PBS supplemented to contain 0.5% Triton X-100. Infectivity studies were performed in triplicate wells. Three fields of view per well were quantified using the Axiovert 200 fluorescence microscope (Carl Zeiss).

To determine the effect of soluble lectins on viral infectivity, cells were incubated with 10 μg/ml of *Sambucs nigra*, *Maackia Amurensis*, or *Aleuria Aurantia* lectins (Vector Labs) at room temperature for 1 h. Excess lectins were removed, and virus was adsorbed to MEFs (MOI of 100 PFU/cell as titered on L cells) at room temperature for 1 h. Cells were washed twice, and infectivity was determined by indirect immunofluorescence.

To determine the effect of soluble glycans on infectivity, virus was incubated with 5mM 3'SL (Carbosynth and Sigma Aldrich) or various concentrations of GM2 or GM3 glycan (Elicityl) at room temperature for 1 h. The virus-glycan mixture was adsorbed to MEFs (MOI of 100 PFU/cell as titered on L cells) at room temperature for 1 h. Cells were washed twice, and infectivity was determined by indirect immunofluorescence.

JAM-A Expression

To determine the relative amount of JAM-A on L cells and MEFs, 5 x 10^5 cells were stained with rat anti-mouse JAM-A at a dilution of 1:200 followed by

staining with Alexa-488 labeled goat anti-rat Ig at 1:1000. All staining was done in PBS supplemented to contain 2% FBS. Fluorescence was quantified using an LSRII (BD, Vanderbilt University Flow Cytometry Shared Resource). Mean fluorescence intensity of a forward and side scatter gated population was determined using FlowJo software (Treestar).

T1L σ1 Protein Expression and Purification

Construct $\sigma1_{long}$ comprises the three most C-terminal predicted β-spirals of T1L σ1 and the head domain (amino acids 261-470). Construct $\sigma1_{short}$ comprises the most C-terminal predicted β-spiral of T1L σ1 and the head domain (amino acids 300-470). Expression and purification of T1L $\sigma1_{long}$ and T1L $\sigma1_{short}$ were facilitated by attaching a trimeric version of the GCN4 leucine zipper (10) to the N-terminus of the σ1 sequence, similar to the strategy we used to express T3D σ1 (9). The σ1 construct was cloned into the pQE-80L expression vector (Qiagen), which includes a non-cleavable N-terminal His_6-tag. The protein was expressed in *E. coli* Rosetta 2 (DE3) (Novagen) by autoinduction at 20°C for 48 to 72 h. Bacteria were lysed using an EmulsiFlex (Avestin) homogenizer and purified via Ni-affinity chromatography (His-Trap FF column, GE Healthcare). chromatography (His-Trap FF column, GE Healthcare). The fusion protein was eluted from the column, and the protein solution was desalted using a PD10 desalting column (GE Healthcare). The GCN4 domain and the His_6-tag were removed from the fusion protein using 1 μg trypsin per mg protein at 20°C for 4 h.

The resultant products were subjected to size-exclusion chromatography (Superdex 200) to remove the tags, trypsin, and other minor impurities. Undigested versions of both constructs were used for glycan array screening. STD NMR experiments were performed using $\sigma1_{long}$. Both constructs were used for structural analysis. Uncleaved $\sigma1_{short}$ yielded crystals diffracting to 2.6 Å resolution. This higher resolution structure was used as a reference model for refinement of the lower-resolution structures of cleaved $\sigma1_{long}$ in complex with the GM2 glycan.

Glycan Microarray Analyses

Microarrays were composed of lipid-linked oligosaccharide probes, neoglycolipids (NGLs) and glycolipids, robotically printed on nitrocellulose-coated glass slides at 2 and 7 fmol per spot using a non-contact instrument, and analyses were performed as described (10). T1L $\sigma1_{long}$, was used in the first glycan array comprising 124 oligosaccharide probes (5 non-sialylated and 119 sialylated, Glycosciences Array Set 40-41), at 5 fmol per spot T1L $\sigma1_{short}$, was used on the second array, designed in the Feizi laboratory (in house designation Ganglioside Dose Response Array set 1) comprising 21 ganglioside-related probes each arrayed at four levels: 0.3, 0.8, 1.7 and 5.0 fmol/spot.

For the initial analysis of His-tagged T1L $\sigma1_{long}$, the protein was incubated with mouse monoclonal anti-poly-histidine (Ab1) and biotinylated anti-mouse IgG antibodies (Ab2) (both antibodies from Sigma) at a ratio of 4:2:1 (by weight). The $\sigma1_{long}$-antibody complexes were prepared by preincubating Ab1 with Ab2 at

ambient temperature for 15 min, followed by addition of His-tagged T1L $\sigma1_{long}$ and incubation on ice for 15 min. The $\sigma1_{long}$-antibody complexes were diluted in 5 mM HEPES (pH 7.4), 150 mM NaCl, 0.3% (v/v) Blocker Casein (Pierce), 0.3% (w/v) bovine serum albumin (Sigma), 5 mM $CaCl_2$ and 40 mM imidazole (referred to as HBS-Casein/BSA-imidazole), to provide a final $\sigma1_{long}$ concentration of 150 µg/ml, and overlaid onto the arrays at 20 °C for 2 h. Binding was detected using Alexa Fluor 647-labeled streptavidin (Molecular Probes) at 1 µg/ml. Microarray data analyses and presentation were facilitated using dedicated software as described (10).

For the analyses of His-tagged T1L $\sigma1_{short}$, different assay conditions were evaluated with and without complexation (not shown). The condition selected as optimal was without precomplexation. His-tagged $\sigma1_{short}$ was diluted in HBS-Casein/BSA-imidazole, overlaid at 300 µg/ml, followed by incubation with Ab1 and Ab2 (each at 10 mg/ml, precomplexed at ambient temperature for 15 min). Binding was detected using Alexa Fluor 647-labeled streptavidin.

Crystallization, X-Ray Structure Determination, and Refinement

Crystals of uncleaved $\sigma1_{short}$ formed in 0.1 M MES/imidazole (pH 6.5), 10% PEG 4000, 20 % glycerol, 0.02 M sodium formate, 0.02 M ammonium acetate, 0.02 M trisodium citrate, 0.02 M sodium potassium L-tartrate, 0.02 M sodium oxamate at 4°C using the sitting-drop-vapor-diffusion method. No additional cryoprotection was necessary. Crystals of $\sigma1_{long}$ formed in 0.1 M Na cacodylate (pH 6.0-6.6), 1.2-1.5 M $(NH_4)_2SO_4$ at 4°C using the sitting-drop-vapor-

diffusion method. For preparation of complexes, these crystals were transferred to 20 mM GM2 (Elicityl) for soaking in the crystallization solution for 5-10 min. Prior to flash-freezing, the crystals were transferred to a solution containing 0.1 M Na cacodylate, 1.34 M $(NH_4)_2SO_4$, 25% glycerol, and 20 mM GM2 or GM3 glycan.

The crystals belonged to space group $P3_221$ and contained one trimer in the asymmetric unit. A complete data set was collected at the Swiss Light Source, beamline X06SA. XDS was used to index and scale the reflection data. The structure was determined by molecular replacement with Phaser (CCP4) using the coordinates of T1L σ1 derived from the previously determined T1L σ1-JAM-A complex structure as a search model (130). Manual model building was carried out using coot. Structural refinement was performed using Refmac5 (CCP4), Phenix, and autoBUSTER.

Refinement of the ligands was performed using the CCP4 library and user-defined constraints. Structure images were created using PyMOL. Coordinates and structure factors of the complex have been deposited in the Protein Data Bank by Dr. Thilo Stehle with accession code 4GU3 (T1L-σ1-GM2 glycan complex).

Sequence and Structural Analysis

Sequence alignments were performed using T-Coffee and analyzed using Jalview (10). Structure alignments were calculated by secondary-structure matching (SSM) superposition in coot. The Ramachandran plot was generated

with Rampage (CCP4). Buried surface areas were calculated using AreaImol (CCP4) (10). Sequence analysis of available reovirus strains were aligned using CLC sequence viewer.

Viral Replication Assays

Confluent monolayers of L cells in 24-well plates (Corning) were adsorbed in triplicate with the various reovirus strains at room temperature for 1 h in PBS. Cells were washed twice with PBS, fresh medium was added, and cells were incubated at 37°C for various intervals. Cells were frozen and thawed twice prior to quantification of viral titer by plaque assay using L cells (117). Viral yield was calculated using the formula $Log_{10}yield_{tx} = log_{10}\ (PFU/mL)_{tx} - log_{10}\ (PFU/mL)_0$, where t is the time post-inoculation.

Conformation-Specific Antibody Neutralization

The capacity of T1 σ1 conformation-specific antibody to block wildtype and mutant virus infectivity was assessed by incubating virus strains with 10 μg/ml of 5C6 or an mouse IgG2α isotype control at room temperature for 1 h prior to adsorption onto L929 cells seeded in confluent monolayers in 24-well plates (Corning). Cells were inoculated with the virus antibody mixture at room temperature for 1 h. Cells were washed twice with PBS and fresh medium added. After incubation at 37°C for 20 h, cells were fixed and infectivity determined by indirect immunofluorescence (Figure III-6) or flow cytometry (Figure III-10).

Hemagglutination Assay

Purified reovirus virions (10^{11} particles) were distributed into 96-well U-bottom microtiter plates (Costar) and serially diluted twofold in 0.05 ml of PBS. Human type O erythrocytes (Vanderbilt University Blood Bank) were washed twice with PBS and resuspended at a concentration of 1% (vol/vol). In some assays, erythrocytes were treated with PBS or *A. ureafaciens* neuraminidase (MP Biomedicals, LLC) at room temperature for 1 h prior to virus adsorption. Erythrocytes (0.05 ml) were added to wells containing virus particles and incubated at 4°C for 3 h. A partial or complete shield of erythrocytes on the well bottom was interpreted as a positive HA result; a smooth, round button of erythrocytes was interpreted as a negative result. HA titer is expressed as 10^{11} particles divided by the number of particles/HA unit. One HA unit equals the number of particles sufficient to produce HA.

Hemagglutination Inhibition Assay

Human erythrocytes were treated with *A. ureafaciens* neuraminidase at room temperature for 1 h, incubated with 4 HA units of various virus strains, incubated at 4°C for 3 h, and scored for agglutination.

STD NMR Spectroscopy

NMR spectra were recorded using 3 mm tubes and a Bruker AVIII-600 spectrometer equipped with a room temperature probe head at 283 K and

processed with TOPSPIN 3.0 (Bruker). Samples containing 2 mM GM2 glycan (Elicityl), 20 mM potassium phosphate (pH 7.4), and 150 mM NaCl with and without 16.8 μM of T1L σ1 or the mutant proteins were used for the STD NMR measurements and the frequency control, respectively. Samples were prepared in D_2O, and no additional water suppression was used to preserve the anomeric proton signals. The sample without protein also was used for spectral assignment. The off- and on-resonance irradiation frequencies were set to -30 ppm and 7.3 ppm, respectively. The irradiation power of the selective pulses was 57 Hz, the saturation time was 2 s, and the total relaxation delay was 3 s. A 50 ms continuous-wave spin-lock pulse with a strength of 3.2 kHz was employed to suppress residual protein signals. Spectra were multiplied with a Gaussian window function prior to Fourier transformation. Spectra were referenced using HDO as an internal standard as described (10).

Virus Attachment by Flow Cytometry

MEFs were adsorbed with reovirus strains at 4°C for 1 h to prevent internalization. Cells were washed twice in PBS and stained with Alexa-647 labeled reovirus antiserum. Labeling was performed using the AlexaFluor® Antibody Labeling kit (Molecular Probes) according to manufacturer's instructions. The percentage of cells bound by virus was quantified using an LSR-II flow cytometer (Vanderbilt Flow Cytometry Core). Analysis was performed using FlowJo software (Tree Star).

Infection of Mice

C57Bl/6 mice were obtained from the Jackson Laboratory to establish a breeding colony at Vanderbilt University. The $GM2^{-/-}$ mice lack functional copies of *galgt1* and *galgt2*. These mice are on a C57Bl/6 background and were provided by Dr. Dapeng Zhou (MD Anderson Cancer Center). Two-to-three day old mice were inoculated perorally or intracranially with reovirus diluted in PBS. For co-infection experiments, strains were mixed and inoculated into mice. Peroral inoculations (50 µL) were administered using a Hamilton syringe, 30-gauge needle, and Intramedic PE-10 polyethylene tubing (BD Biosciences) (12). Intracranial inoculations (5 µL) were delivered into the right cerebral hemisphere using a Hamilton syringe and 30-gauge needle. For analysis of viral replication, mice were euthanized at various intervals post-inoculation, organs were excised, collected in 1 mL of PBS, frozen and thawed twice prior to homogenization using a TissueLyser (Qiagen). Viral titer was quantified by plaque assay using L929 cells.

For littermate transmission studies, two two-to-three day old pups were inoculated perorally with either T1L or S370P/Q371E and placed into cages with 6-8 uninoculated littermates. Eight days post-inoculation, inoculated and uninoculated mice were euthanized, and viral titers in organs targeted by reovirus were quantified by plaque assay.

For immunohistochemical and pathology analysis, mice were euthanized at various intervals following inoculation, and organs were excised and fixed overnight in 10% formalin. Fixed organs were paraffin-embedded, and 6 µM

sections were prepared (Vanderbilt University Translational Pathology Shared Resource). Sections were evaluated for histological damage following hematoxylin and eosin staining. Reovirus proteins were detected using polyclonal reovirus antisera. Proliferation, apoptosis, and ganglioside GM2 were detected using Ki-67-, caspase-3-, and GM2-spcecific antibodies, respectively.
All animal husbandry and experimental procedures were performed in accordance with Public Health Service policy and approved by the Vanderbilt University School of Medicine Institutional Animal Care and Use Committee. Unless otherwise stated in the appendices, all animal work presented in in this thesis was performed under Terence Dermody's animal protocol M/05/198.

Magnetic Resonance Imaging

Mice were inoculated with 10^8 PFU of wildtype and mutant reovirus strains. Twenty-one days post-inoculation, mice were anesthetized via inhalation of 2%/98% isoflurane/oxygen. Animals were secured in a prone position with the head placed in a 25-mm inner diameter radiofrequency (RF) coil. A rigid bite-bar and head restraint were used to ensure proper positioning and reduce motion-induced artifacts. Animals were placed in a Varian 7T horizontal bore magnetic resonance imaging system (Varian Inc, Palo Alto, CA) to collect imaging data. Respiration rate and internal body temperature were continuously monitored. A constant body temperature of 37° C was maintained using heated air flow.

For each animal, multi-slice scout images were collected in all three imaging planes (axial, sagittal, and coronal) using a gradient echo sequence with

repetition time (TR) = 75ms, echo time (TE) = 5ms, slice thickness = 2mm, and flip angle = 35 °. An average of four acquisitions was obtained for each animal. Additional parameters include field of view (FOV) = 50mm x 50mm and data matrix = 128 x 128.

Following localization of the brain, T2-weighted fast-spin echo images were collected over 12-20 imaging slices for all three imaging planes (axial, coronal, and sagittal), with FOV = 20mm x 20mm, slice thickness = 0.75mm, and data matrix = 128 x 128. Additional parameters include TR = 5 seconds, echo train length = 16, echo spacing = 8ms, TE = 64ms, and number of experiments = 10.

Ventricular Quantification

Ventricle volume measurements were performed using Matlab 2013a (The MathWorks, Inc, Natick, MA). A region of interest encompassing the entire brain was manually drawn for each slice, and a signal intensity threshold 1.25 times the mean signal intensity in a manually drawn region of cortical gray matter was used to segment voxels within the ROI corresponding to ventricle/cerebrospinal fluid. The total ventricular volume was calculated as the sum of the number of voxels within the segmented ventricle region multiplied by the volume of each voxel. The appearance of both eyes in the plane of analysis was used as a marker to standardize regions for ventricular volume quantification. Following the appearance of both eyes, used as a landmark, one slice was skipped and the next 8 slices quantified.

Statistical Analysis

Statistical analyses were performed using Prism (Graphpad). *P* values of less than 0.05 were considered to be statistically significant. Descriptions of the specific tests are found in the figure legends. Viral replication assays, hemagglutination assays, infectivity assays comprising more than two virus strains, and animal studies were analyzed by ANOVA followed by a Bonferroni's correction for multiple tests. Student's *t* tests were used for analysis of infectivity and binding experiments where only two strains were compared.

APPENDIX 1

REOVIRUS INFECTION ABROGATES ORAL TOLERANCE IN MICE

Introduction

Celiac disease is characterized by a loss of tolerance to dietary gluten peptides found in wheat, barley, and rye, resulting in a robust inflammatory response in the small intestine. Celiac disease manifests as varying degrees of small intestinal injury, ranging from increased intestinal epithelial leukocyte infiltration to total villous atrophy (213-215). The pathogenesis of celiac disease displays characteristics of both allergic and autoimmune conditions, as individuals with this disorder have gluten-specific antibodies and $CD4^+$ T cells (216) as well as auto-antibodies directed against tissue transglutaminase 2 (TG2) (216).

The risk of developing celiac disease is higher in persons who have a sibling, especially a monozygotic twin, with the disease, indicating that there is a strong genetic component (217). Genome-wide-association-studies (GWAS) identified genes associated with inflammatory cytokines, antigen presentation, NF-κB, and T cell and NK cell activation as risk factors for developing celiac disease (218, 219). Human major histocompatibility complex (MHC) genes, specifically those encoding human leukocyte antigens (HLA)-DQ2 and DQ8

molecules, also are associated with an increased risk of celiac disease development. Remarkably, these alleles are expressed in more than 99 percent of persons with celiac disease (219). HLA-DQ2 and DQ8 molecules present (220-223) gluten peptides to potentiate generation of gluten-specific $CD4^+$ T cells. The high proline content of gluten renders it difficult to digest. Upon reaching the intestine, long gluten peptides serve as substrates for TG2, which preferentially recognizes proteins, such as gluten, that contain a Gln-X-Pro motif. TG2 postranslationally modifies the glutamine residues to glutamate (220-224). These negatively charged, deamidated gluten peptides interact with the positively charged pockets in the HLA-DQ2 and DQ8 molecules (225-227), thereby increasing binding affinity, enhancing peptide-MHC complex stability, and promoting gluten-specific $CD4^+$ T cell generation (228). Deamindation enhances the interaction of gluten with these HLA molecules, but the T-cell receptor (TCR) does not have a preference for the native or deamidated form of the gluten peptide (229). Furthermore, gluten-specific $CD4^+$ T cells may recognize B cells presenting gluten-TG2 complexes and thereby provide help to B cells to generate TG2-specific autoantibodies (230). Taken together, these findings suggest that the MHC risk alleles have a functional role in celiac disease progression. However, these molecules also are found in persons without celiac disease, indicating that these alleles are by no means sufficient to induce the illness (231).

It is possible that enteric viral infections enhance the risk of celiac disease onset in persons with HLA-DQ2 or DQ8 alleles. Epidemiological studies have linked rotavirus infections with celiac disease in genetically susceptible

individuals (232). Astroviruses have been isolated from some individuals at the onset of celiac disease but were not found in persons presenting with diarrhea that was unrelated to celiac disease (233). Finally, adenovirus type 12 antibodies are more prevalent in individuals with celiac disease compared with healthy controls (234). Thus, it appears that some enteric viruses may trigger celiac disease, in a subset of individuals.

Enteric viral infections may alter the cytokine profile in the gut and consequentially alter the immune response to dietary antigens. Type 1 interferons (IFNs) released in response to viral infection may potentiate the loss of tolerance to gluten in humans. In support of this idea, IFNα levels are elevated relative to controls in the mucosa of some individuals with celiac disease (235) (Jabri, unpublished). Moreover, IFNα treatment of hepatitis C virus infection leads to celiac disease in some persons (236). Peroral administration of IFNβ to mice results in increased lymphocyte production of inflammatory cytokine IFNγ (237), which is a hallmark of loss of oral tolerance.

Oral tolerance is a term used to describe systemic immune unresponsiveness to previously fed antigen. Understanding mechanisms of oral tolerance induction and maintenance will provide insight into the pathogenesis of diseases such as celiac disease in which oral tolerance is abrogated. The concept of oral tolerance was introduced by Merril Chase in 1946 when he showed that peroral administration of contact-sensitizing agent 2-4-dinitrochlorobenzene does not lead to sensitization as expected, but rather protects mice from an inflammatory response upon subsequent challenge (238).

In a traditional experimental set up of oral tolerance (an example is provided in Figure AI-1), low doses of antigen are administered perorally to mice over time. Animals are subsequently challenged subcutaneously with that antigen mixed with an adjuvant. Mice that received the oral antigen display reduced T cell proliferation and reduced inflammatory cytokine levels (chiefly IFNγ) in response to the challenge compared with mice that did not receive the oral antigen (238). Additionally, mice that are tolerized do not mount B cell responses to fed antigen in contrast to those that first receive the antigen subcutaneously. The concomitant peroral administration of ovalbumin (OVA), a common antigen used in oral tolerance experiments, and IFNα, leads to an increase in levels of OVA-specific antibodies (239). Antibody levels in mice that receive IFNα approximate those observed in mice that did not receive antigen perorally. This finding suggests that type 1 IFN administration abrogates oral tolerance induction in mice.

I hypothesized that enteric viral infection promotes a loss of oral tolerance to fed antigen as a consequence of increased type 1 IFN production. I tested the capacity of poly (I:C), a dsRNA analog, and mammalian reovirus, an enteric pathogen in humans and mice, to alter the immune response to OVA. This project was performed in collaboration with the laboratory of Dr. Bana Jabri at the University of Chicago. The results section of this chapter encompasses only experiments that I designed and conducted. Karl Boehme, a former postdoctoral fellow in the Dermody laboratory, engineered the reassortant virus, T3Drv, described below. Romain Bouziat, a postdoctoral fellow in the Jabri laboratory,

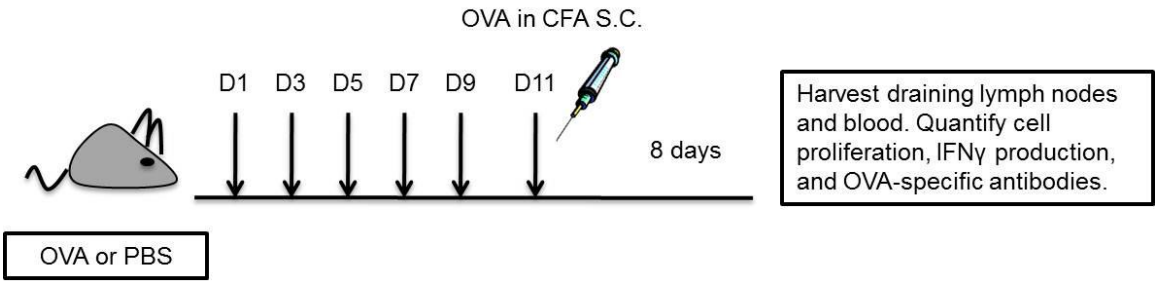

Figure A1-1. Schematic of oral tolerance experimental design. Mice are fed ovalbumin (OVA) or PBS vehicle control every other day for 10 days. Mice are then primed with a subcutaneous injection of OVA in complete Freund's adjuvant (CFA). Eight days after the Ova/CFA challenge, draining lymph nodes were resected, and cells were isolated and restimulated with Ova *ex vivo*. Cell proliferation, IFNγ levels in the draining lymph node, and presence of OVA-specific antibodies are quantified.

performed the quantitative PCR experiment shown in Figure AI-7 after I inoculated and harvested the tissue. Collectively, we found that reovirus infection of mice alters the immune response to dietary antigen and abrogates tolerance to fed OVA. These findings establish a model system for studies to determine how viral infection precipitates celiac disease onset in mice, which in turn may enhance an understanding of celiac disease pathogenesis in humans.

Results

Pilot experiments using poly (I:C)

Initial experiments used poly (I:C), a dsRNA analog, to study the effect of TLR signaling on oral tolerance induction and regulatory T cell generation. To assess the influence of poly (I:C) on oral tolerance induction, mice were fed OVA alone (positive control) or in combination with poly (I:C) every other day for 10 days. Mice were then primed with a subcutaneous injection of OVA emulsified in adjuvant 24 hours after the last feeding. Seven days after this injection, mice were euthanized, and the draining lymph nodes were resected, homogenized, and restimulated *ex vivo* with OVA. Mice that received poly (I:C) displayed enhanced T cell proliferation as assessed by tritiated thymidine incorporation (Figure AI-2A) and increased levels of IFNγ in the draining lymph node following OVA-restimulation (Figure AI-2B). In an additional experiment, poly (I:C) treatment did not abrogate oral tolerance in IFNαβR$^{-/-}$ mice (Figure AI-3). These

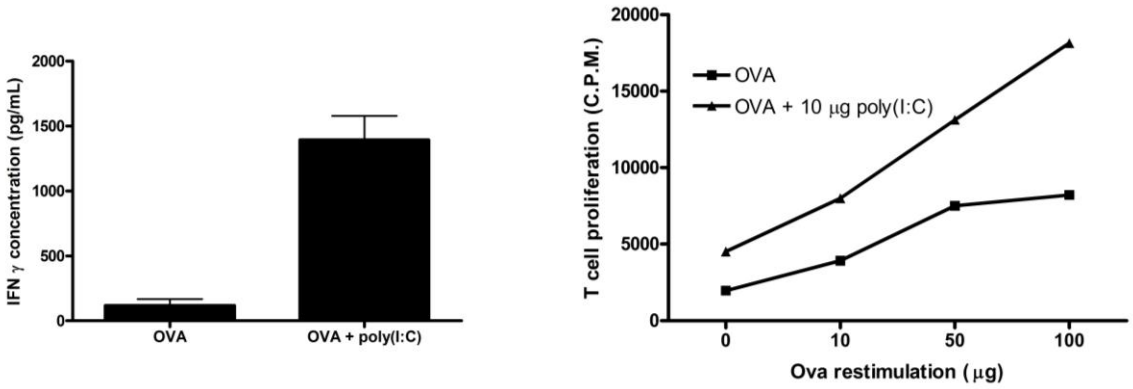

Figure AI-2. Poly(I:C) abrogates oral tolerance. C57Bl/6 mice were fed OVA alone or in combination with poly(I:C) every other day for 10 days. Twenty-four hours after the last feeding, mice were primed with a subcutaneous injection of OVA in complete Freund's adjuvant (CFA). Eight days post-challenge with OVA/CFA, draining lymph nodes were resected, and cells were isolated and restimulated with OVA at 37ºC for 48 h. Cell proliferation was quantified by tritiated thymidine incorporation (left). IFNγ levels in the draining lymph node were quantified by ELISA (left panel). Data shown are from a representative experiment of two performed with three mice. Cell proliferation and ELISA assays were performed with three technical replicates per mouse. Error bars represent standard deviation.

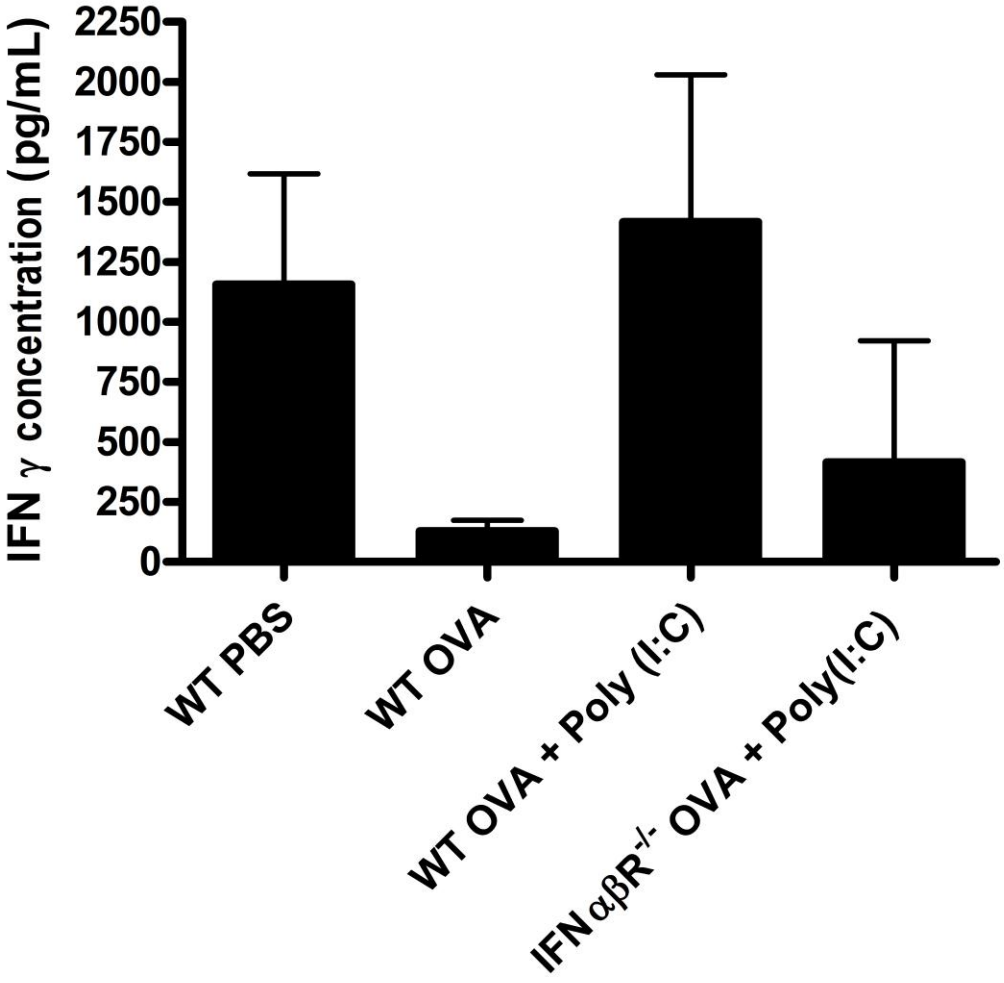

Figure AI-3. Poly(I:C)-mediated abrogation of oral tolerance is dependent on type 1 IFNs. Wildtype or IFNαβR$^{-/-}$ mice were fed OVA alone or in combination with poly(I:C) every other day for 10 days. Twenty four hours after the last feeding, mice were primed with a subcutaneous injection of OVA in complete Freund's adjuvant (CFA). Eight days after the OVA/CFA challenge, draining lymph nodes were resected, and cells were isolated and restimulated with OVA at 37ºC for 48 h. IFNγ levels in the draining lymph node were quantified by ELISA. Data are from one experiment performed in triplicate for wildtype mice and in duplicate for IFNαβR$^{-/-}$ mice. Error bars represent standard deviation.

findings suggest that poly (I:C) stimulates type 1 IFN production, which in turn mediates loss of oral tolerance in mice.

Oral tolerance is thought to depend on generation of regulatory T cells (Tregs) (238, 240). As poly (I:C) treatment abrogated oral tolerance, I hypothesized that poly (I:C) inhibits regulatory T cell induction. Naïve $CD4^+$ T cells can be induced to form Foxp3+ Tregs following co-culture with dendritic cells and treatment with TGFβ and retinoic acid (241). To determine whether poly (I:C) prevents Foxp3+ cell induction, I isolated, co-cultured, and treated naïve $CD4^+$ T cells and $CD11C^+$ dendritic cells harvested from mouse spleens with TGFβ and retinoic acid. After 3 days in co-culture, I quantified the percentage of Tregs by flow cytometry. Treatment with poly (I:C) hindered Treg generation *in vitro* (Figure AI-4), suggesting that the poly (I:C) induction of type 1 IFNs impairs Treg differentiation and tolerance to fed antigen.

Reovirus abrogates oral tolerance in mice

As viruses have been implicated in celiac disease onset in humans (232, 233), I next sought to assess how enteric viral infection, and not a synthetic analog, influences oral tolerance in mice. Following peroral inoculation, reoviruses infect the murine alimentary tract, but in adult animals these viruses do not disseminate to cause systemic disease (103, 115). Moreover, the reovirus serotypes differ in the magnitude of the type 1 IFN response (242-244). While infection with either T1 or T3 reovirus leads to IFN production, T1 reovirus encodes an IFN antagonist and consequentially produces less type 1 IFN than

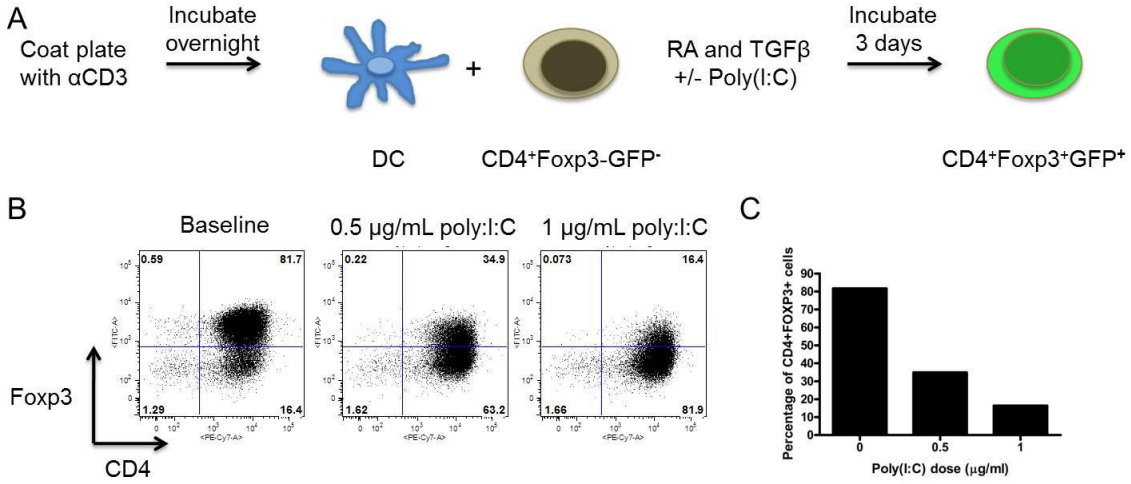

Figure AI- 4. Poly(I:C) inhibits the induction of regulatory T cells. (A) Summary of the experimental protocol. (B) Splenic dendritic cells (DCs) were co-cultured with naive splenic $CD4^{+}Foxp3^{-}$ T cells at 37ºC for 3 days in the presence of TGFβ and retinoic acid (RA) alone or in combination with 0.5 µg/ml or 1 µg/ml of poly(I:C). $CD4^{+}$Foxp3+ regulatory T cell induction was quantified by flow cytometry. (C). Graphical representation of the flow cytometry shown in B.

does T3D (242, 243). We sought to use T1 and T3 reoviruses to evaluate the effect of reovirus infection on oral tolerance induction. However, prototype T3D does not efficiently infect the murine intestine, a property that genetically segregates with the viral S1 and L2 gene segments (245). Therefore, we engineered a T1L/T3D-S1L2 reassortant reovirus, herein referred to at T3Drv, for these studies. Following peroral inoculation, T1L and T3Drv produce equivalent titers in the intestine, mesenteric lymph node (MLN), and Peyer's patches (Figure AI-5).

To assess the influence of reovirus infection on oral tolerance induction, mice were fed with OVA alone (positive control) or in combination with T1L or T3Drv on the first feeding. OVA was administered to the mice perorally every other day for four additional feedings. Mice were then primed with a subcutaneous injection of OVA emulsified in adjuvant 24 hours after the last feeding. Seven days later, mice were euthanized, and the draining, inguinal lymph nodes were resected, homogenized, and restimulated with OVA. Remarkably, levels of IFNγ in the draining lymph node were higher in mice that received OVA in combination with T1L, but not T3Drv, compared with mice that received OVA alone (Figure AI-6). This finding demonstrates that infection with certain reovirus strains diminishes the induction of tolerance to orally fed antigens.

Surprisingly, while T3D induces higher levels of type 1 IFNs than does T1L *in vitro* (242, 243), both viruses produced comparable levels of type 1 IFN in the Peyer's patches. However, infection with T1L led to increased type 1 IFN

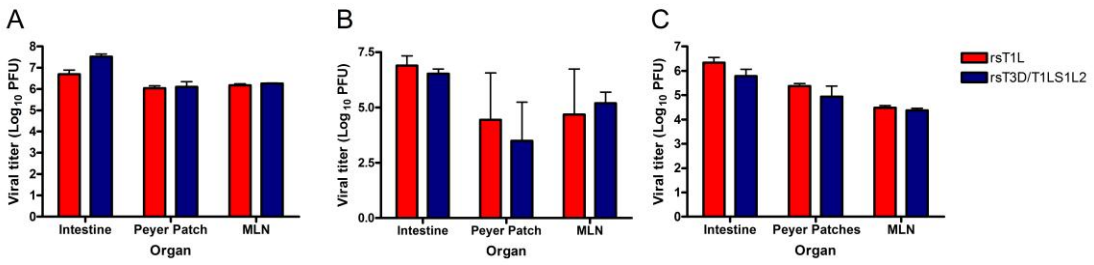

Figure AI-5. T1L and T3Drv produce comparable titers in the intestine. C57BL/6 mice at 6-8 weeks of age were inoculated with 10^{10} PFU of either T1L or T3Drv. At days 1 (A), 2 (B), and 4 (C) post-inoculation, mice were euthanized, and the intestine, Peyer's patches, and mesenteric lymph nodes (MLN) were excised and homogenized. Viral titers in tissue homogenates were determined by plaque assay. Results are expressed as mean viral titers for 3 mice per virus strain per time point. Error bars represent standard deviation. Differences are not significant by one-way ANOVA followed by Bonferroni's correction for multiple tests.

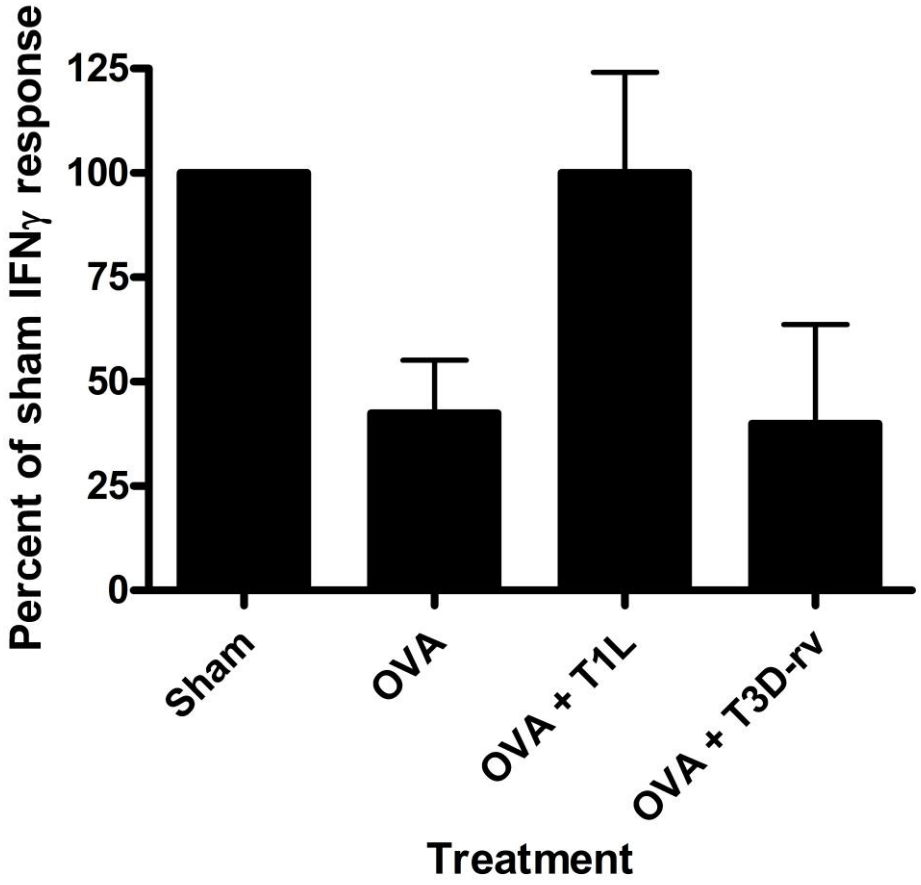

Figure AI-6. T1L but not T3Drv abrogates oral tolerance. C57BL/6 mice were fed OVA every other day for 10 days. Some mice received T1L or T3Drv with OVA during the first feeding. Twenty-four hours after the last feeding, mice were primed with a subcutaneous injection of OVA in complete Freund's adjuvant (CFA). Eight days post-injection with OVA/CFA, draining lymph nodes were resected, and cells were isolated and restimulated with OVA. IFNγ levels in the draining lymph node were quantifiedd by ELISA. IFNγ levels were normalized to the sham (non-tolerized) group for each experiment. Data represent the means of four independent experiments with 3 mice per treatment per experiment. Error bars represent standard error of the mean.

production in the lamina propria and intestinal epithelium compared with T3Drv (Figure AI-7). These findings suggest that T1L infection leads to inflammatory cytokine production in the intestine, which may potentiate a loss of oral tolerance in mice.

Conclusions and Future Directions

Summary

Experiments presented in this chapter demonstrate that infection with T1L reovirus (Figure AI-6) or treatment with poly (I:C) (Figure AI-2), an analog of dsRNA, used as a model antagonist in pilot studies, abrogates oral tolerance induction in mice. Studies using poly (I:C) in mice lacking the type IFN receptor (Figure AI-3) suggest that this TLR3 agonist blocks formation of oral tolerance through the production of type 1 IFNs. Concordant with a function of IFN in tolerance abrogation, infection with T1L leads to higher levels of type 1 IFNs in the gut (Figure AI-7). Interestingly, T1L but not T3Drv abrogates oral tolerance in mice. While type 1 IFN induction by T1L and T3Drv is comparable in the Peyer's patches, T1L induces higher levels of type 1 IFNs in the lamina propria and intestinal epithelium, suggesting that inflammation at these sites prevents a tolerogenic response to fed antigen. Moreover, poly (I:C) blocks the generation of inducible Tregs *in vitro* (Figure AI-4), raising the possibility that diminished Treg responses contribute to oral tolerance abrogation. Taken together, these experiments suggest that viral infection promotes an inflammatory environment in

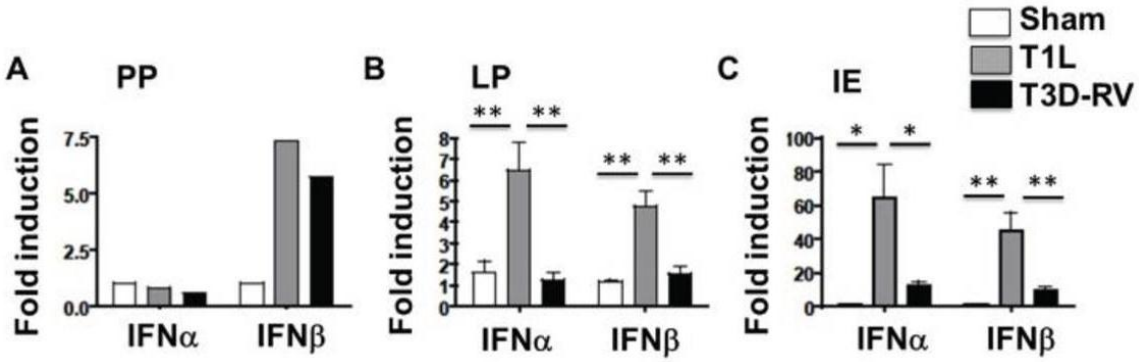

Figure AI-7. T1L induces higher levels of type 1 IFNs in the lamina propria and intestinal epithelium than does T3Drv. C57BL/6 mice were inoculated perorally with 10^{10} PFU of either T1L or T3Drv. Forty-eight hours post-inoculation, the Peyer's patches (A), lamina propria (B), and intestinal epithelium (C) were isolated. Levels of IFNα and IFNβ were assessed by quantitative PCR. Levels of target mRNAs were normalized to GAPDH, and the results are expressed relative to type 1 IFN transcripts found in mice treated with PBS vehicle control (sham). Error bars represent standard deviation. Results are from a representative experiment of 3 mice per experimental condition.

the gut, which prevents generation of Tregs and impedes tolerance to oral antigen (Figure AI-8).

Future directions

Experiments presented in this chapter revealed that T1L but not T3Drv has the capacity to block oral tolerance induction in mice (Figure AI-6). These viruses replicate with comparable efficiency in the MLN, Peyer's patches, and intestine, suggesting that differences in viral replication do not account for differences in type 1 IFN induction and loss of oral tolerance. While T1L and T3Drv induce comparable levels of type 1 IFNs in the Peyer's patches, T1L induces more T1 IFN than does T3Drv in the intestinal epithelium and lamina propria. This finding suggests that the virus-host interaction contributes to the development of oral tolerance. These viruses provide a framework to define viral determinants of oral tolerance abrogation. T1L and T3Drv both contain the T1L S1 and L2 genes, but they differ in expression of the other eight reovirus gene segments. Using reverse genetics, it is possible to generate a panel of reassortant viruses to identify gene segments that contribute to loss of tolerance to fed antigens (Table AI-1). It would be informative to quantify type 1 IFN production in the lamina propria and intestinal epithelium following infection with these reassortant strains and evaluate the capacity of these viruses to block oral tolerance induction in mice. Since functions of the reovirus gene products are

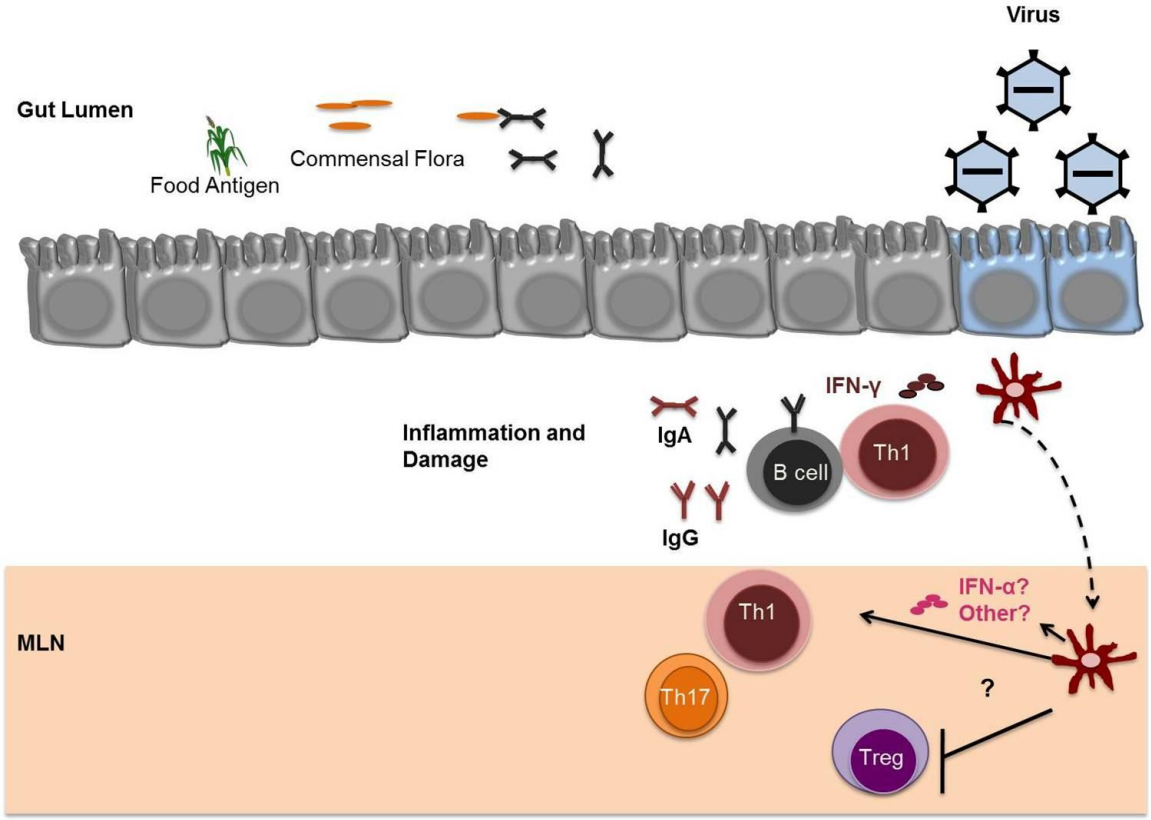

Figure AI-8. Model of reovirus-induced loss of oral tolerance. Reovirus infection promotes an inflammatory environment within the intestine. Reovirus may trigger innate signaling pathways to activate dendritic cells, which in turn prime T cells to generate inflammatory $CD4^+$ T cell subsets at the expense of regulatory T cell induction. Future experiments will determine whether infection promotes anti-OVA and autoantibody production following infection.

Name										
Parent T1L	S1	S2	S3	S4	M1	M2	M3	L1	L2	L3
Parent T3Drv	S1	S2	S3	S4	M1	M2	M3	L1	L2	L3
A	S1	S2	S3	S4	M1	M2	M3	L1	L2	L3
B	S1	S2	S3	S4	M1	M2	M3	L1	L2	L3
C	S1	S2	S3	S4	M1	M2	M3	L1	L2	L3
D	S1	S2	S3	S4	M1	M2	M3	L1	L2	L3
E	S1	S2	S3	S4	M1	M2	M3	L1	L2	L3
F	S1	S2	S3	S4	M1	M2	M3	L1	L2	L3
G	S1	S2	S3	S4	M1	M2	M3	L1	L2	L3
H	S1	S2	S3	S4	M1	M2	M3	L1	L2	L3

Table AI-1. Panel of T1L and T3D-rv reassortants. Eight reassortant viruses were generated using reverse genetics. These viruses can be used to study viral determinants of reovirus-mediated oral tolerance abrogation.

well understood, such experiments will provide the first steps in defining mechanisms by which viral infections lead to loss of oral tolerance.

The finding that T1L but not T3Drv abrogates oral tolerance in mice illustrates the concept that some but not all enteric viruses have the capacity to alter the immune response to dietary antigens. There is evidence to support this contention from studies of celiac disease patients. Persons with celiac disease display higher titers of adenovirus type 12-specific antibodies than controls, yet celiac disease cases and controls have comparable levels of antibodies to the related adenovirus type 18 (234, 246). In addition to reovirus, rotavirus (232), a double-stranded RNA virus virus, astrovirus (233), a positive-sense, single-stranded RNA virus, and adenovirus (234, 246), a double-stranded DNA virus, are associated with celiac disease. These observations indicate that the genome type of the virus is insufficient to promote loss of oral tolerance.

The mechanism by which certain viruses promote an inflammatory response to fed antigen is not understood. It would be useful to determine whether these viruses share any common properties. For example, adenovirus type 12 displays some sequence similarity to α-gliadin (246). In a specific region of the viral E1b protein, 8 of 12 amino acids are identical between adenovirus 12 and α-gliadin, including 5 consecutive amino acids. Analysis of other eukaryotic, prokaryotic, and animal virus proteins did not reveal sequence similarities to that degree (246). It is unclear which animal viruses were included in the analysis. Sequences of rotavirus, reovirus, astrovirus, and adenovirus type 12 should be compared to each other and to gluten peptides to determine whether there is

sequence similarity. Alternatively, the immune response, particularly production of type 1 IFNs in intestinal epithelial cells or intestinal cell lines, could be assessed for T1L, T3Drv, adenovirus 12, and adenovirus 18. While adenovirus has only been correlated with celiac disease, it would be interesting to test whether T1L and adenovirus 12 induce similar immune signatures in comparison to those induced by T3Drv and adenovirus 18.

Celiac disease is characterized by the presence of gluten-specific T cells and antibodies as well as antibodies against TG2. Experiments presented in this chapter examined the T cell arm of this disease. The effect of reovirus infection on antibody production is unknown. Using ELISAs, the levels of OVA-specific antibodies and TG2-specific antibodies in mice following peroral administration of T1L and OVA could be quantified to answer this question.

Studies using poly (I:C) suggest that this analog of dsRNA blocks the generation of inducible regulatory T cells *in vitro*. These experiments should be repeated using T1L and T3Drv to determine whether reovirus also has the capacity to block Treg differentiation. It would be useful to determine whether this phenomenon also is observed in infected mice as well. Such experiments would enhance an understanding of the function of Tregs in virus-mediated abrogation of oral tolerance.

Celiac disease is a gluten-sensitive enteropathy, and experiments presented in this chapter used OVA as a model antigen. OVA is a more convenient antigen to use because it can be easily administered and is not

included in standard mouse chow. Thus, the timing of antigen introduction into the diet can be manipulated as an experimental variable to facilitate development of a mouse model of celiac disease. Mice that lack expression of native MHC class II molecules but instead express human HLA-DQ8 are available. Our collaborators in the Jabri laboratory have maintained these mice on a gluten-free diet and introduced gluten orally in the presence and absence of reovirus infection. Mice that received gluten and T1L developed anti-gluten antibodies. These conditions also led to the activation of TG2 in the duodenum (Bouziat and Jabri, unpublished). It will be informative to perform similar oral tolerance experiments using gluten as the antigen to determine whether T1L induces gluten-specific T cells and villous atrophy. The possibility that T1L and T3Drv differ in induction of these phenotypes also should be assessed.

A remaining question is whether reovirus infection has the capacity to break established tolerance to fed antigen. In my experiments, mice were inoculated with reovirus and fed OVA at the same time. While celiac disease is most prevalent in children, disease onset does not perfectly correlate with the introduction of gluten into the diet. Therefore, it would be useful to establish tolerance in mice by feeding low doses of either OVA or gluten every other day for ten days, wait one week, and then begin a second round of feeding in the presence or absence of T1L. Mice would then be primed 24 hours after the last feeding, and responses to the fed antigens would be assessed one week after the subcutaneous challenge.

Repeated viral infections are associated with increased rates of celiac disease in genetically susceptible persons (232). To determine whether multiple infections promote celiac disease pathology in mice, HLA-DQ8 mice could be maintained on a gluten-containing diet and repeatedly infected with reovirus. At certain intervals, mice could be euthanized, and the presence of gluten-specific T cells, gluten- and TG2-specific antibodies, TG2 activation, and villous atrophy could be assessed.

I found it intriguing that some individuals with celiac disease, particularly those who manifest nervous system symptoms, contain anti-ganglioside antibodies (247-250). Some of these antibodies are directed against ganglioside GM2, which serves as a glycan receptor for serotype 1 reovirus (10) (Chapters 2-5). One study examined the interaction of glaidin with ganglioside GM1 (251). Gliadin binds GM1 both *in vitro* and on the intestinal epithelium. It would be informative to determine whether GM2 also binds gliadin. One possibility is that reovirus and gliadin interact through mutual association with GM2. To test this hypothesis, wildtype or HLA-DQ8 mice could be inoculated with either T1L or a virus containing the S370P/Q371E mutations in σ1. If GM2-reovirus interactions are required for reovirus-mediated loss of oral tolerance, then T1L but not the mutant virus would abrogate tolerance induction and perhaps facilitate generation of anti-gliadin antibodies in mice.

Conclusions

Experiments presented in this chapter demonstrate that infection with T1L but not T3Drv breaks immune tolerance to OVA as a model dietary antigen. This finding provides a tractable system that can be used to identify viral determinants of oral tolerance abrogation. Moreover, these studies, coupled with findings using HLA-DQ8-expressing mice in the Jabri laboratory (Bouziat and Jabri, unpublished), suggest that reovirus infection triggers pathology in mice that resembles celiac disease in humans. Moving forward, new studies inspired by this research will determine mechanisms of oral tolerance abrogation and investigate the contribution of reovirus infection to celiac disease onset in humans.

Methods

Medium

RPMI 1640 (Gibco) was supplemented to contain 10% FBS (Gibco), 1% penicillin-streptomycin (Gibco), 5 µg/mL gentamicin, and 0.05 mM β-mercaptoethanol (Sigma). Complete RPMI was used for most assays, except for isolation of the intestinal epithelial and lamina propria cells.

Mice

C57Bl/6 mice were purchased from Jackson Laboratory. IFNαβ$^{-/-}$ mice on a C57Bl/6 background were provided by Tatyana Golovkina (University of

Chicago). Mice at an age of 6-8 weeks were used for all experiments. T cells were isolated from FOXP3-eGFP mice as described (252, 253). All experiments were performed in accordance with the Institutional Biosafety Committees and Institutional Animal Care and Use Committees at the University of Chicago and Vanderbilt University.

T cell isolation

Spleens and peripheral lymph nodes from FOXP3-eGFP mice were isolated and mechanically disrupted by passage through a 70 μm cell strainer. $CD4^+$ cells were isolated using CD4-specific microbeads (Miltenyi Biotech). $FOXP3^-$ $CD4^+$ cells were isolated using a BD FACS Aria (BD Bioscience) as described (252).

Splenic dendritic cell isolation

Spleens were excised from wildtype C57Bl/6 mice, digested using 400 U/ml of type IV collagenase (Sigma-Aldrich), and mechanically disrupted by passage through a 100 μm cell strainer. Cells were resuspended in an OptiPrep (Sigma-Aldrich) density gradient (252) and centrifuged at 700 x g for 30 min. $CD11c^+$ dendritic cells were isolated using CD11c-specific magnetic beads (Miltenyi Biotech) according to the manufacturer's instructions.

In vitro regulatory T cell induction assay

Wells of 96-well plates (Co-Star) were coated with 1 μg/ml of anti-CD3 antibody (eBioscience) at 4ºC overnight. Plates were washed, and 10^5 $CD4^+FOXP3^-$ T cells were co-cultured with 4 x 10^4 splenic $CD11C^+$ dendritic cells at 37ºC for 3 days in the presence and absence of recombinant TGFβ (2 μg/ml)

(R&D) and retinoic acid (10 nM) (Sigma-Aldrich) to induce regulatory T cells (DePaolo and Mucida Science 2007). Poly (I:C) (Invivogen) was added to some assays.

Administration of oral antigen

OVA (Sigma-Aldrich) was dissolved in PBS and administered by intragastric gavage using 18-20 gauge round-tipped needles. In some experiments, either poly (I:C) (10 μg) or reovirus (10^{10} PFU) was included in the inoculum. Mice were fed every other day for a total of five feedings. When used, poly (I:C) was included in every feeding, whereas reovirus was inoculated only during the first feeding, followed by four feedings with OVA alone.

Analysis of the intestinal response to fed antigen

Intestinal epithelial cells and lamina propria cells were isolated as described (252). The small intestine was resected and bisected longitudinally. Intestinal contents were removed by washing twice with PBS. The bisected intestine was divided into small pieces, resuspended in RPMI 1640 supplemented to contain 1% dialyzed FBS (Gibco), 2 mM EDTA, and 1 mM $MgCl_2$, and shaken at 37°C for 15 min. The supernatant was set aside, and the process was repeated with 15 mL of fresh medium. After the second incubation, cells were centrifuged at 500 x g for 5 min and resuspended in complete RPMI. Lamina propria cells were isolated from the remaining intestinal fragments using RPMI 1640 supplemented to contain 20% FBS and 100 U/mL of type VIII collagenase (Sigma). Samples were shaken at 37°C for 15 min. The supernatant was removed, and this process was repeated using fresh medium. The

supernatant from both incubations was centrifuged at 500 x g for 5 min. Cell pellets were resuspended in complete RPMI. The MLN and Peyer's patches were excised and mechanically disrupted by passage through a 100 μm cell strainer. Cells were resuspended in complete RPMI and stimulated with 50 μg of OVA to detect antigen-specific cytokine responses. Cytokine levels in cell supernatants were analyzed by ELISA (BD Biosciences and eBioscience) according to the manufacturer's instructions. Cytokine mRNA levels in cell pellets were analyzed by quantitative PCR (Life Technologies).

Oral tolerance induction

OVA (100 μg) was emulsified in a 1:1 ratio vol/vol of complete Freund's adjuvant (CFA) and administered to mice via subcutanenous (50 μL) injection in the flanks 24 hours after the last dose of oral antigen was delivered. Eight days post-injection, mice were euthanized, the draining lymph nodes were removed, and single-cell suspensions were generated by mechanically disrupting the tissue and passage through a 100 μm cell strainer. Cells were resuspended at a density of 2 x 10^6/mL in complete RPMI and stimulated with OVA (50 μg) for 48 hours. Supernatants were analyzed by ELISA (BD bioscience and eBioscience) according to the manufacturer's instructions.

T cell proliferation assays

Following oral tolerance experiments, the draining lymph nodes were resected and mechanically disrupted by passage through a 70 μM filter and resuspended in complete RPMI at a concentration of 5 x 10^6 cells/mL. Cells in a volume of 100 μL were added to each each well of a 96-well plate. OVA protein

was suspended in PBS at a concentration of 1 mg/mL. Working dilutions of OVA ranging from 0 to 100 µg/mL were prepared using complete RPMI. Each dilution in a volume of 100 µL was added to cells. Cells were incubated at 37ºC for 48 h and then incubated with 1 µCi of ^{3}H. Cells were incubated for an additional 18-24 h and frozen. Counts per minute (CPM) were quantified using a liquid scintillation counter (University of Chicago).

REFERENCES

1. **Dalgleish AG, Beverley PCL, Clapham PR, Crawford DH, Greaves MF, Weiss RA.** 1984. The CD4 (T4) antigen is an essential component of the receptor for the AIDS retrovirus. Nature **312:**763-767.
2. **Feng Y, Broder CC, Kennedy PE, Berger EA.** 1996. HIV-1 entry cofactor: functional cDNA cloning of a seven-transmembrane, G protein-coupled receptor. Science **272:**872-877.
3. **Dragic T, Litwin V, Allaway GP, Martin SR, Huang Y, Nagashima KA, Cayanan C, Maddon PJ, Koup RA, Moore JP, Paxton WA.** 1996. HIV-1 entry into CD4+ cells is mediated by the chemokine receptor CC-CKR-5. Nature **381:**667-673.
4. **Bergelson JM, Cunningham JA, Droguett G, Kurt-Jones EA, Krithivas A, Hong JS, Horwitz MS, Crowell RL, Finberg RW.** 1997. Isolation of a common receptor for Coxsackie B viruses and adenoviruses 2 and 5. Science **275:**1320-1323.
5. **Mathias P, Wickham T, Moore M, Nemerow G.** 1994. Multiple adenovirus serotypes use αv integrins for infection. J. Virol. **68:**6811-6814.
6. **Nemerow GR, Cheresh DA, Wickham TJ.** 1994. Adenovirus entry into host cells: a role for alpha(v) integrins. Trends Cell Biol **4:**52-55.
7. **Barton ES, Connolly JL, Forrest JC, Chappell JD, Dermody TS.** 2001. Utilization of sialic acid as a coreceptor enhances reovirus attachment by multistep adhesion strengthening. J. Biol. Chem. **276:**2200-2211.
8. **Chappell JD, Duong JL, Wright BW, Dermody TS.** 2000. Identification of carbohydrate-binding domains in the attachment proteins of type 1 and type 3 reoviruses. J. Virol. **74:**8472-8479.
9. **Reiter DM, Frierson JM, Halvorson EE, Kobayashi T, Dermody TS, Stehle T.** 2011. Crystal structure of reovirus attachment protein sigma1 in complex with sialylated oligosaccharides. PLoS Path. **7:**e1002166.
10. **Reiss K, Stencel JE, Liu Y, Blaum BS, Reiter DM, Feizi T, Dermody TS, Stehle T.** 2012. The GM2 glycan serves as a functional co-receptor for serotype 1 reovirus. PLoS Path. **8:**e1003078.
11. **Barton ES, Forrest JC, Connolly JL, Chappell JD, Liu Y, Schnell F, Nusrat A, Parkos CA, Dermody TS.** 2001. Junction adhesion molecule is a receptor for reovirus. Cell **104:**441-451.
12. **Antar AAR, Konopka JL, Campbell JA, Henry RA, Perdigoto AL, Carter BD, Pozzi A, Abel TW, Dermody TS.** 2009. Junctional adhesion molecule-A is required for hematogenous dissemination of reovirus. Cell Host Microbe **5:**59-71.
13. **Maginnis MS, Forrest JC, Kopecky-Bromberg SA, Dickeson SK, Santoro SA, Zutter MM, Nemerow GR, Bergelson JM, Dermody TS.** 2006. β1 integrin mediates internalization of mammalian reovirus. J. Virol. **80:**2760-2770.

14. **Maginnis MS, Mainou BA, Derdowski AM, Johnson EM, Zent R, Dermody TS.** 2008. NPXY motifs in the β1 integrin cytoplasmic tail are required for functional reovirus entry. J. Virol. **82:**3181-3191.
15. **Konopka-Anstadt JL, Mainou BA, Sutherland DM, Sekine Y, Strittmatter SM, Dermody TS.** 2014. The Nogo Receptor NgR1 Mediates Infection by Mammalian Reovirus. Cell Host Microbe **15:**681-691.
16. **Kilham L, Margolis G.** 1969. Hydrocephalus in hamsters, ferrets, rats, and mice following inoculations with reovirus type 1. Laboratory Investigations **22:**183-188.
17. **Weiner HL, Drayna D, Averill DR, Jr, Fields BN.** 1977. Molecular basis of reovirus virulence: role of the S1 gene. Proc. Natl. Acad. Sci. U. S. A. **74:**5744-5748.
18. **Tan CW, Poh CL, Sam IC, Chan YF.** 2013. Enterovirus 71 uses cell surface heparan sulfate glycosaminoglycan as an attachment receptor. J. Virol. **87:**611-620.
19. **Gardner CL, Ebel GD, Ryman KD, Klimstra WB.** 2011. Heparan sulfate binding by natural eastern equine encephalitis viruses promotes neurovirulence. Proc Natl Acad Sci U S A **108:**16026-16031.
20. **Chen Y, Maguire T, Hileman RE, Fromm JR, Esko JD, Linhardt RJ, Marks RM.** 1997. Dengue virus infectivity depends on envelope protein binding to target cell heparan sulfate. Nat. Med. **3:**866-871.
21. **Silva LA, Khomandiak S, Ashbrook AW, Weller R, Heise MT, Morrison TE, Dermody TS.** 2014. A single-amino-acid polymorphism in Chikungunya virus E2 glycoprotein influences glycosaminoglycan utilization. J. Virol. **88:**2385-2397.
22. **Hu L, Crawford SE, Czako R, Cortes-Penfield NW, Smith DF, Le Pendu J, Estes MK, Prasad BV.** 2012. Cell attachment protein VP8* of a human rotavirus specifically interacts with A-type histo-blood group antigen. Nature **485:**256-259.
23. **Ramani S, Cortes-Penfield NW, Hu L, Crawford SE, Czako R, Smith DF, Kang G, Ramig RF, Le Pendu J, Prasad BV, Estes MK.** 2013. The VP8* domain of neonatal rotavirus strain G10P[11] binds to type II precursor glycans. J. Virol. **87:**7255-7264.
24. **Chappell JD, Gunn VL, Wetzel JD, Baer GS, Dermody TS.** 1997. Mutations in type 3 reovirus that determine binding to sialic acid are contained in the fibrous tail domain of viral attachment protein σ1. J. Virol. **71:**1834-1841.
25. **Tsai B, Gilbert JM, Stehle T, Lencer W, Benjamin TL, Rapoport TA.** 2003. Gangliosides are receptors for murine polyoma virus and SV40. EMBO J **22:**4346-4355.
26. **Rogers GN, Paulson JC, Daniels RS, Skehel JJ, Wilson IA, Wiley DC.** 1983. Single amino acid substitutions in influenza haemagglutinin change receptor binding specificity. Nature **304:**76-78.
27. **Neu U, Bauer J, Stehle T.** 2011. Viruses and sialic acids: rules of engagement. Curr. Opin. Struct. Biol. **21:**610-618.

28. **Varki NM, Varki A.** 2007. Diversity in cell surface sialic acid presentations: implications for biology and disease. Lab Invest **87:**851-857.
29. **Varki A.** 2009. Multiple changes in sialic acid biology during human evolution. Glycoconjugate journal **26:**231-245.
30. **Varki A.** 2007. Glycan-based interactions involving vertebrate sialic-acid-recognizing proteins. Nature **446:**1023-1029.
31. **Schwarzkopf M, Knobeloch KP, Rohde E, Hinderlich S, Wiechens N, Lucka L, Horak I, Reutter W, Horstkorte R.** 2002. Sialylation is essential for early development in mice. Proc Natl Acad Sci U S A **99:**5267-5270.
32. **Schnaar RL.** 2010. Brain gangliosides in axon-myelin stability and axon regeneration. FEBS Lett **584:**1741-1747.
33. **Varki A, Schauer R.** 2009. Sialic Acids. *In* Varki A, Cummings RD, Esko JD, Freeze HH, Stanley P, Bertozzi CR, Hart GW, Etzler ME (ed.), Essentials of Glycobiology, 2nd ed, Cold Spring Harbor (NY).
34. **Bauer PH, Cui C, Stehle T, Harrison SC, DeCaprio JA, Benjamin TL.** 1999. Discrimination between sialic acid-containing receptors and pseudoreceptors regulates polyomavirus spread in the mouse. J. Virol. **73:**5826-5832.
35. **Qian M, Tsai B.** 2010. Lipids and proteins act in opposing manners to regulate polyomavirus infection. J. Virol. **84:**9840-9852.
36. **Nilsson EC, Storm RJ, Bauer J, Johansson SM, Lookene A, Angstrom J, Hedenstrom M, Eriksson TL, Frangsmyr L, Rinaldi S, Willison HJ, Pedrosa Domellof F, Stehle T, Arnberg N.** 2011. The GD1a glycan is a cellular receptor for adenoviruses causing epidemic keratoconjunctivitis. Nat. Med. **17:**105-109.
37. **Furukawa K, Takamiya K, Furukawa K.** 2002. Beta1,4-N-acetylgalactosaminyltransferase--GM2/GD2 synthase: a key enzyme to control the synthesis of brain-enriched complex gangliosides. Biochim Biophys Acta **1573:**356-362.
38. **Liu Y, Yan S, Wondimu A, Bob D, Weiss M, Sliwinski K, Villar J, Notario V, Sutherland M, Colberg-Poley AM, Ladisch S.** 2010. Ganglioside synthase knockout in oncogene-transformed fibroblasts depletes gangliosides and impairs tumor growth. Oncogene **29:**3297-3306.
39. **Taube S, Jiang M, Wobus CE.** 2010. Glycosphingolipids as receptors for non-enveloped viruses. Viruses **2:**1011-1049.
40. **Liu Y, Palma AS, Feizi T.** 2009. Carbohydrate microarrays: key developments in glycobiology. Biol Chem **390:**647-656.
41. **Boehme KW, Ikizler M, Kobayashi T, Dermody TS.** 2011. Reverse genetics for mammalian reovirus. Methods **55:**109-113.
42. **Kobayashi T, Antar AAR, Boehme KW, Danthi P, Eby EA, Guglielmi KM, Holm GH, Johnson EM, Maginnis MS, Naik S, Skelton WB, Wetzel JD, Wilson GJ, Chappell JD, Dermody TS.** 2007. A plasmid-based reverse genetics system for animal double-stranded RNA viruses. Cell Host Microbe **1:**147-157.

43. **Miller-Podraza H, Bradley RM, Fishman PH.** 1982. Biosynthesis and localization of gangliosides in cultured cells. Biochemistry **21:**3260-3265.
44. **Blixt O, Head S, Mondala T, Scanlan C, Huflejt ME, Alvarez R, Bryan MC, Fazio F, Calarese D, Stevens J, Razi N, Stevens DJ, Skehel JJ, van Die I, Burton DR, Wilson IA, Cummings R, Bovin N, Wong CH, Paulson JC.** 2004. Printed covalent glycan array for ligand profiling of diverse glycan binding proteins. Proc. Natl. Acad. Sci. U.S.A. **101:**17033-17038.
45. **Feizi T, Fazio F, Chai W, Wong CH.** 2003. Carbohydrate microarrays - a new set of technologies at the frontiers of glycomics. Curr Opin Struct Biol **13:**637-645.
46. **Liu Y, Childs RA, Palma AS, Campanero-Rhodes MA, Stoll MS, Chai W, Feizi T.** 2012. Neoglycolipid-based oligosaccharide microarray system: preparation of NGLs and their noncovalent immobilization on nitrocellulose-coated glass slides for microarray analyses. Methods Mol Biol **808:**117-136.
47. **Childs RA, Palma AS, Wharton S, Matrosovich T, Liu Y, Chai W, Campanero-Rhodes MA, Zhang Y, Eickmann M, Kiso M, Hay A, Matrosovich M, Feizi T.** 2009. Receptor-binding specificity of pandemic influenza A (H1N1) 2009 virus determined by carbohydrate microarray. Nat Biotechnol **27:**797-799.
48. **Stevens J, Blixt O, Glaser L, Taubenberger JK, Palese P, Paulson JC, Wilson IA.** 2006. Glycan microarray analysis of the hemagglutinins from modern and pandemic influenza viruses reveals different receptor specificities. J. Mol. Biol. **355:**1143-1155.
49. **Neu U, Maginnis MS, Palma AS, Stroh LJ, Nelson CDS, Feizi T, Atwood WJ, Stehle T.** 2010. Structure-function analysis of the human JC polyomavirus establishes the LSTc pentasaccharide as a functional receptor motif. Cell Host & Microbe **8:**309-319.
50. **Gamblin SJ, Skehel JJ.** 2010. Influenza hemagglutinin and neuraminidase membrane glycoproteins. J Biol Chem **285:**28403-28409.
51. **Neu U, Allen SA, Blaum BS, Liu Y, Frank M, Palma AS, Stroh LJ, Feizi T, Peters T, Atwood WJ, Stehle T.** 2013. A Structure-guided mutation in the major capsid protein retargets BK polyomavirus. PLoS Pathog **9:**e1003688.
52. **Rogers GN, Pritchett TJ, Lane JL, Paulson JC.** 1983. Differential sensitivity of human, avian, and equine influenza A viruses to a glycoprotein inhibitor of infection: selection of receptor specific variants. Virology **131:**394-408.
53. **Gulati S, Smith DF, Cummings RD, Couch RB, Griesemer SB, St George K, Webster RG, Air GM.** 2013. Human H3N2 Influenza Viruses Isolated from 1968 To 2012 Show Varying Preference for Receptor Substructures with No Apparent Consequences for Disease or Spread. PLoS One **8:**e66325.
54. **Kim CU, Lew W, Williams MA, Liu H, Zhang L, Swaminathan S, Bischofberger N, Chen MS, Mendel DB, Tai CY, Laver WG, Stevens**

RC. 1997. Influenza neuraminidase inhibitors possessing a novel hydrophobic interaction in the enzyme active site: design, synthesis, and structural analysis of carbocyclic sialic acid analogues with potent anti-influenza activity. J Am Chem Soc **119:**681-690.

55. **von Itzstein M, Wu WY, Kok GB, Pegg MS, Dyason JC, Jin B, Van Phan T, Smythe ML, White HF, Oliver SW, et al.** 1993. Rational design of potent sialidase-based inhibitors of influenza virus replication. Nature **363:**418-423.
56. **Xiong X, Martin SR, Haire LF, Wharton SA, Daniels RS, Bennett MS, McCauley JW, Collins PJ, Walker PA, Skehel JJ, Gamblin SJ.** 2013. Receptor binding by an H7N9 influenza virus from humans. Nature **499:**496-499.
57. **Suzuki Y, Ito T, Suzuki T, Holland RE, Jr., Chambers TM, Kiso M, Ishida H, Kawaoka Y.** 2000. Sialic acid species as a determinant of the host range of influenza A viruses. J. Virol. **74:**11825-11831.
58. **Kemp MC, Hierholzer JC, Cabradilla CP, Obijeski JF.** 1983. The changing etiology of epidemic keratoconjunctivitis: antigenic and restriction enzyme analyses of adenovirus types 19 and 37 isolated over a 10-year period. J Infect Dis **148:**24-33.
59. **Arnberg N, Edlund K, Kidd AH, Wadell G.** 2000. Adenovirus type 37 uses sialic acid as a cellular receptor. J. Virol. **74:**42-48.
60. **Wadell G.** 1969. Hemagglutination with adenovirus serotypes belonging to Rosen's subgroups II and 3. Proc Soc Exp Biol Med **132:**413-421.
61. **Qian M, Cai D, Verhey KJ, Tsai B.** 2009. A lipid receptor sorts polyomavirus from the endolysosome to the endoplasmic reticulum to cause infection. PLoS Pathog **5:**e1000465.
62. **Yeager M, Dryden KA, Olson NH, Greenberg HB, Baker TS.** 1990. Three-dimensional structure of rhesus rotavirus by cryoelectron microscopy and image reconstruction. J Cell Biol **110:**2133-2144.
63. **Fiore L, Greenberg HB, Mackow ER.** 1991. The VP8 fragment of VP4 is the rhesus rotavirus hemagglutinin. Virology **181:**553-563.
64. **Denisova E, Dowling W, LaMonica R, Shaw R, Scarlata S, Ruggeri F, Mackow ER.** 1999. Rotavirus capsid protein VP5* permeabilizes membranes. J. Virol. **73:**3147-3153.
65. **Dormitzer PR, Sun ZY, Wagner G, Harrison SC.** 2002. The rhesus rotavirus VP4 sialic acid binding domain has a galectin fold with a novel carbohydrate binding site. EMBO J. **21:**885-897.
66. **Kraschnefski MJ, Bugarcic A, Fleming FE, Yu X, von Itzstein M, Coulson BS, Blanchard H.** 2009. Effects on sialic acid recognition of amino acid mutations in the carbohydrate-binding cleft of the rotavirus spike protein. Glycobiology **19:**194-200.
67. **Blanchard H, Yu X, Coulson BS, von Itzstein M.** 2007. Insight into host cell carbohydrate-recognition by human and porcine rotavirus from crystal structures of the virion spike associated carbohydrate-binding domain (VP8*). J. Mol. Biol. **367:**1215-1226.

68. **Yu X, Dang VT, Fleming FE, von Itzstein M, Coulson BS, Blanchard H.** 2012. Structural basis of rotavirus strain preference toward N-acetyl- or N-glycolylneuraminic acid-containing receptors. J. Virol. **86:**13456-13466.
69. **Monnier N, Higo-Moriguchi K, Sun ZY, Prasad BV, Taniguchi K, Dormitzer PR.** 2006. High-resolution molecular and antigen structure of the VP8* core of a sialic acid-independent human rotavirus strain. J. Virol. **80:**1513-1523.
70. **Haselhorst T, Fiebig T, Dyason JC, Fleming FE, Blanchard H, Coulson BS, von Itzstein M.** 2011. Recognition of the GM3 ganglioside glycan by Rhesus rotavirus particles. Angewandte Chemie **50:**1055-1058.
71. **Haselhorst T, Fleming FE, Dyason JC, Hartnell RD, Yu X, Holloway G, Santegoets K, Kiefel MJ, Blanchard H, Coulson BS, von Itzstein M.** 2009. Sialic acid dependence in rotavirus host cell invasion. Nat. Chem. Biol. **5:**91-93.
72. **Tumpey TM, Maines TR, Van Hoeven N, Glaser L, Solorzano A, Pappas C, Cox NJ, Swayne DE, Palese P, Katz JM, Garcia-Sastre A.** 2007. A two-amino acid change in the hemagglutinin of the 1918 influenza virus abolishes transmission. Science **315:**655-659.
73. **Chen LM, Blixt O, Stevens J, Lipatov AS, Davis CT, Collins BE, Cox NJ, Paulson JC, Donis RO.** 2012. In vitro evolution of H5N1 avian influenza virus toward human-type receptor specificity. Virology **422:**105-113.
74. **Magaldi TG, Buch MH, Murata H, Erickson KD, Neu U, Garcea RL, Peden K, Stehle T, DiMaio D.** 2012. Mutations in the GM1 binding site of simian virus 40 VP1 alter receptor usage and cell tropism. J. Virol. **86:**7028-7042.
75. **Baum LG, Paulson JC.** 1990. Sialyloligosaccharides of the respiratory epithelium in the selection of human influenza virus receptor specificity. Acta histochemica. Supplementband **40:**35-38.
76. **Shinya K, Ebina M, Yamada S, Ono M, Kasai N, Kawaoka Y.** 2006. Avian flu: influenza virus receptors in the human airway. Nature **440:**435-436.
77. **Matrosovich M, Tuzikov A, Bovin N, Gambaryan A, Klimov A, Castrucci MR, Donatelli I, Kawaoka Y.** 2000. Early alterations of the receptor-binding properties of H1, H2, and H3 avian influenza virus hemagglutinins after their introduction into mammals. J. Virol. **74:**8502-8512.
78. **Connor RJ, Kawaoka Y, Webster RG, Paulson JC.** 1994. Receptor specificity in human, avian, and equine H2 and H3 influenza virus isolates. Virology **205:**17-23.
79. **Imai M, Kawaoka Y.** 2012. The role of receptor binding specificity in interspecies transmission of influenza viruses. Current opinion in virology **2:**160-167.
80. **Kumlin U, Olofsson S, Dimock K, Arnberg N.** 2008. Sialic acid tissue distribution and influenza virus tropism. Influenza and other respiratory viruses **2:**147-154.

81. **Stevens J, Blixt O, Tumpey TM, Taubenberger JK, Paulson JC, Wilson IA.** 2006. Structure and receptor specificity of the hemagglutinin from an H5N1 influenza virus. Science **312:**404-410.
82. **Ito T, Suzuki Y, Suzuki T, Takada A, Horimoto T, Wells K, Kida H, Otsuki K, Kiso M, Ishida H, Kawaoka Y.** 2000. Recognition of N-glycolylneuraminic acid linked to galactose by the alpha2,3 linkage is associated with intestinal replication of influenza A virus in ducks. J. Virol. **74:**9300-9305.
83. **Dawe CJ, Freund R, Mandel G, Ballmer-Hofer K, Talmage DA, Benjamin TL.** 1987. Variations in polyoma virus genotype in relation to tumor induction in mice. Characterization of wild type strains with widely differing tumor profiles. Am J Pathol **127:**243-261.
84. **Cahan LD, Singh R, Paulson JC.** 1983. Sialyloligosaccharide receptors of binding variants of polyoma virus. Virology **130:**281-289.
85. **Fried G, Cahan LD, Paulson JC.** 1981. Polyoma virus recognized specific sialyloligosaccharide receptors on host cells. Virology **109:**188-197.
86. **Freund R, Garcea RL, Sahli R, Benjamin TL.** 1991. A single-amino-acid substitution in polyomavirus VP1 correlates with plaque size and hemagglutination behavior. J. Virol. **65:**350-355.
87. **Stehle T, Yan Y, Benjamin TL, Harrison SC.** 1994. Structure of murine polyomavirus complexed with an oligosaccharide receptor fragment. Nature **369:**160-163.
88. **Stehle T, Harrison SC.** 1996. Crystal structures of murine polyomavirus in complex with straight-chain and branched-chain sialyloligosaccharide receptor fragments. Structure **4:**183-194.
89. **Stehle T, Harrison SC.** 1997. High-resolution structure of a polyomavirus VP1-oligosaccharide complex: implications for assembly and receptor binding. Embo J **16:**5139-5148.
90. **Bauer H, Stelzhammer W, Fuchs R, Weiger TM, Danninger C, Probst G, Krizbai IA.** 1999. Astrocytes and neurons express the tight junction-specific protein occludin in vitro. Exp Cell Res **250:**434-438.
91. **Martinez MA, Lopez S, Arias CF, Isa P.** 2013. Gangliosides have a functional role during rotavirus cell entry. J. Virol. **87:**1115-1122.
92. **Yolken RH, Willoughby R, Wee SB, Miskuff R, Vonderfecht S.** 1987. Sialic acid glycoproteins inhibit in vitro and in vivo replication of rotaviruses. J. Clin. Invest. **79:**148-154.
93. **Lee PWK, Hayes EC, Joklik WK.** 1981. Protein σ1 is the reovirus cell attachment protein. Virology **108:**156-163.
94. **Sarkar G, Pelletier J, Bassel-Duby R, Jayasuriya A, Fields BN, Sonenberg N.** 1985. Identification of a new polypeptide coded by reovirus gene S1. J. Virol. **54:**720-725.
95. **Boehme KW, Hammer K, Tollefson WC, Konopka-Anstadt JL, Kobayashi T, Dermody TS.** 2013. Nonstructural Protein sigma1s Mediates Reovirus-Induced Cell Cycle Arrest and Apoptosis. J. Virol.

96. **Tai JH, Williams JV, Edwards KM, Wright PF, Crowe JE, Jr., Dermody TS.** 2005. Prevalence of reovirus-specific antibodies in young children in Nashville, Tennessee. J Infect Dis **191:**1221-1224.
97. **Tyler KL, Barton ES, Ibach ML, Robinson C, Valyi-Nagy T, Campbell JA, Clarke P, O'Donnell SM, Wetzel JD, Dermody TS.** 2004. Isolation and molecular characterization of a novel type 3 reovirus from a child with meningitis. J. Infect. Dis. **189:**1664-1675.
98. **Nason EL, Wetzel JD, Mukherjee SK, Barton ES, Prasad BVV, Dermody TS.** 2001. A monoclonal antibody specific for reovirus outer-capsid protein σ3 inhibits σ1-mediated hemagglutination by steric hindrance. J. Virol. **75:**6625-6634.
99. **Ramos-Alvarez M, Sabin AB.** 1954. Characteristics of poliomyelitis and other enteric viruses recovered in tissue culture from healthy American children. Proc. Soc. Exp. Biol. Med. **87:**655-661.
100. **Ramos-Alvarez M, Sabin AB.** 1958. Enteropathogenic viruses and bacteria. Role in summer diarrheal diseases of infancy and early childhood. Journal of the American Medical Association **167:**147-158.
101. **Sabin AB.** 1956. The significance of viruses recovered from the intestinal tracts of healthy infants and children. Ann N Y Acad Sci **66:**226-230.
102. **Wolf JL, Rubin DH, Finberg R, Kaufman RS, Sharpe AH, Trier JS, Fields BN.** 1981. Intestinal M cells: a pathway of entry of reovirus into the host. Science **212:**471-472.
103. **Gonzalez-Hernandez MB, Liu T, Payne HC, Stencel-Baerenwald JE, Ikizler M, Yagita H, Dermody TS, Williams IR, Wobus CE.** 2014. Efficient Norovirus and Reovirus Replication in the Mouse Intestine Requires Microfold (M) Cells. J. Virol. **88:**6934-6943.
104. **Morrison LA, Sidman RL, Fields BN.** 1991. Direct spread of reovirus from the intestinal lumen to the central nervous system through vagal autonomic nerve fibers. Proc. Natl. Acad. Sci. U. S. A. **88:**3852-3856.
105. **Tardieu M, Weiner HL.** 1982. Viral receptors on isolated murine and human ependymal cells. Science **215:**419-421.
106. **Masters C, Alpers M, Kakulas B.** 1977. Pathogenesis of reovirus type 1 hydrocephalus in mice: significance of aqueductal changes. Arch. Neurol. **34:**18-28.
107. **Phillips PA, Alpers MP, Stanley NF.** 1970. Hydrocephalus in mice inoculated neonatally by the oronasal route with reovirus type 1. Science **168:**858-859.
108. **Margolis G, Kilham L.** 1969. Hydrocephalus in hamsters, ferrets, rats, and mice following inoculations with reovirus type I. II. Pathologic studies. Lab Invest **21:**189-198.
109. **Boehme KW, Frierson JM, Konopka JL, Kobayashi T, Dermody TS.** 2011. The reovirus sigma1s protein is a determinant of hematogenous but not neural virus dissemination in mice. J. Virol. **85:**11781-11790.
110. **Weiner HL, Greene MI, Fields BN.** 1980. Delayed hypersensitivity in mice infected with reovirus. I. Identification of host and viral gene products responsible for the immune response. J. Immunol. **125:**278-282.

111. **Pruijssers AJ, Hengel H, Abel TW, Dermody TS.** 2013. Apoptosis Induction Influences Reovirus Replication and Virulence in Newborn Mice. J. Virol.
112. **Jenson AB, Rabin ER, Phillips CA, al e.** 1965. Reovirus encephalitis in newborn mice: an electron microscopic and virus assay study. Am. J. Pathol. **47:**223-239.
113. **Danthi P, Pruijssers AJ, Berger AK, Holm GH, Zinkel SS, Dermody TS.** 2010. Bid regulates the pathogenesis of neurotropic reovirus. PLoS Path. **6:**e1000980.
114. **Weiner HL, Powers ML, Fields BN.** 1980. Absolute linkage of virulence and central nervous system tropism of reoviruses to viral hemagglutinin. J. Infect. Dis. **141:**609-616.
115. **Tardieu M, Powers ML, Weiner HL.** 1983. Age-dependent susceptibility to reovirus type 3 encephalitis: role of viral and host factors. Ann. Neurol. **13:**602-607.
116. **Virgin HW, Tyler KL.** 1991. Role of immune cells in protection against and control of reovirus infection in neonatal mice. J. Virol. **65:**5157-5164.
117. **Virgin HW, IV, Bassel-Duby R, Fields BN, Tyler KL.** 1988. Antibody protects against lethal infection with the neurally spreading reovirus type 3 (Dearing). J. Virol. **62:**4594-4604.
118. **Tyler KL, Virgin HW, Bassel-Duby R, Fields BN.** 1989. Antibody inhibits defined stages in the pathogenesis of reovirus serotype 3 infection of the central nervous system. J. Exp. Med. **170:**887-900.
119. **George A, Kost SI, Witzleben CL, al e.** 1990. Reovirus-induced liver disease in severe combined immunodeficient (SCID) mice: a model for the study of viral infection, pathogenesis, and clearance. J. Exp. Med. **171:**929-934.
120. **Tyler KL, McPhee DA, Fields BN.** 1986. Distinct pathways of viral spread in the host determined by reovirus S1 gene segment. Science **233:**770-774.
121. **Furlong DB, Nibert ML, Fields BN.** 1988. Sigma 1 protein of mammalian reoviruses extends from the surfaces of viral particles. J. Virol. **62:**246-256.
122. **Dryden KA, Wang G, Yeager M, Nibert ML, Coombs KM, Furlong DB, Fields BN, Baker TS.** 1993. Early steps in reovirus infection are associated with dramatic changes in supramolecular structure and protein conformation: analysis of virions and subviral particles by cryoelectron microscopy and image reconstruction. J. Cell Biol. **122:**1023-1041.
123. **Chappell JD, Prota A, Dermody TS, Stehle T.** 2002. Crystal structure of reovirus attachment protein σ1 reveals evolutionary relationship to adenovirus fiber. EMBO J. **21:**1-11.
124. **Nibert ML, Dermody TS, Fields BN.** 1990. Structure of the reovirus cell-attachment protein: a model for the domain organization of σ1. J. Virol. **64:**2976-2989.
125. **Campbell JA, Shelling P, Wetzel JD, Johnson EM, Wilson GAR, Forrest JC, Aurrand-Lions M, Imhof B, Stehle T, Dermody TS.** 2005.

Junctional adhesion molecule-A serves as a receptor for prototype and field-isolate strains of mammalian reovirus. J. Virol. **79:**7967-7978.
126. **Bazzoni G, Martinez-Estrada OM, Orsenigo F, Cordenonsi M, Citi S, Dejana E.** 2000. Interaction of junctional adhesion molecule with the tight junction components ZO-1, cingulin, and occludin. J. Biol. Chem. **275:**20520-20526.
127. **Ebnet K, Schulz CU, Meyer Zu Brickwedde MK, Pendl GG, Vestweber D.** 2000. Junctional adhesion molecule interacts with the PDZ domain-containing proteins AF-6 and ZO-1. J. Biol. Chem. **275:**27979-27988.
128. **Maschio AD, Luigi AD, Martin-Padura I, Brockhaus M, Bartfai T, Fruscella P, Adorini L, Martino G, Furlan R, DeSimoni MG, Dejana E.** 1999. Leukocyte recruitment in the cerebrospinal fluid of mice with experimental meningitis is inhabited by an antibody to junctional adhesion molecule (JAM). J. Exp. Med. **190:**1351-1356.
129. **Lechner F, Sahrbacher U, Suter T, Frei K, Brockhaus M, Koedel U, Fontana A.** 2000. Antibodies to the junctional adhesion molecule cause disruption of endothelial cells and do not prevent leukocyte influx into the meninges after viral or bacterial infection. J Infect Dis **182:**978-982.
130. **Kirchner E.** 2009. Structural and functional studies of the reovirus attachment protein σ1 and its interaction with the receptor JAM-A. Eberhard Karls University of Tübingen, Eberhard Karls University of Tübingen, Tübingen, Baden-Württemberg, Germany.
131. **Barton WA, Liu BP, Tzvetkova D, Jeffrey PD, Fournier AE, Sah D, Cate R, Strittmatter SM, Nikolov DB.** 2003. Structure and axon outgrowth inhibitor binding of the Nogo-66 receptor and related proteins. EMBO J **22:**3291-3302.
132. **Fournier AE, GrandPre T, Strittmatter SM.** 2001. Identification of a receptor mediating Nogo-66 inhibition of axonal regeneration. Nature **409:**341-346.
133. **He XL, Bazan JF, McDermott G, Park JB, Wang K, Tessier-Lavigne M, He Z, Garcia KC.** 2003. Structure of the Nogo receptor ectodomain: a recognition module implicated in myelin inhibition. Neuron **38:**177-185.
134. **Wang KC, Koprivica V, Kim JA, Sivasankaran R, Guo Y, Neve RL, He Z.** 2002. Oligodendrocyte-myelin glycoprotein is a Nogo receptor ligand that inhibits neurite outgrowth. Nature **417:**941-944.
135. **Hunt D, Coffin RS, Anderson PN.** 2002. The Nogo receptor, its ligands and axonal regeneration in the spinal cord; a review. J Neurocytol **31:**93-120.
136. **McGee AW, Strittmatter SM.** 2003. The Nogo-66 receptor: focusing myelin inhibition of axon regeneration. Trends Neurosci **26:**193-198.
137. **Lerner AM, Cherry JD, Finland M.** 1963. Haemagglutination with reoviruses. Virology **19:**58-65.
138. **Eggers HJ, Gomatos PJ, Tamm I.** 1962. Agglutination of bovine erythrocytes: a general characteristic of reovirus type 3. Proc. Soc. Exp. Biol. Med. **110:**879-881.

139. **Barton ES, Youree BE, Ebert DH, Forrest JC, Connolly JL, Valyi-Nagy T, Washington K, Wetzel JD, Dermody TS.** 2003. Utilization of sialic acid as a coreceptor is required for reovirus-induced biliary disease. J. Clin. Invest. **111:**1823-1833.
140. **Frierson JM, Pruijssers AJ, Konopka JL, Reiter DM, Abel TW, Stehle T, Dermody TS.** 2012. Utilization of sialylated glycans as coreceptors enhances the neurovirulence of serotype 3 reovirus. J. Virol. **86:**13164-13173.
141. **Helander A, Silvey KJ, Mantis NJ, Hutchings AB, Chandran K, Lucas WT, Nibert ML, Neutra MR.** 2003. The viral σ1 protein and glycoconjugates containing α2-3-linked sialic acid are involved in type 1 reovirus adherence to M cell apical surfaces. J. Virol. **77:**7964-7977.
142. **Gollamudi R, Ghalib MH, Desai KK, Chaudhary I, Wong B, Einstein M, Coffey M, Gill GM, Mettinger K, Mariadason JM, Mani S, Goel S.** 2009. Intravenous administration of Reolysin, a live replication competent RNA virus is safe in patients with advanced solid tumors. Invest New Drugs **28:**641-649.
143. **Vidal L, Pandha HS, Yap TA, White CL, Twigger K, Vile RG, Melcher A, Coffey M, Harrington KJ, DeBono JS.** 2008. A phase I study of intravenous oncolytic reovirus type 3 Dearing in patients with advanced cancer. Clin. Cancer. Res. **14:**7127-7137.
144. **Sahin E, Egger M, McMasters K, Zhou H.** 2013. Development of Oncolytic Reovirus for Cancer Therapy. Journal of Cancer Therapy **4:**1100-1115.
145. **Harduin-Lepers A, Krzewinski-Recchi MA, Colomb F, Foulquier F, Groux-Degroote S, Delannoy P.** 2012. Sialyltransferases functions in cancers. Frontiers in bioscience **4:**499-515.
146. **Chappell JD, Duncan R, Mertens PPC, Dermody TS.** 2005. Orthoreovirus, Reoviridae, p. 455-465. *In* Fauquet CM, Mayo, M. A., Maniloff, J., Desselberger, U., and L. A. Ball (ed.), Virus Taxonomy: The Classification and Nomenclature of Viruses. The Eighth Report of the International Committee on Taxonomy of Viruses. Elsevier/Academic Press, London.
147. **Rubin DH, Wetzel JD, Williams WV, Cohen JA, Dworkin C, Dermody TS.** 1992. Binding of type 3 reovirus by a domain of the σ1 protein important for hemagglutination leads to infection of murine erythroleukemia cells. J. Clin. Invest. **90:**2536-2542.
148. **Uchida Y, Tsukada Y, Sugimori T.** 1979. Enzymatic properties of neuraminidases from Arthrobacter ureafaciens. J. Biochem. **86:**1573-1585.
149. **Raval G, Biswas S, Rayman P, Biswas K, Sa G, Ghosh S, Thornton M, Hilston C, Das T, Bukowski R, Finke J, Tannenbaum CS.** 2007. TNF-alpha induction of GM2 expression on renal cell carcinomas promotes T cell dysfunction. The Journal of Immunology **178:**6642-6652.
150. **Yamada T, Bando H, Takeuchi S, Kita K, Li Q, Wang W, Akinaga S, Nishioka Y, Sone S, Yano S.** 2011. Genetically engineered humanized

anti-ganglioside GM2 antibody against multiple organ metastasis produced by GM2-expressing small-cell lung cancer cells. Cancer Sci **102:**2157-2163.

151. **Kobayashi T, Ooms LS, Ikizler M, Chappell JD, Dermody TS.** 2010. An improved reverse genetics system for mammalian orthoreoviruses. Virology **2:**194-200.
152. **Kirchner E, Guglielmi KM, Strauss HM, Dermody TS, Stehle T.** 2008. Structure of reovirus σ1 in complex with its receptor junctional adhesion molecule-A. PLoS Path. **4:**e1000235.
153. **Schelling P, Guglielmi KM, Kirchner E, Paetzold B, Dermody TS, Stehle T.** 2007. The reovirus σ1 aspartic acid sandwich: a trimerization motif poised for conformational change. J. Biol. Chem. **282:**11582-11589.
154. **Dermody TS, Nibert ML, Bassel-Duby R, Fields BN.** 1990. A σ1 region important for hemagglutination by serotype 3 reovirus strains. J. Virol. **64:**5173-5176.
155. **Helander A, Miller CL, Myers KS, Neutra MR, Nibert ML.** 2004. Protective immunoglobulin A and G antibodies bind to overlapping intersubunit epitopes in the head domain of type 1 reovirus adhesin σ1. J. Virol. **78:**10695-10705.
156. **Gentsch JR, Pacitti AF.** 1987. Differential interaction of reovirus type 3 with sialylated receptor components on animal cells. Virology **161:**245-248.
157. **Neu U, Hengel H, Blaum BS, Schowalter RM, Macejak D, Gilbert M, Wakarchuk WW, Imamura A, Ando H, Kiso M, Arnberg N, Garcea RL, Peters T, Buck CB, Stehle T.** 2012. Structures of Merkel cell polyomavirus VP1 complexes define a sialic acid binding site required for infection. PLoS Pathog **8:**e1002738.
158. **Meyer B, Peters T.** 2003. NMR spectroscopy techniques for screening and identifying ligand binding to protein receptors. Angewandte Chemie **42:**864-890.
159. **Brubaker MM, West B, Ellis RJ.** 1964. Human blood group influence on reovirus hemagglutination titers. Proc. Soc. Exp. Biol. Med. **115:**1118.
160. **Sugano Y, Takeuchi M, Hirata A, Matsushita H, Kitamura T, Tanaka M, Miyajima A.** 2008. Junctional adhesion molecule-A, JAM-A, is a novel cell-surface marker for long-term repopulating hematopoietic stem cells. Blood **111:**1167-1172.
161. **Liu Y, Childs RA, Matrosovich T, Wharton S, Palma AS, Chai W, Daniels R, Gregory V, Uhlendorff J, Kiso M, Klenk HD, Hay A, Feizi T, Matrosovich M.** 2010. Altered receptor specificity and cell tropism of D222G hemagglutinin mutants isolated from fatal cases of pandemic A(H1N1) 2009 influenza virus. J. Virol. **84:**12069-12074.
162. **Imai M, Watanabe T, Hatta M, Das SC, Ozawa M, Shinya K, Zhong G, Hanson A, Katsura H, Watanabe S, Li C, Kawakami E, Yamada S, Kiso M, Suzuki Y, Maher EA, Neumann G, Kawaoka Y.** 2012. Experimental adaptation of an influenza H5 HA confers respiratory droplet

transmission to a reassortant H5 HA/H1N1 virus in ferrets. Nature **486:**420-428.
163. **Zhang Y, Zhang Q, Kong H, Jiang Y, Gao Y, Deng G, Shi J, Tian G, Liu L, Liu J, Guan Y, Bu Z, Chen H.** 2013. H5N1 hybrid viruses bearing 2009/H1N1 virus genes transmit in guinea pigs by respiratory droplet. Science **340:**1459-1463.
164. **Margolis G, Kilham L, Gonatos N.** 1971. Reovirus type III encephalitis: observations of virus-cell interactions in neural tissues. I. Light microscopy studies. Laboratory Investigations **24:**91-109.
165. **Prota AE, Campbell JA, Schelling P, Forrest JC, Peters TR, Watson MJ, Aurrand-Lions M, Imhof B, Dermody TS, Stehle T.** 2003. Crystal structure of human junctional adhesion molecule 1: implications for reovirus binding. Proc. Natl. Acad. Sci. U. S. A. **100:**5366-5371.
166. **Cochran FB, Jr., Yu RK, Ledeen RW.** 1982. Myelin gangliosides in vertebrates. J Neurochem **39:**773-779.
167. **Satoh JI, Tai T, Kim SU.** 1996. Differential expression of gangliosides and galactolipids in fetal human oligodendrocytes and astrocytes in culture. Brain research. Developmental brain research **93:**172-181.
168. **Marconi S, De Toni L, Lovato L, Tedeschi E, Gaetti L, Acler M, Bonetti B.** 2005. Expression of gangliosides on glial and neuronal cells in normal and pathological adult human brain. J Neuroimmunol **170:**115-121.
169. **Yu RK, Tsai YT, Ariga T, Yanagisawa M.** 2011. Structures, biosynthesis, and functions of gangliosides--an overview. J Oleo Sci **60:**537-544.
170. **Scholzen T, Gerdes J.** 2000. The Ki-67 protein: from the known and the unknown. J Cell Physiol **182:**311-322.
171. **Venter EH, van der Lugt JJ, Gerdes GH.** 1993. Detection of bluetongue virus RNA in cell cultures and in the central nervous system of experimentally infected mice using in situ hybridization. Onderstepoort J. Vet. Res. **60:**39-45.
172. **Singhal N, Xu R, Martin PT.** 2012. Distinct contributions of Galgt1 and Galgt2 to carbohydrate expression and function at the mouse neuromuscular junction. Molecular and cellular neurosciences **51:**112-126.
173. **Takamiya K, Yamamoto A, Furukawa K, Yamashiro S, Shin M, Okada M, Fukumoto S, Haraguchi M, Takeda N, Fujimura K, Sakae M, Kishikawa M, Shiku H, Furukawa K, Aizawa S.** 1996. Mice with disrupted GM2/GD2 synthase gene lack complex gangliosides but exhibit only subtle defects in their nervous system. Proc Natl Acad Sci U S A **93:**10662-10667.
174. **Sarnat HB.** 1995. Ependymal reactions to injury. A review. J Neuropathol Exp Neurol **54:**1-15.
175. **Yu L, Baxter PA, Voicu H, Gurusiddappa S, Zhao Y, Adesina A, Man TK, Shu Q, Zhang YJ, Zhao XM, Su JM, Perlaky L, Dauser R, Chintagumpala M, Lau CC, Blaney SM, Rao PH, Leung HC, Li XN.** 2010. A clinically relevant orthotopic xenograft model of ependymoma that

maintains the genomic signature of the primary tumor and preserves cancer stem cells in vivo. Neuro-oncology **12:**580-594.
176. **Monnot AD, Zheng W.** 2013. Culture of choroid plexus epithelial cells and in vitro model of blood-CSF barrier. Methods Mol Biol **945:**13-29.
177. **Boehme KW, Guglielmi KM, Dermody TS.** 2009. Reovirus nonstructural protein σ1s is required for establishment of viremia and systemic dissemination. Proc. Natl. Acad. Sci. U. S. A. **106:**19986-19991.
178. **Boehme KW, Frierson JM, Konopka JL, Kobayashi T, Dermody TS.** 2011. The reovirus σ1s protein is a determinant of hematogenous but not neural virus dissemination in mice. J. Virol. **85:**11781-11790.
179. **Dermody TS, Nibert ML, Bassel-Duby R, Fields BN.** 1990. Sequence diversity in S1 genes and S1 translation products of 11 serotype 3 reovirus strains. J. Virol. **64:**4842-4850.
180. **Gulati S, Lasanajak Y, Smith DF, Cummings RD, Air GM.** 2014. Glycan array analysis of influenza H1N1 binding and release. Cancer biomarkers : section A of Disease markers **14:**43-53.
181. **Weis W, Brown JH, Cusack S, Paulson JC, Skehel JJ, Wiley DC.** 1988. Structure of the influenza virus haemagglutinin complexed with its receptor, sialic acid. Nature **333:**426-431.
182. **Nobusawa E, Aoyama T, Kato H, Suzuki Y, Tateno Y, Nakajima K.** 1991. Comparison of complete amino acid sequences and receptor-binding properties among 13 serotypes of hemagglutinins of influenza A viruses. Virology **182:**475-485.
183. **Watowich SJ, Skehel JJ, Wiley DC.** 1994. Crystal structures of influenza virus hemagglutinin in complex with high-affinity receptor analogs. Structure **2:**719-731.
184. **Sauter NK, Hanson JE, Glick GD, Brown JH, Crowther RL, Park SJ, Skehel JJ, Wiley DC.** 1992. Binding of influenza virus hemagglutinin to analogs of its cell-surface receptor, sialic acid: analysis by proton nuclear magnetic resonance spectroscopy and X-ray crystallography. Biochemistry **31:**9609-9621.
185. **Shevchuk NA, Hathout Y, Epifano O, Su Y, Liu Y, Sutherland M, Ladisch S.** 2007. Alteration of ganglioside synthesis by GM3 synthase knockout in murine embryonic fibroblasts. Biochim Biophys Acta **1771:**1226-1234.
186. **Walther T, Karamanska R, Chan RW, Chan MC, Jia N, Air G, Hopton C, Wong MP, Dell A, Malik Peiris JS, Haslam SM, Nicholls JM.** 2013. Glycomic analysis of human respiratory tract tissues and correlation with influenza virus infection. PLoS Pathog **9:**e1003223.
187. **Comelli EM, Head SR, Gilmartin T, Whisenant T, Haslam SM, North SJ, Wong NK, Kudo T, Narimatsu H, Esko JD, Drickamer K, Dell A, Paulson JC.** 2006. A focused microarray approach to functional glycomics: transcriptional regulation of the glycome. Glycobiology **16:**117-131.
188. **Song X, Lasanajak Y, Xia B, Heimburg-Molinaro J, Rhea JM, Ju H, Zhao C, Molinaro RJ, Cummings RD, Smith DF.** 2011. Shotgun

glycomics: a microarray strategy for functional glycomics. Nat Methods **8:**85-90.
189. **Byrd-Leotis L, Liu R, Bradley KC, Lasanajak Y, Cummings SF, Song X, Heimburg-Molinaro J, Galloway SE, Culhane MR, Smith DF, Steinhauer DA, Cummings RD.** 2014. Shotgun glycomics of pig lung identifies natural endogenous receptors for influenza viruses. Proc Natl Acad Sci U S A.
190. **Munch TN, Rasmussen ML, Wohlfahrt J, Juhler M, Melbye M.** 2014. Risk factors for congenital hydrocephalus: a nationwide, register-based, cohort study. Journal of neurology, neurosurgery, and psychiatry.
191. **Simeone RM, Rasmussen SA, Mei JV, Dollard SC, Frias JL, Shaw GM, Canfield MA, Meyer RE, Jones JL, Lorey F, Honein MA.** 2013. A pilot study using residual newborn dried blood spots to assess the potential role of cytomegalovirus and Toxoplasma gondii in the etiology of congenital hydrocephalus. Birth defects research. Part A, Clinical and molecular teratology **97:**431-436.
192. **Enders G, Bader U, Lindemann L, Schalasta G, Daiminger A.** 2001. Prenatal diagnosis of congenital cytomegalovirus infection in 189 pregnancies with known outcome. Prenat Diagn **21:**362-377.
193. **Johnson KP, Johnson RT.** 1972. Granular ependymitis. Occurrence in myxovirus infected rodents and prevalence in man. Am J Pathol **67:**511-526.
194. **Tai JH, Williams JV, Edwards KM, Wright PF, Crowe JE, Dermody TS.** 2005. Prevalence of reovirus-specific antibodies in young children in Nashville, Tennessee. J. Infect. Dis. **191:**1221-1224.
195. **Rosen L, Hovis JF, Mastrota FM, Bell JA, Huebner RJ.** 1960. Observations on a newly recognized virus (Abney) of the reovirus family. American Journal of Hygiene **71:**258-265.
196. **Joske RA, Keall DD, Leak PJ, al e.** 1966. Hepatitis-encephalitis in humans with reovirus infections. Arch Intern Med **113:**811-816.
197. **Rosen L, Evans HE, Spickard A.** 1963. Reovirus infections in human volunteers. American Journal of Hygiene **77:**29-37.
198. **Malakhov MP, Aschenbrenner LM, Smee DF, Wandersee MK, Sidwell RW, Gubareva LV, Mishin VP, Hayden FG, Kim DH, Ing A, Campbell ER, Yu M, Fang F.** 2006. Sialidase fusion protein as a novel broad-spectrum inhibitor of influenza virus infection. Antimicrob Agents Chemother **50:**1470-1479.
199. **Belser JA, Lu X, Szretter KJ, Jin X, Aschenbrenner LM, Lee A, Hawley S, Kim do H, Malakhov MP, Yu M, Fang F, Katz JM.** 2007. DAS181, a novel sialidase fusion protein, protects mice from lethal avian influenza H5N1 virus infection. J Infect Dis **196:**1493-1499.
200. **Wathen MW, Barro M, Bright RA.** 2013. Antivirals in seasonal and pandemic influenza--future perspectives. Influenza Other Respir Viruses **7 Suppl 1:**76-80.
201. **Hashiro G, Loh PC, Yau JT.** 1977. The preferential cytotoxicity of reovirus for certain transformed cell lines. Arch Virol **54:**307-315.

202. **Norman KL, Hirasawa K, Yang AD, Shields MA, Lee PW.** 2004. Reovirus oncolysis: the Ras/RalGEF/p38 pathway dictates host cell permissiveness to reovirus infection. Proc. Natl. Acad. Sci. U. S. A. **101:**11099-11104.
203. **Strong JE, Coffey MC, Tang D, Sabinin P, Lee PW.** 1998. The molecular basis of viral oncolysis: usurpation of the Ras signaling pathway by reovirus. EMBO J **17:**3351-3362.
204. **Coffey MC, Strong JE, Forsyth PA, Lee PW.** 1998. Reovirus therapy of tumors with activated Ras pathway. Science **282:**1332-1334.
205. **Kyula JN, Roulstone V, Karapanagiotou EM, Melcher AA, Harrington KJ.** 2012. Oncolytic reovirus type 3 (Dearing) as a novel therapy in head and neck cancer. Expert Opin Biol Ther **12:**1669-1678.
206. **Kim M, Garant KA, zur Nieden NI, Alain T, Loken SD, Urbanski SJ, Forsyth PA, Rancourt DE, Lee PW, Johnston RN.** 2011. Attenuated reovirus displays oncolysis with reduced host toxicity. Br. J. Cancer **104:**290-299.
207. **van den Wollenberg DJ, Dautzenberg IJ, van den Hengel SK, Cramer SJ, de Groot RJ, Hoeben RC.** 2012. Isolation of reovirus T3D mutants capable of infecting human tumor cells independent of junction adhesion molecule-A. PLoS One **7:**e48064.
208. **Holm GH, Pruijssers AJ, Li L, Danthi P, Sherry B, Dermody TS.** 2010. Interferon regulatory factor 3 attenuates reovirus myocarditis and contributes to viral clearance. J. Virol. **84:**6900-6908.
209. **Smith RE, Zweerink HJ, Joklik WK.** 1969. Polypeptide components of virions, top component and cores of reovirus type 3. Virology **39:**791-810.
210. **Wilson GJ, Wetzel JD, Puryear W, Bassel-Duby R, Dermody TS.** 1996. Persistent reovirus infections of L cells select mutations in viral attachment protein σ1 that alter oligomer stability. J. Virol. **70:**6598-6606.
211. **Wetzel JD, Chappell JD, Fogo AB, Dermody TS.** 1997. Efficiency of viral entry determines the capacity of murine erythroleukemia cells to support persistent infections by mammalian reoviruses. J. Virol. **71:**299-306.
212. **Iskarpatyoti JA, Morse EA, McClung RP, Ikizler M, Wetzel JD, Contractor N, Dermody TS.** 2012. Serotype-specific differences in inhibition of reovirus infectivity by human-milk glycans are determined by viral attachment protein sigma1 Virology **433:**489-497.
213. **Marsh MN.** 1992. Gluten, major histocompatibility complex, and the small intestine. A molecular and immunobiologic approach to the spectrum of gluten sensitivity ('celiac sprue'). Gastroenterology **102:**330-354.
214. **Green PH, Jabri B.** 2003. Coeliac disease. Lancet **362:**383-391.
215. **Ferguson A, McClure JP, Townley RR.** 1976. Intraepithelial lymphocyte counts in small intestinal biopsies from children with diarrhoea. Acta paediatrica Scandinavica **65:**541-546.
216. **Sollid LM.** 2002. Coeliac disease: dissecting a complex inflammatory disorder. Nat Rev Immunol **2:**647-655.

217. **Nistico L, Fagnani C, Coto I, Percopo S, Cotichini R, Limongelli MG, Paparo F, D'Alfonso S, Giordano M, Sferlazzas C, Magazzu G, Momigliano-Richiardi P, Greco L, Stazi MA.** 2006. Concordance, disease progression, and heritability of coeliac disease in Italian twins. Gut **55:**803-808.
218. **Dubois PC, Trynka G, Franke L, Hunt KA, Romanos J, Curtotti A, Zhernakova A, Heap GA, Adany R, Aromaa A, Bardella MT, van den Berg LH, Bockett NA, de la Concha EG, Dema B, Fehrmann RS, Fernandez-Arquero M, Fiatal S, Grandone E, Green PM, Groen HJ, Gwilliam R, Houwen RH, Hunt SE, Kaukinen K, Kelleher D, Korponay-Szabo I, Kurppa K, MacMathuna P, Maki M, Mazzilli MC, McCann OT, Mearin ML, Mein CA, Mirza MM, Mistry V, Mora B, Morley KI, Mulder CJ, Murray JA, Nunez C, Oosterom E, Ophoff RA, Polanco I, Peltonen L, Platteel M, Rybak A, Salomaa V, Schweizer JJ, Sperandeo MP, Tack GJ, Turner G, Veldink JH, Verbeek WH, Weersma RK, Wolters VM, Urcelay E, Cukrowska B, Greco L, Neuhausen SL, McManus R, Barisani D, Deloukas P, Barrett JC, Saavalainen P, Wijmenga C, van Heel DA.** 2010. Multiple common variants for celiac disease influencing immune gene expression. Nat Genet **42:**295-302.
219. **Abadie V, Sollid LM, Barreiro LB, Jabri B.** 2011. Integration of genetic and immunological insights into a model of celiac disease pathogenesis. Annu Rev Immunol **29:**493-525.
220. **Molberg O, McAdam SN, Korner R, Quarsten H, Kristiansen C, Madsen L, Fugger L, Scott H, Noren O, Roepstorff P, Lundin KE, Sjostrom H, Sollid LM.** 1998. Tissue transglutaminase selectively modifies gliadin peptides that are recognized by gut-derived T cells in celiac disease. Nat. Med. **4:**713-717.
221. **van de Wal Y, Kooy Y, van Veelen P, Pena S, Mearin L, Papadopoulos G, Koning F.** 1998. Selective deamidation by tissue transglutaminase strongly enhances gliadin-specific T cell reactivity. J Immunol **161:**1585-1588.
222. **Fleckenstein B, Molberg O, Qiao SW, Schmid DG, von der Mulbe F, Elgstoen K, Jung G, Sollid LM.** 2002. Gliadin T cell epitope selection by tissue transglutaminase in celiac disease. Role of enzyme specificity and pH influence on the transamidation versus deamidation process. J Biol Chem **277:**34109-34116.
223. **Vader LW, de Ru A, van der Wal Y, Kooy YM, Benckhuijsen W, Mearin ML, Drijfhout JW, van Veelen P, Koning F.** 2002. Specificity of tissue transglutaminase explains cereal toxicity in celiac disease. J Exp Med **195:**643-649.
224. **Jabri B, Sollid LM.** 2006. Mechanisms of disease: immunopathogenesis of celiac disease. Nature clinical practice. Gastroenterology & hepatology **3:**516-525.
225. **Arentz-Hansen H, Korner R, Molberg O, Quarsten H, Vader W, Kooy YM, Lundin KE, Koning F, Roepstorff P, Sollid LM, McAdam SN.** 2000. The intestinal T cell response to alpha-gliadin in adult celiac disease is

focused on a single deamidated glutamine targeted by tissue transglutaminase. J Exp Med **191:**603-612.
226. **Xia J, Sollid LM, Khosla C.** 2005. Equilibrium and kinetic analysis of the unusual binding behavior of a highly immunogenic gluten peptide to HLA-DQ2. Biochemistry **44:**4442-4449.
227. **Fallang LE, Bergseng E, Hotta K, Berg-Larsen A, Kim CY, Sollid LM.** 2009. Differences in the risk of celiac disease associated with HLA-DQ2.5 or HLA-DQ2.2 are related to sustained gluten antigen presentation. Nat Immunol **10:**1096-1101.
228. **Jabri B, Chen X, Sollid LM.** 2014. How T cells taste gluten in celiac disease. Nat Struct Mol Biol **21:**429-431.
229. **Petersen J, Montserrat V, Mujico JR, Loh KL, Beringer DX, van Lummel M, Thompson A, Mearin ML, Schweizer J, Kooy-Winkelaar Y, van Bergen J, Drijfhout JW, Kan WT, La Gruta NL, Anderson RP, Reid HH, Koning F, Rossjohn J.** 2014. T-cell receptor recognition of HLA-DQ2-gliadin complexes associated with celiac disease. Nat Struct Mol Biol **21:**480-488.
230. **Sollid LM, Molberg O, McAdam S, Lundin KE.** 1997. Autoantibodies in coeliac disease: tissue transglutaminase--guilt by association? Gut **41:**851-852.
231. **Kagnoff MF.** 2007. Celiac disease: pathogenesis of a model immunogenetic disease. J Clin Invest **117:**41-49.
232. **Stene LC, Honeyman MC, Hoffenberg EJ, Haas JE, Sokol RJ, Emery L, Taki I, Norris JM, Erlich HA, Eisenbarth GS, Rewers M.** 2006. Rotavirus infection frequency and risk of celiac disease autoimmunity in early childhood: a longitudinal study. The American journal of gastroenterology **101:**2333-2340.
233. **Smits SL, van Leeuwen M, van der Eijk AA, Fraaij PL, Escher JC, Simon JH, Osterhaus AD.** 2010. Human astrovirus infection in a patient with new-onset celiac disease. J Clin Microbiol **48:**3416-3418.
234. **Kagnoff MF, Paterson YJ, Kumar PJ, Kasarda DD, Carbone FR, Unsworth DJ, Austin RK.** 1987. Evidence for the role of a human intestinal adenovirus in the pathogenesis of coeliac disease. Gut **28:**995-1001.
235. **Monteleone G, Pender SL, Alstead E, Hauer AC, Lionetti P, McKenzie C, MacDonald TT.** 2001. Role of interferon alpha in promoting T helper cell type 1 responses in the small intestine in coeliac disease. Gut **48:**425-429.
236. **Cammarota G, Cuoco L, Cianci R, Pandolfi F, Gasbarrini G.** 2000. Onset of coeliac disease during treatment with interferon for chronic hepatitis C. Lancet **356:**1494-1495.
237. **Nelson PA, Akselband Y, Dearborn SM, Al-Sabbagh A, Tian ZJ, Gonnella PA, Zamvil SS, Chen Y, Weiner HL.** 1996. Effect of oral beta interferon on subsequent immune responsiveness. Ann N Y Acad Sci **778:**145-155.

238. **Mayer L, Shao L.** 2004. Therapeutic potential of oral tolerance. Nat Rev Immunol **4:**407-419.
239. **Takayama S, Iwaki K, Nishida Y, Tanaka M, Fujii M, Ohashi K, Ikeda M, Kurimoto M.** 1999. Effects of oral administration of interferon-alpha on antibody production in mice with induced tolerance. J Interferon Cytokine Res **19:**895-900.
240. **Zhang X, Izikson L, Liu L, Weiner HL.** 2001. Activation of CD25(+)CD4(+) regulatory T cells by oral antigen administration. J Immunol **167:**4245-4253.
241. **Mucida D, Park Y, Kim G, Turovskaya O, Scott I, Kronenberg M, Cheroutre H.** 2007. Reciprocal TH17 and regulatory T cell differentiation mediated by retinoic acid. Science **317:**256-260.
242. **Zurney J, Kobayashi T, Holm GH, Dermody TS, Sherry B.** 2009. The reovirus μ2 protein inhibits interferon signaling through a novel mechanism involving nuclear accumulation of interferon regulatory factor 9. J. Virol. **83:**2178-2187.
243. **Irvin SC, Zurney J, Ooms LS, Chappell JD, Dermody TS, Sherry B.** 2012. A single amino acid polymorphism in reovirus protein μ2 determines repression of interferon signaling and modulates myocarditis. J. Virol. **86:**2302-2311.
244. **Bischoff JR, Samuel CE.** 1989. Mechanism of interferon action. Activation of the human P1/eIF-2-α protein kinase by individual reovirus s-class mRNAs: s1 mRNA is a potent activator relative to s4 mRNA. Virology **172:**106-115.
245. **Bodkin DK, Fields BN.** 1989. Growth and survival of reovirus in intestinal tissue: role of the L2 and S1 genes. J. Virol. **63:**1188-1193.
246. **Kagnoff MF, Austin RK, Hubert JJ, Bernardin JE, Kasarda DD.** 1984. Possible role for a human adenovirus in the pathogenesis of celiac disease. J Exp Med **160:**1544-1557.
247. **Alaedini A, Green PH, Sander HW, Hays AP, Gamboa ET, Fasano A, Sonnenberg M, Lewis LD, Latov N.** 2002. Ganglioside reactive antibodies in the neuropathy associated with celiac disease. J Neuroimmunol **127:**145-148.
248. **Chin RL, Sander HW, Brannagan TH, Green PH, Hays AP, Alaedini A, Latov N.** 2003. Celiac neuropathy. Neurology **60:**1581-1585.
249. **Volta U, De Giorgio R, Granito A, Stanghellini V, Barbara G, Avoni P, Liguori R, Petrolini N, Fiorini E, Montagna P, Corinaldesi R, Bianchi FB.** 2006. Anti-ganglioside antibodies in coeliac disease with neurological disorders. Digestive and liver disease : official journal of the Italian Society of Gastroenterology and the Italian Association for the Study of the Liver **38:**183-187.
250. **Briani C, Ruggero S, Zara G, Toffanin E, Ermani M, Betterle C, Guariso G.** 2004. Anti-ganglioside antibodies in children with coeliac disease: correlation with gluten-free diet and neurological complications. Alimentary pharmacology & therapeutics **20:**231-235.

251. **Alaedini A, Latov N.** 2006. Transglutaminase-independent binding of gliadin to intestinal brush border membrane and GM1 ganglioside. J Neuroimmunol **177:**167-172.
252. **DePaolo RW, Abadie V, Tang F, Fehlner-Peach H, Hall JA, Wang W, Marietta EV, Kasarda DD, Waldmann TA, Murray JA, Semrad C, Kupfer SS, Belkaid Y, Guandalini S, Jabri B.** 2011. Co-adjuvant effects of retinoic acid and IL-15 induce inflammatory immunity to dietary antigens. Nature **471:**220-224.
253. **Fontenot JD, Rasmussen JP, Williams LM, Dooley JL, Farr AG, Rudensky AY.** 2005. Regulatory T cell lineage specification by the forkhead transcription factor foxp3. Immunity **22:**329-341.